THE UNIVERSITY OF MANITOBA

CHARACTERIZATION AND SOME SURFACE STUDIES ON THE PROPERTIES OF POROUS TITANIA GLASS

BY

YOU SING YONG

A THESIS

SUBMITTED TO THE FACULTY OF GRADUATE STUDIES

IN PARTIAL FULFILLMENT OF THE REQUIREMENTS FOR THE DEGREE

OF MASTER OF SCIENCE

DEPARTMENT OF CHEMISTRY

1984

CHARACTERIZATION AND SOME SURFACE STUDIES ON THE PROPERTIES OF POROUS TITANIA GLASS

by

You Sing Yong

A thesis submitted to the Faculty of Graduate Studies of the University of Manitoba in partial fulfillment of the requirements of the degree of

MASTER OF SCIENCE

© 1984

Permission has been granted to the LIBRARY OF THE UNIVERSITY OF MANITOBA to lend or sell copies of this thesis, to the NATIONAL LIBRARY OF CANADA to microfilm this thesis and to lend or sell copies of the film, and UNIVERSITY MICROFILMS to publish an abstract of this thesis.

The author reserves other publication rights, and neither the thesis nor extensive extracts from it may be printed or otherwise reproduced without the author's written permission.

Acknowledgements

The author expresses his sincerest thanks to his supervisor, Dr. H. D. Gesser for his invaluable guidance and advice throughout this project.

Deep appreciation is also expressed to Dr. L. Kruczynski for his encouragement and assistance in this project.

Appreciation is also expressed to my examining committee: Dr. E. Bock and Dr. H. C. Card for their helpful suggestions and comments.

Sincere gratitude to Dr. C. M. Wong for the unrestricted use of the Infrared spectrometer, Mr. L. Groat for running the XRD patterns without cost and his helpful discussions and Dr. C. E. Burchill for allowing his space to be used for writing the author's thesis.

Thanks are also extended to Patrick Gordon, Werner Fritz, Faizan Ahmad, Khalique Ahmad, Younus Meah, Laurie Morton, Mike Sowa, Vipin Bhayana and Vilayat Ali Sayeed for varying assistance along the way.

Special recognition to my parents for their unrelenting support and encouragement towards a tertiary education.

Thanks to Donna Harris for typing the thesis.

The financial assistance from the Chemistry Department, University of Manitoba and the research funds to Dr. H. D. Gesser is gratefully acknowledged.

I. ABSTRACT

Monolithic transparent Porous Titania Glass (PTG) has been successfully fabricated by the controlled hydrolysis of titanium tetrachloride and careful dehydration. X-ray diffraction studies (XRD) indicated that the samples were predominantly amorphous at lower annealing temperature but crystallized to anatase and eventually to rutile at elevated temperature. Surface areas were determined using the conventional volumetric method at 77K. Annealing temperature was found to have a significant effect on the surface area and pore size. Degassing temperature and length of annealing time at constant annealing temperature did not affect the morphology of the sample significantly. PTG, coated with a uniform layer of platinum was used as a hydrogen detector, its sensitivity enhanced by recyling in hydrogen and increasing loading. O_2^- species is proposed as the prerequisite for Ti^{3+} formation by a hydrogen spillover mechanism. The presence of oxygen and/or moisture enhanced the sensitivity of the detector but hydrochloric acid vapour completely destroyed its sensitivity to hydrogen. The energy separation (of plain PTG300R) between the conduction band, E_c, and Fermi level, E_f, decreased with electroreduction time. Infra-red studies on the surface hydroxyl groups indicated that PTG resembled anatase more than rutile.

TABLE OF CONTENTS

Chapter 4

Chapter 5

List of Tables

List of Figures

CHAPTER 1

GENERAL INTRODUCTION

In the last few decades, quite a large volume of literature has been published about anatase and rutile titanium dioxide(TiO_2). The capability of TiO_2 as a support catalyst and photocatalyst [1-8], exhibitions of n-type semiconductor characteristics [9-14] and Strong Metal Support Interaction (SMSI) effect [15-18] has received wide attention. Despite the large volume of work already conducted, research on this subject continues. Recently Gesser et al [19] reported the fabrication of monolithic transparent Porous Titania Glass (PTG) by controlled hydrolysis of titanium tetrachloride ($TiCl_4$) and careful dehydration. Surface area was reported to depend on the thermal history of the titania glass. Earlier, El-Akkad [20] reported on the characterisation of anatase titania gel. Subsequent studies by Gesser and co-workers [21] revealed the use of palladium photodeposited on titania glass as a hydrogen detector. Harris [22] had constructed a similar device by depositing platinum on polycrystalline (anatase) TiO_2. Temperature was reported to influence the response of the detector to hydrogen. The infra-red studies on the surface hydroxyl groups of TiO_2 have also been reviewed quite extensively [23-31].

To my knowledge, little work was done regarding PTG apart from the few publications from Gesser et al [19,21,32]. In this dissertation, PTG will be characterised using the widely applied "two-parameter" BET equation developed by Brunauer et al [33]. Pore size and pore size distribution will be evaluated using the methods adopted by Foster [34] and Lippens et al [35]. The effects of the parameters - annealing temperature, length of annealing time at fixed temperature and degassing temperature on surface area and pore size will be discussed in detail.

The other aspect of the dissertation will focus on some surface properties of PTG. PTG, coated with a uniform layer of platinum, will be discussed. It's use as a hydrogen detector and "ingredients" that enhances/affects its response to hydrogen will also be discussed, together with an attempt to correlate the deep blue colour of plain PTG after electroreduction with the energy separation, between the conduction band, E_c, and the Fermi level, E_f. Finally, infra-red study on the dehydroxylation process will be correlated with the slight decrease in surface area upon subjecting PTG to high temperature-high vacuum treatment.

CHAPTER 2

A THEORETICAL BACKGROUND OF THE ADSORPTION THEORIES AND THE ELUCIDATION OF SURFACE AREA AND PORE SIZE

2-1 INTRODUCTION

When a gas is permitted to come into contact with an evacuated solid in a "restricted" environment, quite a considerable amount of the gas is taken up (adsorbed) by the solid. For example, charcoal has the ability to take up several times it's own volume of various gases under the above conditions. This power depends on the amount of surface area that is exposed. The first systematic investigations on the above phenomenon were conducted by de Saussure [cited from S. Brunauer, ref. [36]] in 1814 when he analysed the uptake of gases by several solids. In this dissertation, the historical interests of the above events will not be emphasized but a review of the theories of the above phenomenon will be presented in the course of this work.

How do the gas molecules disappear from the gas phase upon contact with the solid? Before that detail is presented, there are a few terms which ought to be defined.

i) Adsorption - This is the condensation of gas molecules on the surface of the solid.

ii) Absorption - This process involves the diffusion of gas molecules into the bulk of the solid (or liquid) via the pores, etc.

iii) Sorption - This is the term used to describe the simultaneous occurrence of both adsorption and absorption.

iv) Adsorbent - The solid that adsorbs the gas molecules from the gas or vapour phase.

v) Adsorbate - The gas or vapour that attaches to the surface of the adsorbent.

In spite of the above definitions, it is difficult to determine whether the adsorbate is inside or outside the adsorbent. For a highly porous material like charcoal, only a fraction of the total surface area is exposed, even under the microscope. So long as the adsorbates do not penetrate into the "force field" exerted by the atoms, ions or molecules inside the solid, they are considered to be residing on the external surface though it may be on the inside of the adsorbent.

If the gas molecules enter the inside of the solid, the following may occur:

1) it may form a 'solid' solution by just dissolving into the cracks or fissures

OR

2) it may react with the adsorbent forming a compound.

Upon warming or degassing, the first case may exhibit a phenomenon termed "hysteresis" which will be dealt with in the later section. Suppose the gas remains on the surface of the adsorbents, then two situations may arise:

1) a weak adsorbate-adsorbent interaction may occur, a process identical to condensation

OR

2) a strong adsorbate-adsorbent interaction occurs, resulting in the equivalence of a chemical reaction.

The former case is termed physical adsorption or physiosorption whereas the latter is called chemical adsorption or chemisorption.
Van der Waals adsorption is occasionally used to describe the former case, implying that van der Waals forces are being utilized. Activated adsorption, a term coined by Taylor [37] in 1931 is used to indicate the

latter case as it involves an activation energy just as most chemical reactions do.

2-2 The Solid-Gas Interface

Regardless of the nature of the surface or the adsorbate, the concentration of the adsorbate is always found to be greater near the immediate vicinity of the surface relative to the gaseous phase if equilibrium exists in the system. In any solid (or liquid), the atoms at the surface are always subjected to unbalanced attractive forces acting normal to the plane of the surface. This defect is partially restored by adsorbing the adsorbate. This process is usually exothermic and it is a spontaneous occurring process. Hence the Gibbs free energy ΔG is negative, indicating that the term $(\Delta H - T\Delta S)$ must also be negative.

$$\Delta G = \Delta H - T\Delta S \qquad (2.01)$$

where ΔH = heat of reaction

ΔS = entropy change of the process

T = absolute temperature

The gaseous phase is the most disordered state. If the molecule is being adsorbed by the surface, it loses some of it's degree of freedom, thus producing a more ordered state. Therefore the entropy term becomes negative. In other words, the ΔH term must also be negative, thus making ΔG negative or $\Delta H < T\Delta S$.

As mentioned earlier, gas molecules can be physically or chemically adsorbed on the surface. In the former case, van der Waals interaction is involved and the energy release is tantamount to the enthalpy of condensation of the gas molecules. For example, the heat of physical adsorption of nitrogen on an iron catalyst is between 9-12 kJ $mole^{-1}$

whereas the heat of liquefaction of gaseous nitrogen is about 6 kJ $mole^{-1}$. This small amount of energy can easily be eliminated as vibrations of the lattice and dissipated as heat. On the other hand, a bond (usually a covalent bond) is formed between the adsorbate and ignored adsorbent in chemisorption. A molecule undergoing such process may be torn apart in order to satisfy the valencies of the surface atoms, thus loosing its identity. For instance, nitrogen molecule becomes nitrogen atoms upon adsorbing onto the surface of the iron catalyst, the heat of adsorption being 146 kJ $mole^{-1}$. Briefly, the following points can be used to distinguish physiosorption and chemisorption:

a) For physiosorption, the heat of adsorption H_{ads} is of the order of magnitude as the heat of liquefaction of the gas molecules and is rarely more than two or three times as large. Typically, the values are less than 20 kJ $mole^{-1}$. In contrast, chemisorption results in the formation of bonds and the range of H_{ads} falling between 40-800 kJ $mole^{-1}$.

b) Physical adsorption permits the formation of multi-layers whereas only a monolayer is permitted by chemisorption.

c) The rate of physical adsorption is always fast, as in the condensation of a vapour on the surface of its own liquid because there is no appreciable activation energy. The process of chemisorption, in contrast has an activation energy barrier as illustrated in Fig. 1 [75].

d) Physiosorption, like condensation will occur with any gas-solid system provided that the conditions of the temperature and pressure are suitable. Chemical adsorption will only occur if the gas is capable of forming a chemical bond with the surface.

Fig 1: Potential energy diagram for the adsorption of hydrogen on nickel (reproduced from ref: 75).

$D.E_{H-H}$ = Dissociation energy of hydrogen ($\approx$434 KJ $mole^{-1}$).

ΔH_P = Enthalpy of physical adsorption (negligible).

ΔH_C = Enthalpy of chemisorption ($\approx$125 KJ $mole^{-1}$).

ΔE = Activation energy for chemisorption.

P = Physical adsorption.

C = Chemisorption.

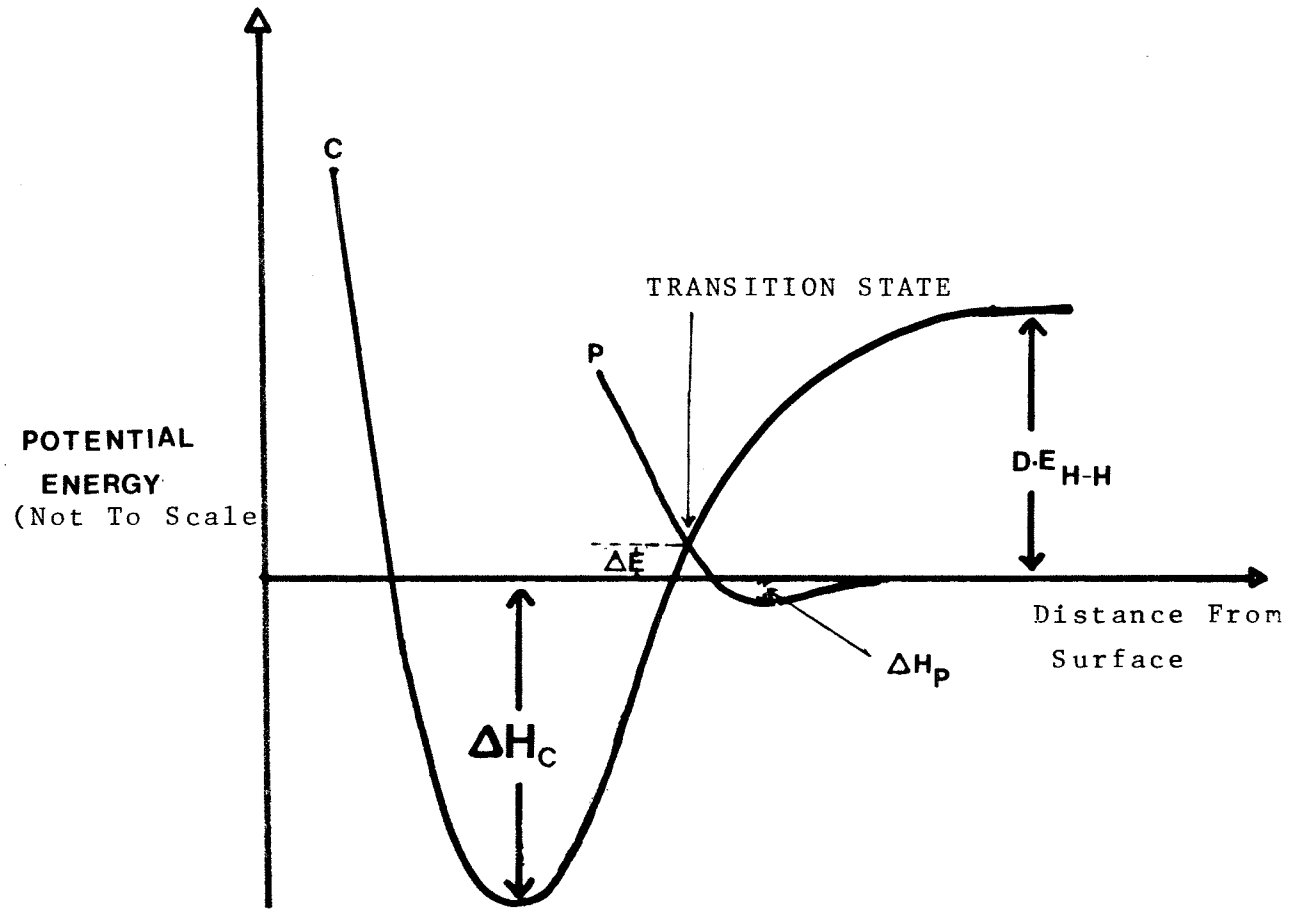
C
TRANSITION STATE
P
POTENTIAL
ENERGY
(Not To Scale
D·E H-H
ΔE
Distance From
Surface
ΔH P
ΔH C

e) A physiosorbed layer may be removed by reducing the pressure, at the temperature at which adsorption occurred, although it may be slow on account of diffusion effects. The removal of a chemisorbed layer usually requires more drastic measures such as high temperature.

f) Physiosorption is usually related to liquefaction. This only occurs to an appreciable extent at pressures and temperatures close to those required for liquefaction. Although these criteria are unquestionably useful, it can be misleading if the material is highly porous. Chemisorption, being associated with much stronger forces should be capable of occurring at higher temperature, well above the boiling point of the adsorbate at the operative pressure.

2-3 Theory of Adsorption of Gases on Solid Surfaces

Let us consider a surface on which a certain number of molecules are already adsorbed. There is a probability that an impinging molecule will not strike an empty site but on top of an adsorbed molecule which is already physically adsorbed there. The probability of the above happening increases with the number of molecules adsorbed. If the molecules, when striking on a layer of molecules which are already adsorbed are attracted by sufficiently great forces, multilayer adsorption occurs.

In the above phenomenon, several theories have been developed in order to correlate and explain experimental data with a theoretical approach. Polanyi [cited from Young and Crowell in ref. [38]] in 1914 extended the idea of de Saussure to construct the potential theory. Briefly, it is assumed that the "adsorption space" has the same

adsorption potential in the vicinity of the adsorbent's surface as illustrated in Fig. 2. Let ABCD be a section through the "adsorption space" (see Fig. 3) and abAB corresponding an equipotential surface. When the space of volume V between CDcd and ABab is filled with adsorbate, the adsorption potential ε at the surface of ABab is

$$\varepsilon = RT/\ln ({}^{P_o}/_{P}) \qquad (2.02)$$

where P_o = saturated vapour pressure of adsorbate

P = equilibrium pressure of adsorbate

Assuming that the adsorbed adsorbate exists as a liquid, then the volume V will be given by

$$V = W/\rho \qquad (2.03)$$

where W = adsorption in grams corresponding to pressure P

ρ = density of liquid adsorbate

Since both V and ε can be evaluated from the experimental data, V can thus be represented as

$$V = f(\varepsilon) \qquad (2.04)$$

No attempt was made to derive an expression for the adsorption isotherm from the potential theory until Dubinin et al. [39] presented a derivation in 1947.

The attempt to explain the sigmoid or S-shaped adsorption isotherms commonly encountered at high relative pressures was first undertaken by

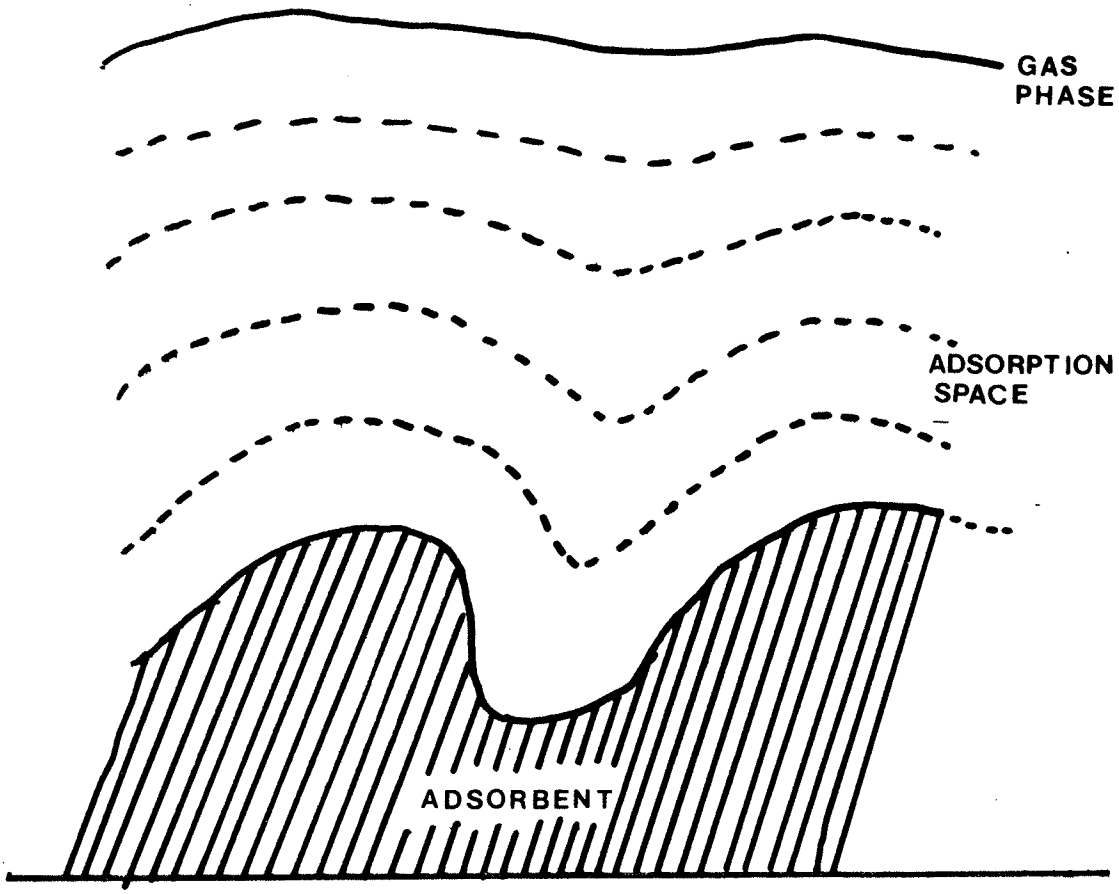

Fig 2 Cross-Section Of The Adsorbed Layer According To The Potential Theory(reproduced from reference (36)).

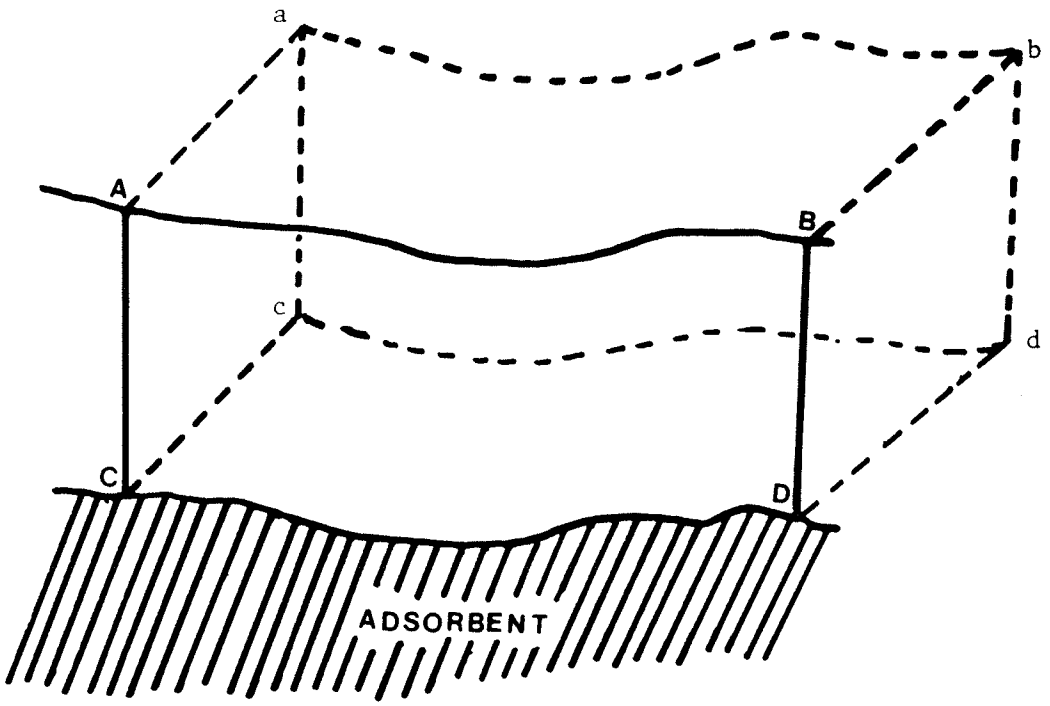

Fig 3: A Diagramatic Representation of The Adsorption Space In The Vicinity Of An Adsorbent.

CDcd is the region of the adsorbent surface.

ABab is an equipotential surface which will be approximately parallel to CDcd (reproduced from reference (36)).

de Boer and Zwikker in 1929 [cited from ref. [33]]. Again briefly, the surface is assumed to induce dipoles in the first layer of adsorbed molecules and these dipoles in turn induce dipoles in the second layer and so on. The magnitude of the induced dipole moment decreases exponentially as the number of layers increases. The final isotherm equation is given by

$$\frac{\ln(P/P_o)}{K_3} = K_2 K_1^{\theta} \tag{2.05}$$

where

K_1 , K_2, K_3 = constants

and θ = coverage which is equal to V/V_m, V_m being the volume of adsorbate required to completely form a monolayer.

If K_3 is unity, then equation (2.05) transforms to

$$\ln(P/P_o) = K_2 K_1^{\theta} \tag{2.06}$$

or

$$\ln(\ln(P/P_o)) = \ln K_2 + \theta \ln K_1$$

$$= \ln K_2 + V/V_m \ln K_1 \tag{2.07}$$

Since $\theta = V/V_m$.

However, the above concepts are obsolete now, and hence the reader is requested to refer to the reference quoted [33,39].

The first theoretical approach to descibe the relationship between the amount of gas adsorbed and the equilibrium pressure of the gas at constant temperature was due to I. Langmuir in 1915 [40]. But prior to the discussion of the theory and subsequently it's modification to

explain multilayer adsorptions, let us not neglect the various type of adsorption isotherm encountered by earlier studies [41].

2-4 The Adsorption Isotherm

As stated earlier, a solid that has been evacuated and degassed will adsorb a large volume of adsorbate if exposed in a closed space at some definite pressure. This is manifested by a gradual reduction in pressure of the adsorbate and an increase in the weight of the solid. Eventually the pressure becomes constant at a value say P and correspondingly, the weight ceases to increase any further. The amount of adsorbate adsorbed can thus be calculated from the fall in pressure by the application of the gas laws if the volume of the vessel, temperature and the adsorbent is known, or it can be determined directly as the increase in weight of the adsorbent in the case where a spring balance is used.

The adsorption process is a consequence of the field force at the surface of the adsorbent which attracts the adsorbate, either physiosorbed or chemisorbed depending on the forces of attraction emanating from the adsorbent. In any event, the amount adsorbed depends on the equilibrium pressure P, the temperature T and the nature of the adsorbate and adsorbent. In other words, the amount adsorbed can be represented as

$$V = f(P, T, \text{adsorbate}, \text{adsorbent}) \qquad (2.08)$$

where V is the volume adsorbed.

If the temperature is kept constant, then

$$V = f(P)_{T,\text{adsorbate, adsorbent}} \qquad (2.09)$$

If the experiment is conducted below the critical temperature of the adsorbate, that is in the vapour state, then

$$V = f(P)_{T,\text{adsorbate, adsorbent}} \qquad (2.10)$$

where P_o is the saturated vapour pressure of the adsorbate. A plot of V against P/P_o represents the relationship between the amount adsorbed and the pressure. These plots are called adsorption isotherms.

A literature survey on physical adsorption will reveal an enormous amount of work done on the above subject on a wide variety of adsorbents. Nevertheless, the majority of the isotherms can be classified into six types, the first five types essentially those proposed by Brunauer, Deming, Deming and Teller [41] (BDDT classification or commonly refered to as BET classification) whereas the last type is more recent [42]. Examples of these isotherms are illustrated in Fig. 4.

2-5 Types of Adsorption Isotherms

Type I

The typical characteristic of this type of isotherm is its long flat branch which is quite horizontal. In most cases, it cuts the relative pressure axis $P/P_o = 1$ sharply but others produce a "tail". This characteristic may be caused by the microporous nature of the adsorbent, in other words the pores are very narrow and are less than a few molecular diameters wide. Langmuir [40] considered this horizontal region as the completion of a monolayer but Sing [42] attributed it to be the primary adsorption process whereby pore filling occurred. "Molecular sieve zeolite" exhibits an isotherm with a horizontal plane over a huge range of P/P_o. This suggests that the adsorption is

Fig 4: Types Of Physical Adsorption [42]

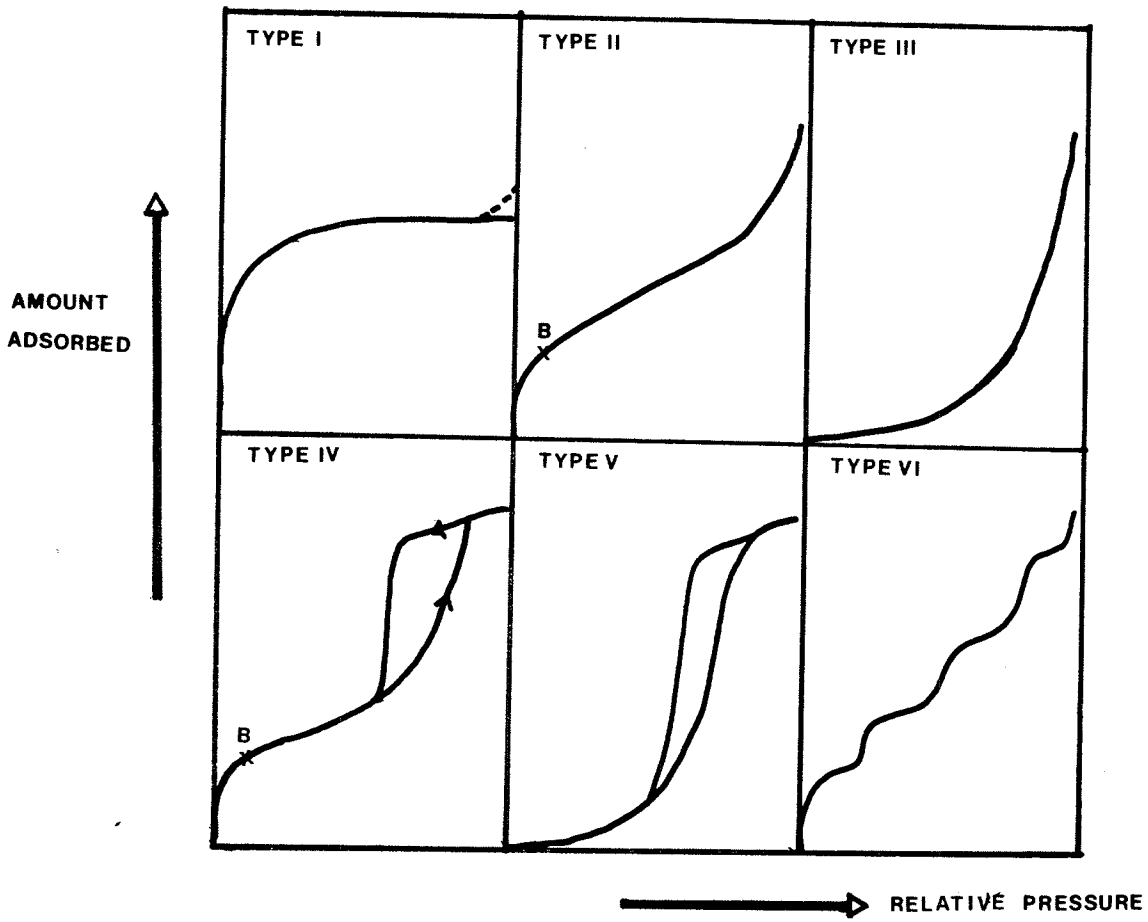

controlled by the micropores' volume beside revealing that the external surface area is small. Note that this is a reversible isotherm and though hysteresis effect is seldom encountered, it is sometimes observed, for example in the adsorption of benzene on activated coconut shell charcoals. However, no explanation was forwarded by the authors to explain the hysteresis effect [43]. In some cases, low pressure hysteresis may be associated with "activated" entry of adsorbate molecules through the fine capillaries or constrictions [42]. An example which illustrates Type I isotherm is the adsorption of oxygen on carbon.

Type II

This type of isotherm is usually associated with the physical adsorption of nitrogen and other non-porous on non-porous or macroporous materials. It is usually called the sigmoid or "S-shaped" isotherm. This characteristic is caused by the lack of "restriction" imposed on the physiosorption on a heterogenous surface (in particular), whereby multilayer adsorption can occur. The adsorbate-adsorbate and adsorbate-adsorbent interactions have a pronounced influence on the features exhibited by this isotherm. The linear portion of this isotherm corresponds to the formation of a complete monolayer and the beginning of the formation of the second layer. The value V_m derived from this isotherm (so called Point B method) can be used to derive the surface area of the adsorbent. This procedure will be reviewed later. The adsorption of nitrogen on iron catalyst at 77K follows this isotherm.

Type III

This type of isotherm is seldom encountered. It does not exhibit "Point B" though some systems did give a gradual curvature at the point equivalent to Point B of Type II. It is convex to the relative pressure axis over it's entire range, thus making the identification of Point B extremely difficult or virtually impossible. Usually the adsorbate-adsorbent interaction is very weak if the adsorbent obeys the above plot. An example is the adsorption of bromine on non-porous silica at 77K.

Type IV

The initial part of the isotherm follows precisely the same pattern as that of Type II except that adsorption increases as the pressure of the adsorbate approaches the saturated vapour pressure P_o in Type IV. In Type II, maximum or almost maximum adsorption is achieved at some pressure much lower than the saturated vapour pressure of the adsorbate. However, the exhibition of hysteresis effect is the most prominent feature of Type IV isotherm. Sing [42] attributed this to be associated with the secondary pore-filling process, and this is the portion of the isotherm which can be used to determine the pore size and the pore volume.

Type V

This is probably the most difficult isotherm to interpret. A hysteresis which is often observed is generally related to capillary condensation. Adsorbate-adsorbent interaction is also very weak. Neither the surface area nor the pore size distribution can be evaluated with confidence. In some cases, a low pressure hysteresis had been

observed and this is attributed to the slow rehydration of the surface, for example the adsorption of water vapour on charcoal at 373 K.

Type VI

This type of isotherm does not fit into the conventional BDDT classification. A step-wise multilayer formation occurs on a uniform surface whereby each of the first few layers is adsorbed over a restricted range of pressure. The step height which corresponds to the monolayer capacity will remain constant for two or three layers. At very low pressure, the isotherm is convex. An example of this isotherm is illustrated by krypton on carbon (graphitized at 2700°C) at 90K.

As mentioned earlier, Langmuir [40] initiated the theoretical approach to explain the adsorption of gases on the surface. Since his theory serves as the basis for the development of other theories to explain multilayer adsorption, it would therefore be inappropriate to neglect it.

2-6 The Langmuir Theory

Langmuir [40] visualized the adsorption process at equilibrium to be dynamic whereby the adsorbate molecule will be adsorbed if it impinges on a vacant site but elastically reflected away if it impinges on an occupied site. The adsorbed molecule will relinquish it's kinetic energy to the surface of the adsorbent which in turn will either lose it by vibration of the lattice or dissipated it as heat. If these adsorbed species manage to acquire sufficient energy, they will desorb from the surface. However, Langmuir assumed that there is a time lapse during

the acquisition of this energy and this is what causes the adsorption phenomenon.

At equilibrium, the rate of adsorption equals the rate of desorption. The number of molecules impinging on a unit area of surface per unit time is given by

$$\nu = P(2\pi mkT)^{-\frac{1}{2}} \tag{2.11}$$

where

P = pressure

m = mass of adsorbate molecule

k = Boltzmann constant

and T = absolute temperature

The following assumptions were introduced:

i) The probability of evaporation of an adsorbate molecule from the surface is identical irrespective of whether the neighbouring site on the surface is occupied or not. In other words, the adsorbate-adsorbate interaction is assumed to be negligible or absent.

ii) A molecule that impinges on a vacant site will be adsorbed but reflected away elastically if it impinges on an occupied site, that is there is no loss of kinetic energy, if it collides with an adsorbed molecule.

iii) The heat of adsorption on all sites are equivalent.

iv) Only a monolayer is formed.

Based on the above assumptions, the rate of adsorption R_A can be represented as

$$R_A = \alpha_o(1-\theta)\nu \tag{2.12}$$

where

θ = coverage

and α_o = condensation coefficient, that is, the ratio of inelastic collisions resulting in adsorption to the total number of collisions of gas molecules with the surface.

Similarly, the rate of desorption R_D is given by:

$$R_D = \mu\theta \tag{2.13}$$

where

μ = number of molecules leaving the surface, a parameter which is dependent on the adsorbate-adsorbent binding energy.

If ϵ is the heat of adsorption, then molecules that have acquired energy E will be able to desorb from the surface provided that $E \geq \epsilon$.

At equilibrium,

$$R_A = R_D \tag{2.14}$$

that is

$$\alpha_o\,(1-\theta) = \mu\theta \tag{2.15}$$

Substituting equation (2.11) into (2.15)

$$\alpha_o P(2\pi mKT)^{-\frac{1}{2}}(1-\theta) = \mu\theta \tag{2.16}$$

Rearranging and solving for θ

$$\theta = \frac{bP}{1 + bP} \tag{2.17}$$

where

$$b = \frac{\alpha_o}{(2\pi mkT)^{\frac{1}{2}}} \tag{2.18}$$

Equation (2.17) is known as the Langmuir adsorption isotherm. Though the above concept is applicable to a certain extent, it received wide criticism. To date, the constant b is found to be [44]

$$b = \frac{h^3 f_a(T) \exp(-\epsilon/kT)}{(2\pi m)^{3/2}(kT)^{5/2} f_g(T)} \tag{2.19}$$

where

h = Planck constant

$f_a(T)$ and $f_g(T)$ = internal partition functions of a molecule in the adsorbed and gaseous state respectively.

ϵ = heat of adsorption which is equivalent to the energy required to transfer a molecule from the lowest adsorbed state to the lowest gaseous state.

The derivation of the Langmuir adsorption isotherm is essentially based on kinetics. Thermodynamic properties are thus liable to be concealed. In other words, the adsorption process depends only on the condensation and evaporation of the adsorbed molecules. The term b is entropy dependent and will only be constant if the free energy of adsorption does not vary with coverage [44]. In reality, the energetic equivalence

of all adsorption sites is not true. Thus the Langmuir adsorption isotherm will not be obeyed unless the surface is uniform and adsorbate-adsorbate interaction is negligible, otherwise the information derived will be misleading. But Brunauer and co-workers [44] disagreed with the above. They pointed that the most important factor is b, a term which involves the heat of adsorption. They argued that the opposing effect of lateral interaction energies between the physiosorbed species and the heat of adsorption of molecules at low coverage when the vacant sites possess the highest energies compensate each other, thus making ϵ approximately constant. The entropy term may partially be compensated by ϵ. Despite all of the criticisms and comments, the Langmuir equation is still applicable if b is constant but the most important contribution is its basis for the development of multilayer adsorption theory by Brunauer et al. [33] who overcame the problem of multilayer adsorption by focussing their attention to the process of interchange of molecules between the gas phase and the adsorbed species.

2-7 The BET Equation

Fig. 5 represents the model proposed by Brunauer and co-workers [33]. In this model, varying numbers of molecules can condense on one site and there is dynamic equilibrium within each layer. For example, the number of molecules desorbing per second in layer n is equivalent to the number condensing per second on the layer immediately below it, that is the $(n-1)^{th}$ layer.

Let A_o, A_1,A_2...A_n be the surface area that is covered by only 0, 1, 2, 3...n... layers of adsorbed molecules. At equilibrium, A_o is assumed to remain constant. Hence the rate of condensation on the

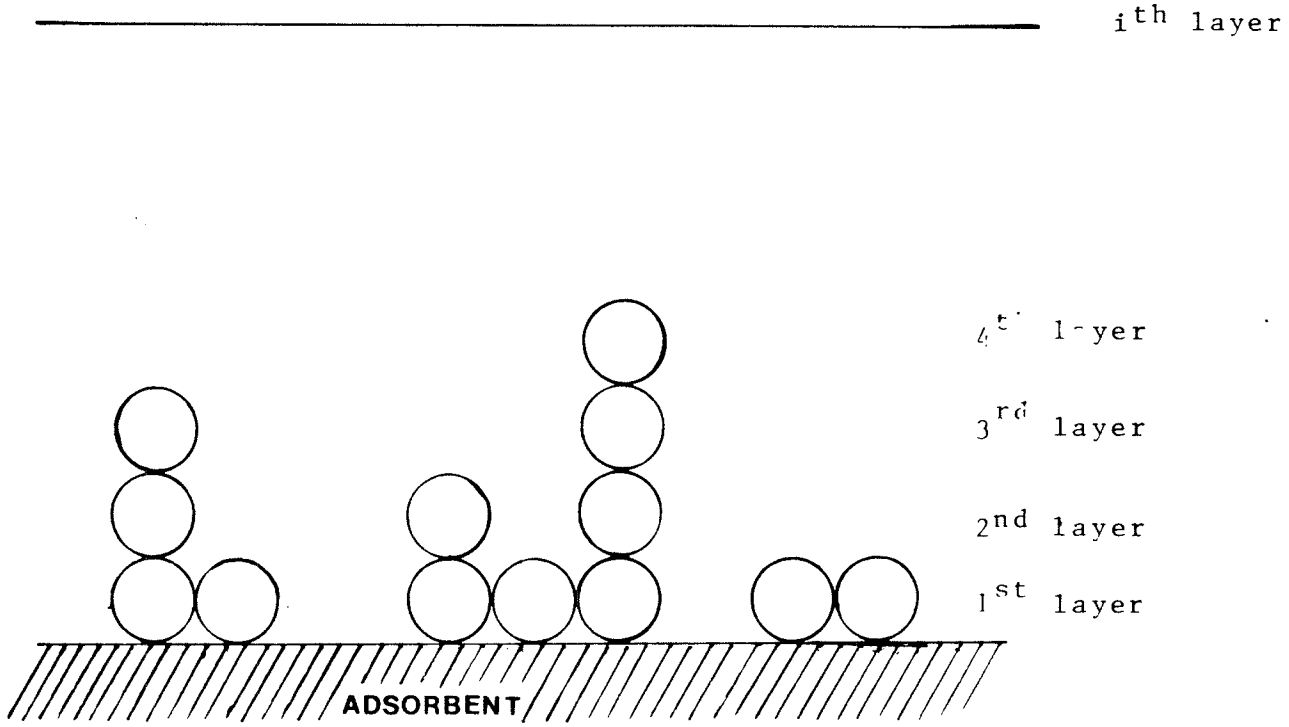

Fig 5: The BET Model For Adsorption

(reproduced from reference (36)).

unoccupied site is equal to the rate of desorption from the first layer. Thus

$$\alpha_1 P A_o = \beta_1 A_1 \exp(-\Delta E_1/RT) \tag{2.20}$$

where

P = equilibrium pressure

ΔE_1 = heat of adsorption of the first layer

and α_1, β_1 = constants.

It is also assumed that α_1, β_1 and ΔE_1 are independent of the number of adsorbed molecules already present in the first layer, an identical assumption made by Langmuir [40] in his derivation of the Langmuir adsorption isotherm. Similarly A_1 must also remain constant at equilibrium. Notice that there are four ways in which A_1 can vary:

i) Adsorption of molecules on vacant sites

ii) Evaporation from the first layer

iii) Condensation on the first layer and lastly

iv) Evaporation from the second layer

The above condition can be expressed mathematically as:

$$\alpha_2 P A_1 + \beta_1 A_1 \exp(-\Delta E_1/RT) = \beta_2 A_2 \exp(-\Delta E_2/RT) + \alpha_1 P A_o \tag{2.21}$$

where α_2, α_2 and E_2 are similarly defined to α_1, β_1 and ΔE_1.

Substituting equation (2.20) into (2.21) and solving the equation yields

$$\alpha_2 P A_1 = \beta_2 A_2 \exp(-\Delta E_2/RT) \tag{2.22}$$

In short, the rate of condensation on top of the first layer is equal to the rate of evaporation of the second layer. Based on the same arguments to the second and consecutive layers, the multilayer formation can be described as

$$\begin{aligned} \alpha_3 P A_2 &= \beta_3 A_3 \exp(-\Delta E_3/RT) \\ &\vdots \\ \alpha_n P A_{n-1} &= \beta_n A_n \exp(-\Delta E_n/RT) \end{aligned} \tag{2.23}$$

The total surface area S_{tot} is defined as the sum of all the areas, that is,

$$S_{tot} = \sum_{n=0}^{\infty} A_n \tag{2.24}$$

and the total volume V_{tot} as

$$V_{tot} = V_o \sum_{n=0}^{\infty} n\, A_n \tag{2.25}$$

where

V_o = volume of adsorbate adsorbed on a square metre of the adsorbent surface when it is covered with a complete unimolecular layer of adsorbed adsorbate.

Divide equation (2.25) by (2.24):

$$\frac{V_{tot}}{S_{tot}} = V_o \sum_{n=0}^{\infty} n\, A_n \Big/ \sum_{n=0}^{\infty} A_n \tag{2.26}$$

that is,

$$\frac{V_{tot}}{S_{tot} \times V_o} = \sum_{n=0}^{\infty} n\, A_n \Big/ \sum_{n=0}^{\infty} A_n \tag{2.27}$$

V_m, the volume of adsorbate required to form a complete monolayer, is given by

$$V_m = V_0 \times S_{tot} \tag{2.28}$$

Substitute equation (2.28) into (2.27) yields

$$\frac{V_{tot}}{V_m} = \sum_{n=0}^{\infty} n A_n \Big/ \sum_{n=0}^{\infty} A_n$$

It is also assumed that

$$\text{i)} \quad \Delta E_2 = \Delta E_3 = ... \Delta E_n = \Delta E_L \tag{2.30}$$

where ΔE_L = heat of liquefaction of adsorbate molecules and

$$\text{ii)} \quad \frac{\beta_2}{\alpha_2} = \frac{\beta_3}{\alpha_3} = ... \frac{\beta_n}{\alpha_n} = g \tag{2.31}$$

where g is a constant.

The above assumptions imply that the second and the consecutive layers have identical properties as those in the liquid state. As mentioned earlier van der Waals forces are involved in physical adsorption. Since the first layer is in contact with the surface of the adsorbent, it therefore experiences this force. The second and higher layers are assumed to be "spared" from this force. Let

$$A_1 = yA_o \tag{2.32}$$

where

$$y = \frac{\alpha_1}{\beta_1} P \exp(\Delta E_1/RT)$$

Similarly,

$$A_2 = XA_1 \tag{2.33}$$

where

$$X = \frac{P \exp(\Delta E_L/RT)}{g}$$

and

$$A_3 = XA_2$$
$$= X^2 A_1$$

Similarly,

$$A_n = XA_{n-1} \tag{2.34}$$
$$= X^{n-1} A_n$$
$$= yX^{n-1} A_o$$
$$= CX^x A_o$$

where

$$C = Y/X$$

$$= \frac{\alpha_1 g \exp[(\Delta E_1 - \Delta E_L)/RT]}{\beta_1} \tag{2.35}$$

Substitute equation (2.35) into (2.29) and simplifying

$$\frac{V_{tot}}{V_m} = C A_o \sum_{n=1}^{\infty} n X^n \Big/ A_o[1 + C \sum_{n=1}^{\infty} X^n] \tag{2.36}$$

The summation term in the denominator is the sum of an infinite geometric progression.

$$X \sum_{n=1}^{\infty} X^n \approx \frac{X}{1-X} \tag{2.37}$$

The numerator is thus equivalent to the differential of equation (2.37), that is,

$$X \frac{d}{dX} \sum_{n=1}^{\infty} X^n \approx X \frac{d}{dX} \left(X \Big/ 1-X \right)$$

$$\approx \frac{X}{(1 - X)^2} \qquad (2.38)$$

Substitute equation (2.37) and (2.38) and simplifying

$$\frac{V_{tot}}{V_m} = \frac{CX}{(1 - X)(1 - X + CX)} \qquad (2.39)$$

On a free surface, an infinite number of layers can build up on the surface when the pressure approaches the saturated vapour pressure of the adsorbate. To make $V_{tot} = \infty$ when $P = P_o$, X must be unity in equation (2.39). Thus

$$1 = (P/g)\exp(\Delta E_L/RT)$$
$$= (P_o/g)\exp(\Delta E_L/RT) \qquad (2.40)$$

In other words,

$$1 = X = P/P_o \qquad (2.41)$$

Substitute equation (2.41) into (2.39)

$$\frac{V_{tot}}{V_m} = \frac{C(P/P_o)}{(1 - P/P_o)(1 - P/P_o + C(P/P_o))} \qquad (2.42)$$

On rearranging equation (2.42),

$$V_{tot} = \frac{V_m CP}{(P_o - P)[1 + (C - 1)(P/P_o)]} \qquad (2.43)$$

This equation (equation (2.43)) is known as the "simple" or "ω-form" BET equation. For the purpose of testing equation (2.43), it can be expressed as

$$\frac{P}{V_{tot}(P_o - P)} = \frac{1}{V_m C} + \frac{(C-1)P}{V_m C P} \qquad (2.44)$$

As the equilibrium pressure P, approaches the saturated vapour pressure P_o of the adsorbate, the graph becomes convex to the pressure axis. Likewise, the graph will be concave in the low pressure region since the constant C is larger than unity, thus resulting in two regions. Note that equation (2.44) is commonly referred as the BET "two-parameter" equation for obvious reason. If $P \ll P_o$, then equation (2.44) transforms as

$$V_{tot} = \frac{V_m C P}{P_o} \Big/ \left(1 + \frac{CP}{P_o}\right) \qquad (2.45)$$

Provided that $(\alpha_1\beta_2/\alpha_2\beta_1)$ does not deviate much from unity, then the average heat of adsorption in the first layer can be determined as:

$$C = \frac{\alpha_1 \beta_2}{\alpha_2 \beta_1} \exp[(\Delta E_1 - \Delta E_L)/RT] \qquad (2.46)$$

$$\approx \exp[\Delta E_1 - \Delta E_L] \qquad (2.47)$$

Suppose the adsorption occurs in a restricted area and not on a free surface, then only finite layers n can be built on the surface of the adsorbent when $P=P_o$. Thus the summation of the two series in equation (2.36) is to be expanded to the n^{th} term only. Therefore

$$V_{tot} = \frac{V_m C X}{(1-X)} \left(\frac{1 - (n+1)X^n + n X^{n+1}}{1 + (C-1)X - C X^{n+1}} \right) \qquad (2.48)$$

the terms X, V_m, V_{tot}, C and n as defined earlier. This equation is

referred as BET "three-parameter" equation. i) When $n=\infty$, equation (2.48) becomes equation (2.43). ii) When n=1, equation (2.48) reduces to equation (2.45).

In the development of the BET theory, it was assumed that the adsorbed molecule is unable to evaporate if there is another adsorbed molecule on top of it. On the other hand, Huttig [cited from Young and Crowell [38]] argued that evaporation is possible if there is another adsorbed species on top of it. His equation is

$$\frac{V_{tot}}{V_m} = \left(\frac{CP/P_o}{1 + \frac{CP}{P_o}}\right)\left(1 + \frac{P}{P_o}\right) \qquad (2.49)$$

There are two points to note in this equation:

i) At $P=P_o$, the maximum number of layers that can occur on the surface is finite and is given by $2C/(1+C)$.

ii) Equation (2.49) is an extension of Langmuir adsorption isotherm by a factor $(1 + P/P_o)$.

The other modification was by McMillan and Teller [45]. They argued that surface tension would oppose the build-up of the thickness of the adsorbed layers. The final form of the isotherm is given by

$$-\ln X = \sigma\theta^{-3} \qquad (2.50)$$

where

$X = P/P_o$

σ = proportionality function which is temperature dependent and is given by $kT/18\pi\omega\tau^2$, ω being energy per unit surface and τ, the interlayer spacing

and θ = coverage

For further details about the modifications, the reader is referred to the book by Young and Crowell on "Physical Adsorption of Gases" [38].

The BET theory, though achieving much success, has had several defects too. The BET constant C (from equation (2.35)) which determines the nature of the plot is not unity at all in a majority of cases. At the present moment, there is still no definite way of determining C precisely. Secondly, the assumption that an energetically equivalent surface exists is often misleading. Joyner and Emmett [46] found that the differential heat of adsorption of nitrogen on pre- and post-graphitized carbon blacks (Temp = 3000°C) varied. Thirdly, the horizontal adsorbate-adsorbate interaction becomes more pronounced as the number of layers increases. Despite these setbacks, the BET equation is still the most practical and impressive theory developed to date for the determination of surface areas.

As mentioned earlier, the almost linear portion contains a point called "Point B" which Brunauer and Emmett [47] concluded to be the completion of a monolayer. By extrapolating the linear portion to P=0, the authors found that the surface areas derived were very satisfactory. Halsey [48] pointed out that "Point B" is the region where dramatic adsorption of molecules occurs. By treating the surface of the adsorbent as a uniform surface and letting the effect of heat of adsorption in the n^{th} layer be a function of n, he found that the surface areas derived by using "Point B" are comparable to the BET analogues. White [49] concluded that accurate surface area determination was possible provided C is greater than 9. Though experimental data such as heat of adsorption, etc, lent much support to

this method, the reliability of this method is still in doubt due to the difficulty in locating the precise "Point B".

From the above discussion, the relationship between the adsorption isotherm, the surface area and pore structure is indeed very intimate. Very often, a highly porous material has large surface area. In such a system, it is desirable to have a huge internal microporous network where total contribution to the total surface area is great. These networks are composed of pores - big or small. Adopting the IUPAC classification [42], these pores can be classified into three categories:

i) Macropores - pores with width greater than 500Å

ii) Mesopores - pores with width between 20Å and 500Å

iii) Micropores - pores with width less than 20Å

There are several ways in which pores arise, namely precipitation, sublimation, thermal decomposition and leaching of substances. These pores, in various sizes and shapes, will influence the form of the adsorption isotherms. For example, wedge- or cone-shaped systems will result in Type III, IV or V isotherms [49] apart from the hysteresis effect [50].

But what is hysteresis? Gas molecules will condense in some empty pores at a certain pressure depending on the size and shape of the pores. These condensed molecules will desorb from the pores at a pressure which is lower than the adsorption pressure. Under these circumstances, the adsorption and desorption branches will not coincide, therefore a hysteresis is said to have occurred. In other words, when an independent variable changes direction, the dependent variable fails

to retrace the forward path and hence it "lags" behind. A hysteresis loop thus formed.

As in the case of adsorption, hysteresis loops are also classified into five groups viz: type A-E depending on the steepness of the adsorption and desorption branches or the pressure range. The various types of hysteresis loops are illustrated in Fig. 6 together with the possible pore shapes that causes it [51]. Several theories have been proposed to explain the hysteresis phenomenon but due to the enormous volume available only some suggestions will be mentioned. Zsigmondy [cited from Flood [51]] reckoned that insufficient time is allocated for equilibrium to exist due to the "permanent" impurities in the gas or the surface of the adsorbent. An increase in pressure removes the impurities and eventually total "wetting" of the pores occurs when the pressure approaches the saturated vapour pressure of the adsorbate. The contact angle Φ thus becomes zero and on desorption, the adsorption path is not traced due to difference of pressure ($P_A > P_D$). However, Cohan [52] argued that hysteresis will occur in any systems even if complete "wetting" has yet to occur. If there is impurity, then the hysteresis should spread over the entire isotherm. McBain [53] attributed the phenomenon to be caused by pores possessing narrow neck and wider body - the so-called "Ink Bottle" effect. The pore will not be filled until it reaches a pressure corresponding to the radius of the body (r_{body}) and desorbs at a pressure corresponding to the radius of the neck (r_{neck}). Since $r_{neck} < r_{body}$, desorption occurs at a lower pressure than adsorption. Cohan [54] in his later paper extended McBain's "Ink Bottle" hypothesis. He postulated that a meniscus should form at the neck during adsorption at a pressure given by

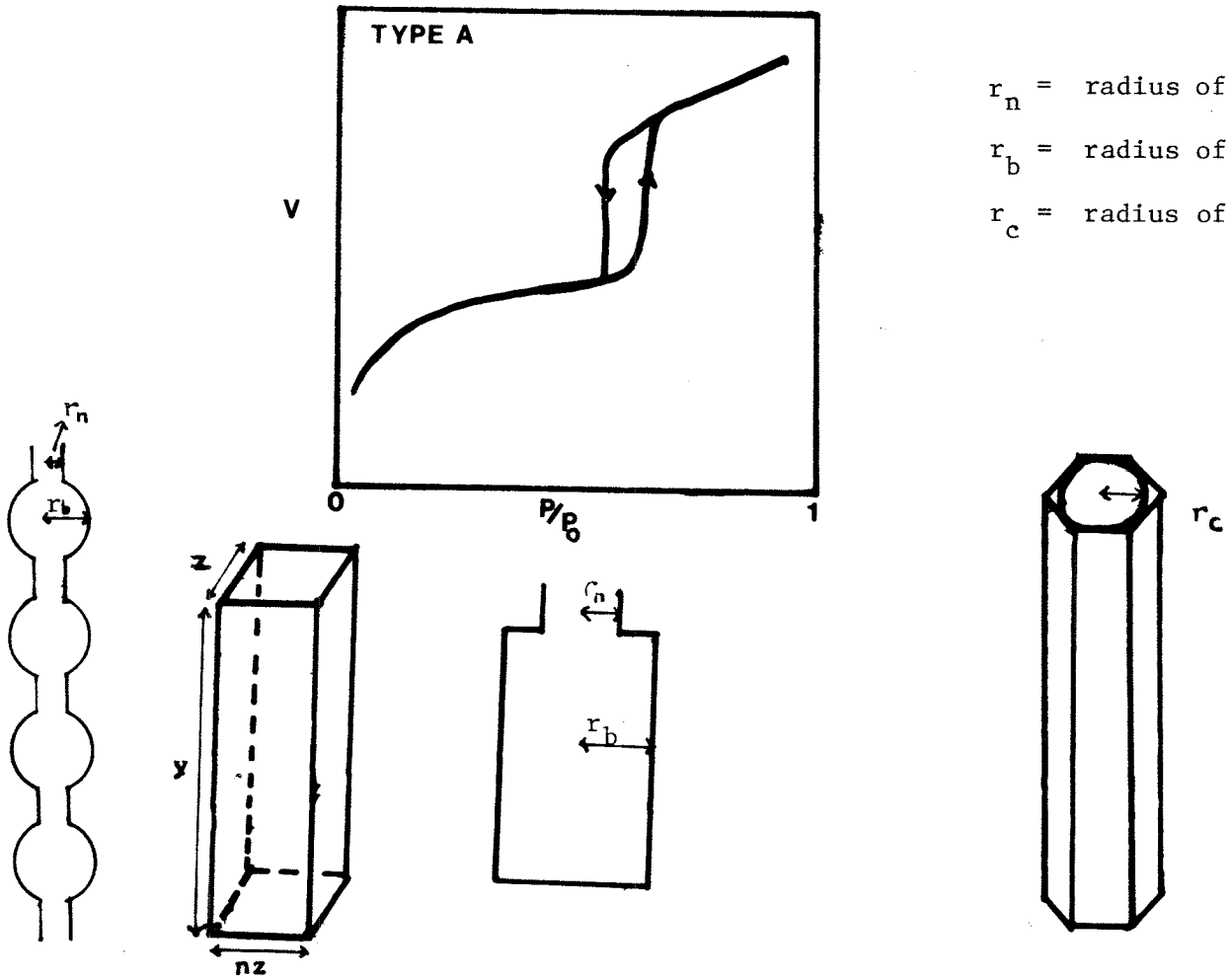

r_n = radius of neck

r_b = radius of body

r_c = radius of capillary

Fig 6.1: Shapes Responsible For Type A Hysteresis(reproduced from reference (76)).

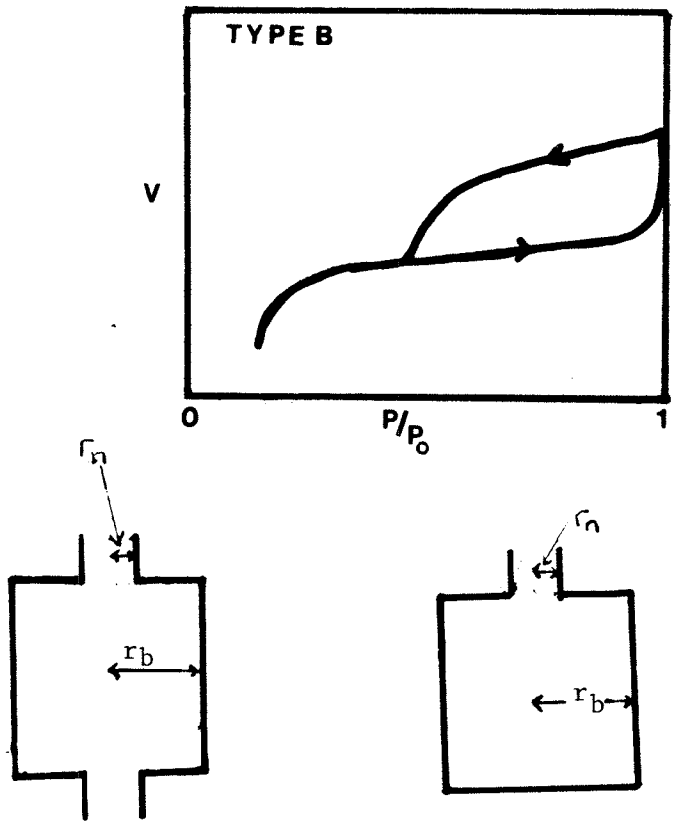

Fig 6.2: Shapes Responsible For Type B Hysteresis.

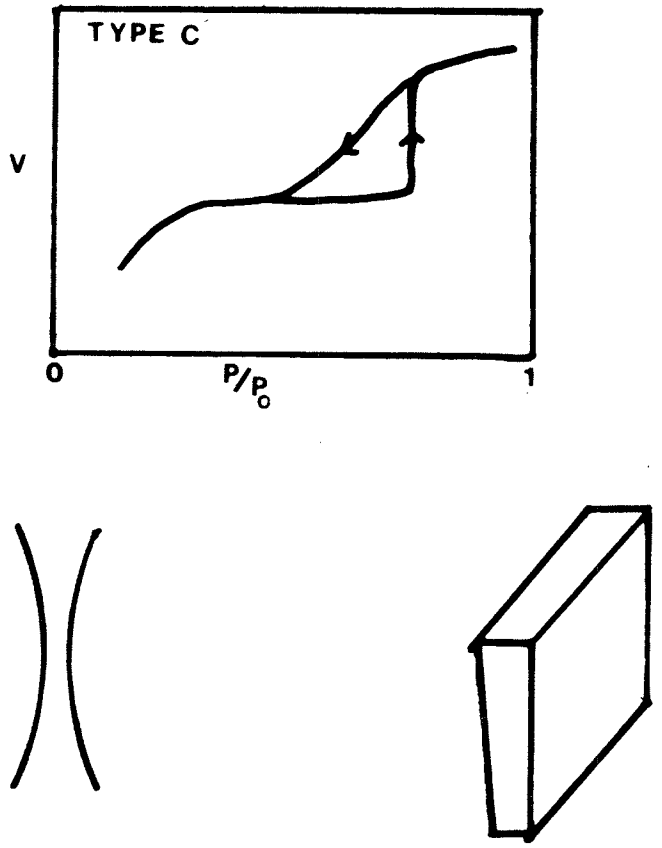

Fig 6.3: Shapes Responsible For Type C Hysteresis.

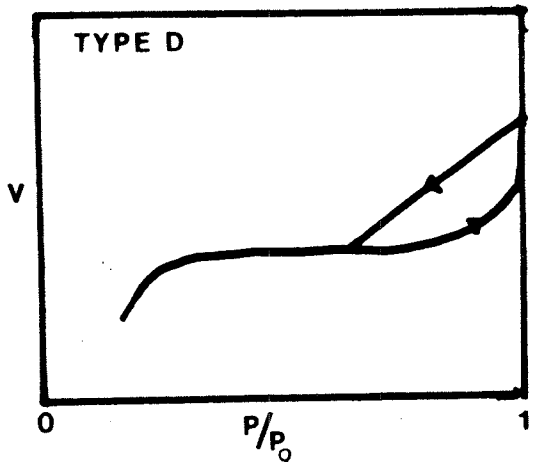

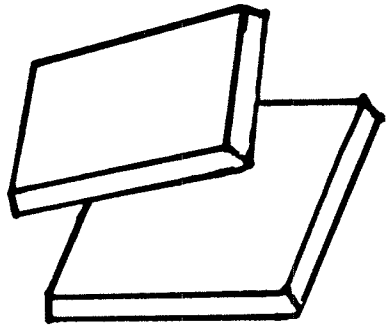

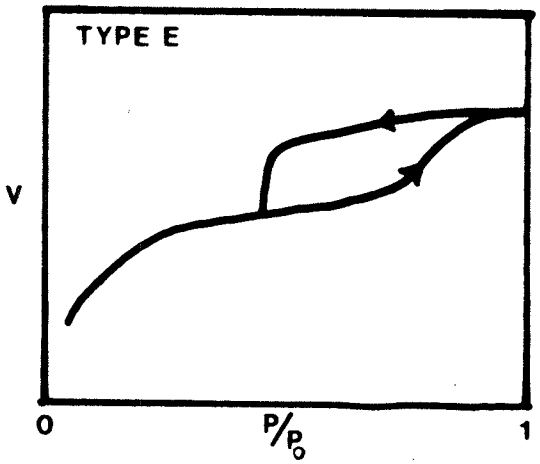

Fig 6.4: Shape responsible for Type D hysteresis.

$$\ln(P/P_o) = \frac{-\gamma \bar{V} \cos\Phi}{r_K RT} \qquad (2.51)$$

but the body will ($r_{body} > r_{neck}$) only be filled at a much higher pressure than the above case. The pressure required to fill the body is given by

$$\ln(P/P_o) = \frac{-2\gamma \bar{V} \cos\Phi}{r_K RT} \qquad (2.52)$$

where

$\bar{V}$ = molar volume of adsorbate

γ = surface tension of liquid adsorbate

r_K = Kelvin radius

Foster [34] viewed the hysteresis effect as a delay in the formation of the meniscus. The adsorption branch is under the influence of the pressure that results in the formation of multi-layer in accordance to the BET equation. However, the desorption pressure which is a result of the evaporation of the spherical meniscus is given by the Kelvin equation (equation (2.52)). Naturally the two pressures differ and hence hysteresis occurs. There are other theories such as the domain concept, phase change, etc. which the reader is referred to in Flood [56] on the Solid-Gas Interface.

2-8 Kelvin Equation

The estimation of pore size is commonly based on the fact that the adsorbate will condense in narrow pores at pressures less than the

saturated vapour pressure of the adsorbate. This phenomenon can be pictured as equivalent ot the work done in enlarging a cavity of radius r to r + dr by removing dn moles of liquid from the wall of cavity and transferring it to the bulk liquid. By transferring the droplet into the interior of the bulk, the change in chemical potential is given by

$$(\mu - \mu_d)dn = G \tag{2.53}$$

where μ and μ_d are the chemical potential of bulk and droplet respectively.

At constant pressure and temperature, surface tension γ is equal to the partial derivative of the Gibbs free energy with respect to surface area ∂A, that is

$$\left(\frac{\partial G}{\partial A}\right)_{T,P} = \gamma \tag{2.54}$$

Thus at constant temperature and pressure,

$$(\mu - \mu_d)dn = \gamma \partial A \tag{2.55}$$

But area (A) of sphere = $4\pi r^2$

Hence

$$\partial A = 8\pi r dr \tag{2.56}$$

Thus

$$(\mu - \mu_d)dn = 8\pi r \partial r \tag{2.57}$$

Let v be the molar volume of adsorbate. By the addition of the tiny droplet, the change in volume of bulk is given by

$$\partial v = v dn \tag{2.58}$$

But the volume of sphere is given by

$$v = 4\pi r^3/3$$

Hence

$$\gamma v = 4\pi r^2 \, dr \tag{2.59}$$

From equations (2.58) and (2.59), dn is given by

$$dn = 4\pi r^2/v \tag{2.60}$$

Comparing equations (2.57) and (2.60), the change in chemical potential $(\mu - \mu_d)$ is given by

$$(\mu - \mu_d) = \frac{2\gamma v}{r} \tag{2.61}$$

For ideal vapours, μ and μ_d can be represented as

$$\mu = \mu_o + RT \ln P_o \tag{2.62}$$

and

$$\mu_d = \mu_o + RT \ln P \tag{2.63}$$

where P is the equilibrium pressure over the curved surface and P_o, the saturated vapour pressure of adsorbate. Comparing equations (2.62) and (2.63), $(\mu - \mu_d)$ is represented by

$$(\mu - \mu_d) = RT \ln (P_o/P) \tag{2.64}$$

Hence

$$RT \ln (P_o/P) = 2\gamma v/ r \tag{2.65}$$

Simplifying equation (2.65) yields

$$\ln (P_o/P) = \frac{2\gamma v}{r \, RT} \tag{2.66}$$

Equation (2.66) is called the Kelvin equation and r is the radius of the pore. If the contact angle Φ between solid and the liquid exists (see diagram below)

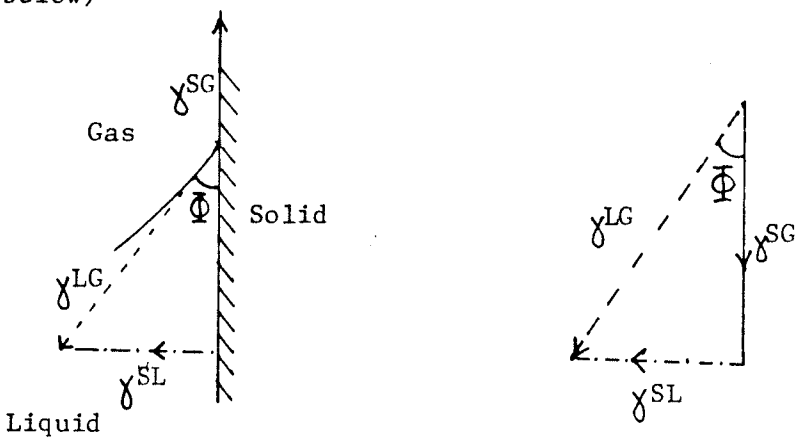

L = liquid G = gas S = solid

Definition of contact angle Φ

then γ will be represented by $\gamma\cos\Phi$ assuming the equilibrium exists in the system. Hence, the Kelvin equation will be altered as

$$\ln (P/P_o) = \frac{-2\gamma v \cos\Phi}{r\,RT} \qquad (2.52)$$

The importance of the desorption branch to the elucidation of pore size cannot be denied. Briefly, as this will be dealt with again later, the pore size can be determined by using the desorption branch of the isotherm and applying the Kelvin equation as used by Lippens et al [35] and others. However, the practical use of the above equation is limited by the assumptions that the contact angle Φ is negligible ($\Phi \approx 0°$), the pores are cylindrical and the assessment of thickness of adsorbed layers. In spite of all the limitations, the equation is still invaluable, for example, in helping us to assess the performance of a

catalyst. From this brief theoretical survey, it is apparent that the characterisation of a support catalyst has been simplified drastically by the application of the simple procedures outlined above. Despite of all the uncertainties and criticisms, the procedures will be utilized in the elucidation of the surface area and pore structure of Porous Titania Glass (PTG) in the subsequent chapter.

Chapter 3

FABRICATION OF MONOLITHIC TRANSPARENT POROUS TITANIA GLASS

3-1 Introduction

Glasses, now widely accepted as an inorganic polymers are produced by solidification of oxides melted at high temperature. This procedure prohibits the precise determination of the molecular weight as there is no control over the degree of polymerisation and occurrence of cross-linking. It has been demonstrated that monolithic oxide glasses can be fabricated at low temperature [57] by the formation of an oxide network, thus allowing glass technologists to exercise significant control over the nature and the extent of polymerisation, an advantage that has benefited organic polymer scientists for a long time. However, the advancement in glass formation is largely attributed to the successful utilisation of metal-organic compounds, particularly metal-alkoxides and their properties plus the low cost of glass forming species themselves such as Si, Al, Ti, etc. which makes it favourable. To date, various monolithic glasses are easily accessible to us with the exception of Porous Titania Glass.

Titania gel was first mentioned by Rose [cited from ref. [19]] in 1823 by the fusion of titanium dioxide and an alkali carbonate and the product treated subsequently by hydrochloric acid. However, no attempt was made to dehydrate it to porous glass. In 1861, Thomas Graham [cited from ref. [58]] successfully produced titania gel by dialysing titanic acid in hydrochloric acid. During the same period, Knop [cited from ref. [58]] obtained a transparent titania gel by neutralizing titanic acid with ammonium hydroxide. In 1925, Klosky and Marzano [58] prepared the titania gel by adding concentrated hydrochloric acid (35%) to sodium titanate solution, a product from the fusion of sodium carbonate and

titanium dioxide. Weiser and co-workers [59] reported that titania gel was formed by partial neutralisation of titanium tetrachloride in concentrated hydrochloric acid below 0°C by ammonium hydroxide and the sol-gel transition will not occur prior to the removal of salts formed. Harris and Whitaker [60] in an effort to eliminate the presence of salts, utilized the hydrolysis of titanium alkoxides which resulted in the production of amorphous powders with large surface areas. Recently Yoldas [57] reported on the formation of monolithic multi-component glasses, for example, silica-titania glass by the polymerisation of a partially slow hydrolysing alkoxide, that is, silicon alkoxide with an unaltered fast hydrolysing alkoxide such as titanium alkoxide. However, the first successful fabrication of monolithic transparent Porous Titania Glass (PTG) was achieved recently by Gesser et al [19] by controlled hydrolysis of titanium tetrachloride and careful dehydration. In this section, a detailed experimental procedure and discussion will be outlined for the preparation of PTG.

3-2 Experimental

The preparation of monolithic transparent PTG consists of six stages:

i) Distillation of doubly distilled water

ii) Low temperature hydrolysis of titanium tetrachloride

iii) Removal of hydrochloric acid by low pressure distillation

iv) Vortexing

v) Dialysis

vi) Dehydrating and annealing

3-2.1 Distillation of doubly distilled water

Potassium permanganate crystals (Fisher certified reagent) and a potassium hydroxide pellet (Fisher certified reagent) were dissolved together in distilled water in a round-bottom flask (Pyrex, 2 litre). A few anti-bumping granules were added to the solution which was then refluxed overnight prior to distillation. This was to ensure the elimination of organic impurities via oxidation. The purity of the distillate was checked spectrometrically using a Beckmann DK-2A double-beam spectrometer and a 10 cm quartz cell.

3-2.2 Low Temperature Hydrolysis

Titanium tetrachloride (25 mL, Fisher certified reagent) was transferred to a dry conical flask using a dry measuring cylinder. The solution was cooled in a liquid nitrogen bath for approximately five minutes with constant swirling. Doubly distilled water was added dropwise to the frozen titanium tetrachloride using a disposable pipette (Eye-dropper, Fisher Scientific). The flask was constantly removed from the liquid nitrogen bath for swirling, thus ensuring that frozen water adhering to the flask would melt. An additional 25 mL of doubly distilled water in 5 mL portions were added to the solution (reactants and products) when the total volume approached 50 mL. The final total volume was 75 mL.

3-2.3 Removal of hydrochloric acid by low pressure distillation

Two 75 mL portions of solution from stage (ii) were mixed in a three-neck round-bottom flask (Pyrex, 500 mL). The mixture was diluted with doubly distilled water to make up a total volume of 200 mL. A magnetic stirrer was placed in the round-bottom flask which was subsequently connected to the low pressure room temperature distillation unit as shown in Fig. 7. The receiving flask was cooled in a liquid nitrogen bath. The mixture was stirred vigorously and distillation commenced by opening stop-cock T1 slowly. The round-bottom flask was carefully immersed in a water bath which was heated electrically ("thermix" heater, Fisher Scientific) to about 60°-70°C. The coolant was constantly replenished and the distillation terminated after the viscous solution became a solid mass (approximately 1 hour). The solid mass was redissolved with doubly distilled water (100 mL) and the solidified hydrochloric acid (white solid) discarded by dissolving it in water. The distillation was repeated as outlined above and finally terminated after a clear viscous solution was obtained (about 45 minutes). The viscous solution was transferred to a clean conical flask (Pyrex, 250 mL) and diluted to 200 mL with doubly distilled water. It was stoppered and stored in a refrigerator. This solution was referred as "50/200" P HCl.

3-2.4 Vortexing

A known volume (usually 20 mL) of "50/200" P HCl was transferred to a clean conical flask and diluted to 100 mL with doubly distilled water.

Fig 7: Low pressure distillation unit.

H = "Thermix" heating mantle.

J = Mercury thermometer.

MS = Magnetic stirrer.

LNB = Liquid nitrogen bath.

R = $TiCl_{4-n}(OH)_n$ solution.

S = Solidified hydrochloric acid.

Tl = Stopcock.

VLNT = To vacuum line with liquid nitrogen trap.

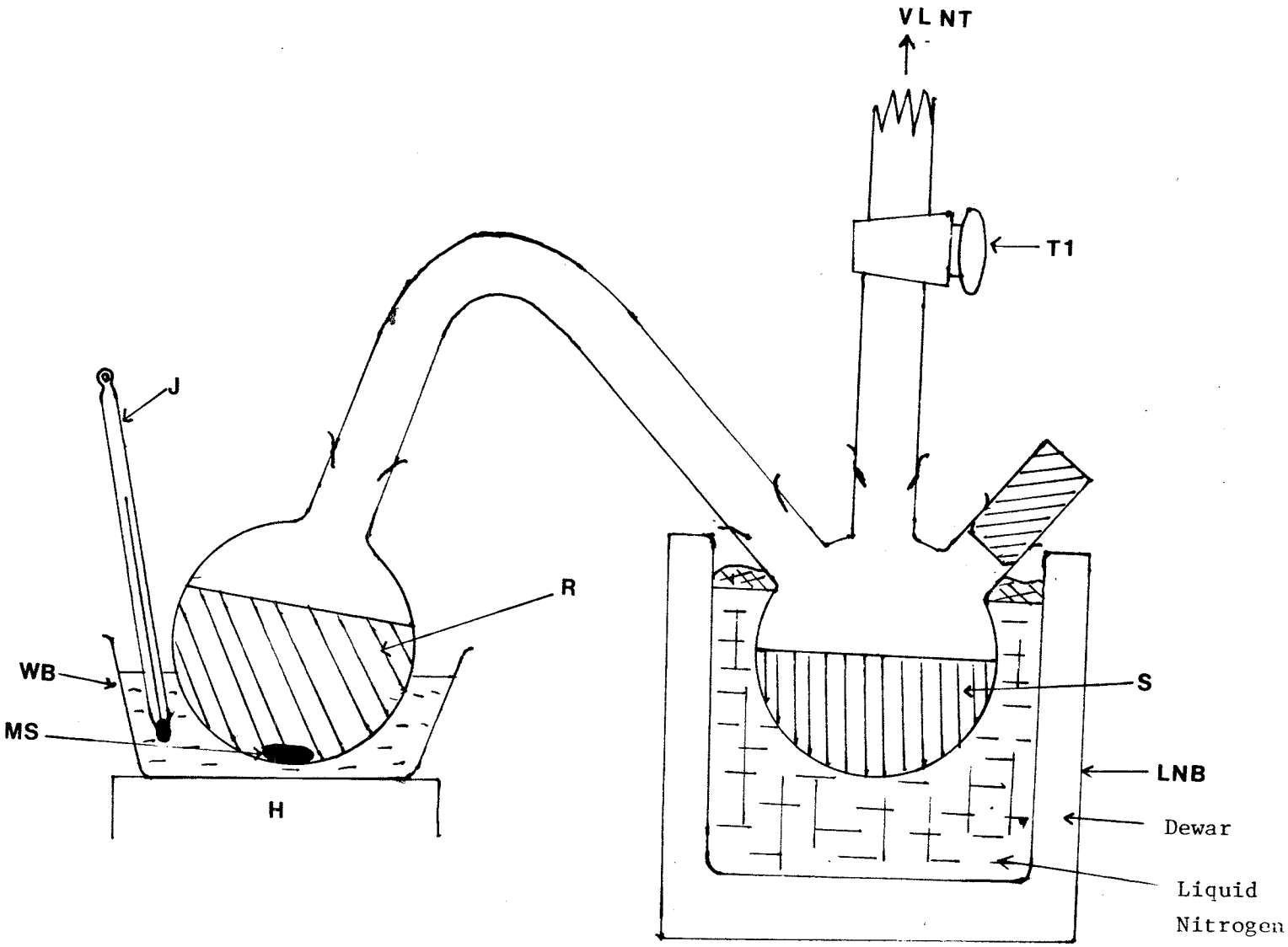

Fig 7.Low Pressure Distillation Unit.

It was stoppered and cooled in a refrigerator. A stock solution of potassium hydroxide (2g, 20 mL) was prepared and cooled. The cooled and diluted "50/200" P HCl solution was stirred vigorously until a vortex was created. Into the vortex, potassium hydroxide solution was added dropwise using a disposable pipette (see Fig. 8). Vortexing was continued at room temperature until cloudiness partially or completely disappeared (approximately five hours). The vortexed solution was stoppered and left to stand overnight in a refrigerator.

3-2.5 Dialysis

Dialysis tubing (Fisher, 3.1 cm width, cat. number 08-667C) of length 45 cm was soaked in distilled water for 10-15 minutes. One end of the soft tubing was tied with cotton thread and the cold vortexed solution was transferred into it. The remaining end was then tied as illustrated in Fig. 9. The filled tubing was dialysed with distilled water and continuously stirring the distilled water with a magnetic stirrer. The tubing was occassionally inverted to ensure an even mixing of the content and the distilled water changed constantly. The dialysis was terminated when the viscosity of the solution reached the point that the velocity of the smallest bubble was approximately 0.5-0.2 mms^{-1} (about 3 hours). The content was then transferred to four greased (Vaseline, Cheesebrough Ponds (Canada) Ltd.) petri dishes (10 cm x 2 cm high) by cutting one end of the tubing. Air bubbles were removed with a clean disposable pipette and the filled petri dishes were left to set.

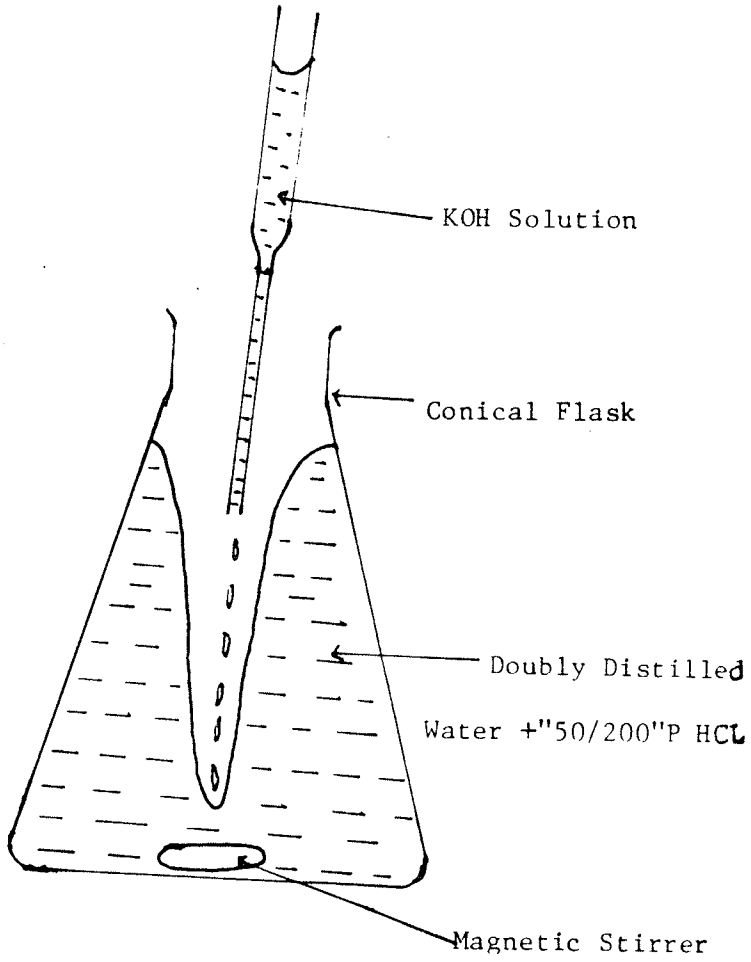

Fig 8: Vortexing.

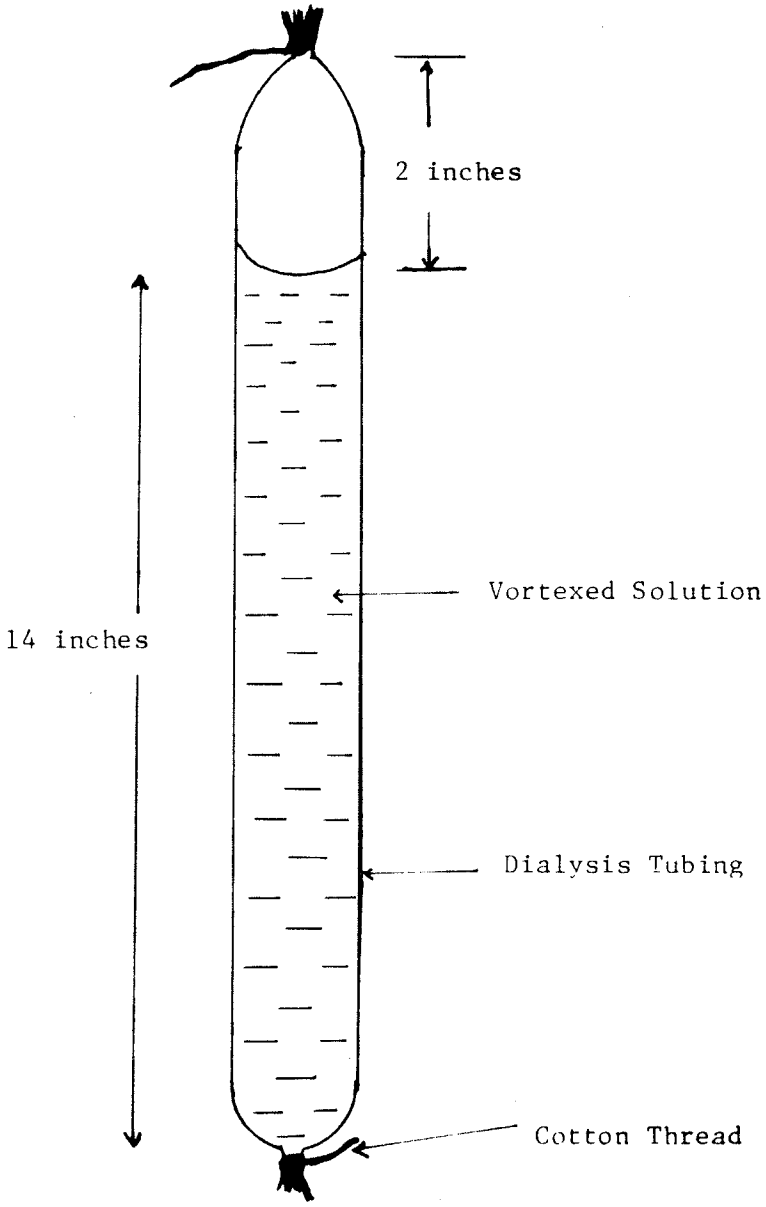

Fig 9: Dialysis

3-2.6 Dehydration and annealing

The petri dishes were placed in a dust-free constant temperature (20°C) and humidity controlled (79% humidity, achieved by bubbling air into saturated ammonium chloride solution [61]) chamber. The gels were left to dehydrate and shrink (this process took about 10-14 days). The air-dried glass was carefully removed by sliding a flexible wire underneath the glass, thus breaking the surface tension. It was then gently lifted off using the flexible wire and the adhered grease removed with Kleenex tissue [Scotch (Canada) Ltd.]. The glass was left to air-dry for 2-3 days. At this stage, the glass, when wetted with water, would fracture into many pieces.

The thin fragile wafers (2 cm diameter, 0.1 cm thick) were annealed slowly at 5°C/six hours initially (1 day). The rate of annealing was then increased to 10°C/six hours. When the annealing temperature approached 200°C, the temperature was maintained for twenty-four hours and subsequently cooled to room temperature in the oven [The first stage of annealing was done by INRAD, Winnipeg. Total time taken for the whole annealing process was four days]. The sample was re-heated at 20°C/five hours. When the annealing temperature reached 300°C, the temperature was maintained for 3-10 hours (depending on the porosity desired) and subsequently cooled to room temperature.

The dark brown wafers were reannealed to 300° at 30°C/hour. This annealing temperature was maintained [this stage was done at the Chemistry Department, University of Manitoba, Winnipeg, and the total duration of annealing was 14 hours] and subsequently cooled to room temperature (12 hours). Residual potassium chloride that adhered to the

surface of the glass was removed by soaking in doubly distilled water (24 hours). The wafers were then air-dried (2-3 days) and were designated PTG300R, indicating that they were annealed at 300°C and rinsed in doubly distilled water.

3-3 Results

Titanium tetrachloride ($TiCl_4$) is a hygroscopic, volatile fuming liquid (melting point = -23°C, boiling point = 136°C [61]). It is easily hydrolysed, forming a series of stable oxychlorides: $TiCl_3(OH)$, $TiCl_2(OH)_2$, $TiCl(OH)_3$ and with excess water titanium hydoxide ($Ti(OH)_4$) results. This non-violent hydrolysis can be represented as

$$TiCl_4 + nH_2O \longrightarrow TiCl_{4-n}(OH)_n + nHCl \qquad (3a)$$

where n = 1,2,3 or 4.

This hydrolysis is highly exothermic and hydrochloric acid (HCl) is produced simultaneously as white fumes, the majority of HCl remaining in the conical flask as frozen aqueous HCl. When 15 mL of doubly distilled water was added to the system, a yellow solid which did not melt at room temperature resulted. Further addition of doubly distilled water redissolved the solid, transforming it into a yellowish solution which eventually went colourless when the total volume reached 70 mL.

HCl was removed according to the procedures outlined by Kruczynski [62]. Further elimination of HCl or chloride from the oxychloride

species was achieved by the addition of potassium hydroxide (KOH) solution via the vortexing process.

$$TiCl_3(OH) + KOH \longrightarrow TiCl_2(OH)_2 + KCl \qquad (3b)$$

$$TiCl_2(OH)_2 + KOH \longrightarrow TiCl(OH)_3 + KCl \qquad (3c)$$

$$TiCl(OH)_3 + KOH \longrightarrow Ti(OH)_4 + KCl \qquad (3d)$$

The appearance of a white precipitate during the addition of KOH solution to the vortexed solution was attributed to the formation of hydrated titanium dioxide (TiO_2). It redissolved by prolong vortexing at room temperature, the disappearance was observed to be dependant on the size of the particles formed in the vortex addition.

$$Ti(OH)_{4(l)} \longrightarrow TiO_{2(s)} + H_2O \qquad (3e)$$

The presence of KOH in the solution containing TiO_2 may cause the formation of soluble hydrated "titanates" having formulae such as $M_2^{I}TiO_3n.H_2O$ and $M_2^{I}Ti_2O_5.n.H_2O$ but of unknown structure. This possibility, however, cannot be neglected. The idea of using lithium hydroxide or sodium hydroxide as the neutralizing reagents had been discarded due to the production of soft and easily scratched glass and the extrusion of sodium chloride and the ease of cracking [21]. Gesser et al. [64] found that the most stable glass was formed using KOH as the neutralizing reagent. Exposure of the vortexed solution to ambient temperature for more than twelve hours resulted in the precipitation of amorphous TiO_2, a white pigment whose solubility depends largely on its chemical and thermal history.

Condensation reactions occurred on dialysing which led to the production of titania jelly. Monolithic transparent PTG were produced after careful dehydration. These glasses shattered violently on contact with water. Upon annealing at 300°C, the shattering characteristic disappeared but still retaining the slight yellowish transparent colour. A 2% loss of weight by annealing PTG300R to 360°C was observed and this was attributed to the loss of surface hydroxyl group and residual molecular water molecules. Subjecting the glass to higher annealing temperature turned the glass completely hard and opaque.

3-4 Discussion

As mentioned earlier, copious amounts of HCl were produced during the course of this reaction. Long and Davies [63] obtained a yellow solid when the colourless $TiCl_4$ was added to concentrated HCl and which subsequently redissolved to give a yellow solution. From the Raman studies, the authors suggested that the yellowish solid could be titanium oxide chloride $TiOCl_2$.

$$TiCl_4 + H_2O \longrightarrow TiOCl_2 + 2HCl$$

In the same piece of work, they confirmed that the yellowish solution could be oxychloride species of type $[TiO_2Cl_4]^{-4}$ or $[TiOCl_5]^{3-}$.

$$TiCl_4 + nH_2O \longrightarrow TiCl_{4-n}(OH)_n + nH_2O \qquad (3f)$$

$$TiCl_3(OH) + 2HCl \longrightarrow H_3TiOCl_5 \qquad (3g)$$

$$TiCl_2(OH)_2 + 2HCl \longrightarrow H_4TiO_2Cl_4 \qquad (3h)$$

In view of the fact that HCl in the hydrolysis process was not removed prior to distillation, the possibility of the presence of $TiOCl_2$ and $[TiOCl_5]^{-3}$ or $[TiO_2Cl_4]^{4-}$ as the yellow solid and yellow solution respectively cannot be denied. The existence of titanium hexachloride species ($TiCl_6^{2-}$) in the solution can be neglected since it was proven by Long and Davies [63] to be the wrong species. Apparently increasing concentration of water molecules in the system favours the existence of species $TiCl_3(OH)$, $TiCl_2(OH)_2$, $TiCl(OH)_3$ or perhaps $Ti(OH)_4$, a pathway favoured by some glass producing species such as boron alkoxides. The relative concentration of each of these transient species will depend on the availibility of water and the dilution of the system. Completion of the hydrolysis which results in the formation of $Ti(OH)_4$ or TiO_2 couple by the cooling effect inhibits polymerisation. By dialysing the solution, the "active" species such as $Ti(OH)_4$ immediately undergo a number of condensation reactions, forming a series of secondary species where bridging occurs.

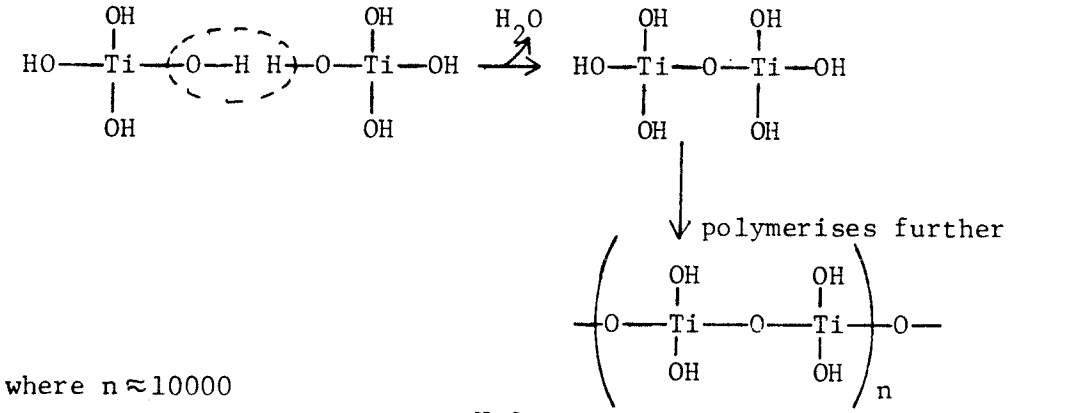

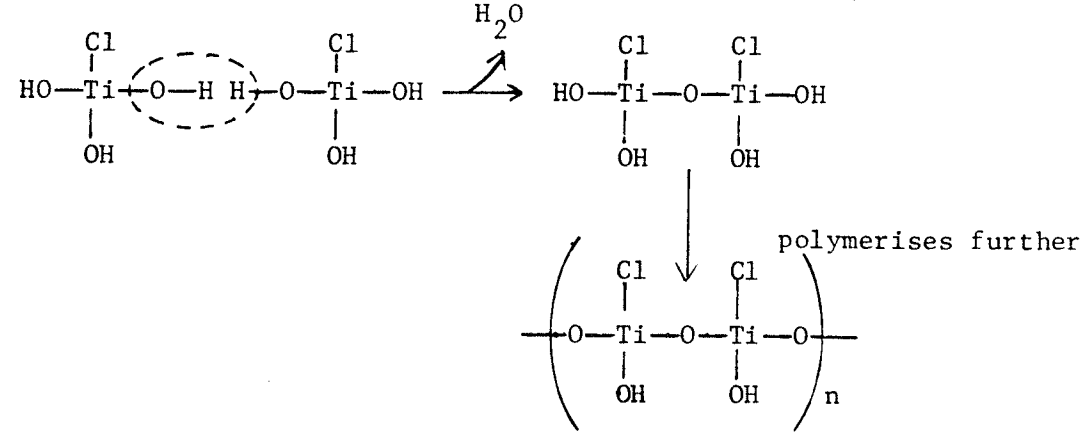

In a homogenous system containing numerous "active" species, the condensation process will only terminate when the "active" species are completely eliminated. In spite of the long chain, the product remains in solution, presumably due to the residual hydroxyls on the polymer.

The presence of K^+ ions in the solution had a pronounced effect on the rate of polymerisation. The OH group is a very polarised group, which favours electrostatic interaction with K^+ ions. Some form of "shield" is apparently formed, thus inhibiting the activity of the "active" species. In other words, no noticeable condensation occurs. This inhibiting effect can easily be eliminated by dialysis as mentioned above.

How does the gel manage to retain its structural integrity during the dehydation and annealing? How could it remain monolithic? Yoldas [57] suggested that it may be due to a requirement for an average interparticle distance which must not exceed a certain limit imposed by the gel. Other gels like silanols retain their integrity by cross-linking and maintaining some hydroxyl and alkyl groups such that the alkyl group is positioned at the terminal of the structural chains rather than in the bridging position. However, there is still no clear evidence as to how glasses are able to maintain their integrity and certainly it will be of great interest to investigate this. Also, the amount of residual K^+ or Cl^- in the annealed gel has not been determined.

CHAPTER 4

SURFACE AREA AND PORE STRUCTURE OF POROUS TITANIA GLASS

4-1 INTRODUCTION

The indispensable BET equation

$$\frac{P}{V_{tot}(P_o - P)} = \frac{1}{V_m C} + \frac{(C-1)P}{V_m C P_o} \qquad (2.42)$$

where P, P_o = equilibrium pressure and saturated vapour pressure of adsorbate molecule respectively,

V_m = volume of adsorbate required to form a monolayer

V_{tot} = volume of adsorbate

and C = BET constant,

is undoubtedly the best known equation today for the determination of the surface area of a sample. Since the derivation of the theory by Brunauer et al. [33] in 1937, the amount of information obtained is enormous. Together with the Kelvin equation

$$\ln(P/P_o) = -2\gamma\bar{V}\cos\Phi / r_k RT \qquad (2.52)$$

(parameters $\gamma, \bar{V}, \Phi, r_k$, R and T as defined on page 38), the characterisation of the sample becomes more meaningful, particularly in assessing the potential of the sample as a catalyst. Earlier, Harris and Whitaker [60] used the above equations to study the surface properties of titania derived from the steam hydrolysis of several titanium tetra-alkoxides. Similarly, El-Akkad [20] characterized anatase titania gel using the approach mentioned earlier. The author reported a decrease in surface area of titania gel with respect to increasing annealing temperature.

An identical trend was observed by Gesser and Speers [64] in Porous Titania Glass (PTG). However, the authors concluded their work without investigating the pore structures since surface areas were determined only by the gas chromatographic method. In this chapter, a detailed picture will be presented for the determination of the effect of the annealing temperature, length of annealing time at constant annealing temperature and the degassing temperature on the surface area and pore structure of PTG using the standard volumetric method at 77K, dry nitrogen being the adsorbate.

4-2. The sample tube

Fig. 10 illustrates the design of the quartz sample tube used in the determination of the surface areas and pore studies of PTG. The upper half (V_{YR-T}) is made of pyrex while the lower half (sample tube, V_{77K}) is made of quartz. A removable capillary tube is always placed in the pyrex region (V_{YR-T}) to decrease the effective volume error to a minimum when the temperature of the surrounding fluctuates due to changing level of the liquid nitrogen.

4-3. Experimental

The complete apparatus is illustrated in Fig. 11 and it consists of the following: a quartz sample tube, two mercury manometers (M1 and M2), gas reservoirs, a mercury reservoir and a high vacuum unit consisting of a mercury diffusion pump, a rotary pump, liquid nitrogen traps and a vacuum gauge. Prior to any experiments, the following portions of the apparatus (Fig. 10) had to be calibrated: i) V_A, ii) V_B, iii) V_C, and iv) V_{eff}, that is V_C immersed in a liquid nitrogen bath.

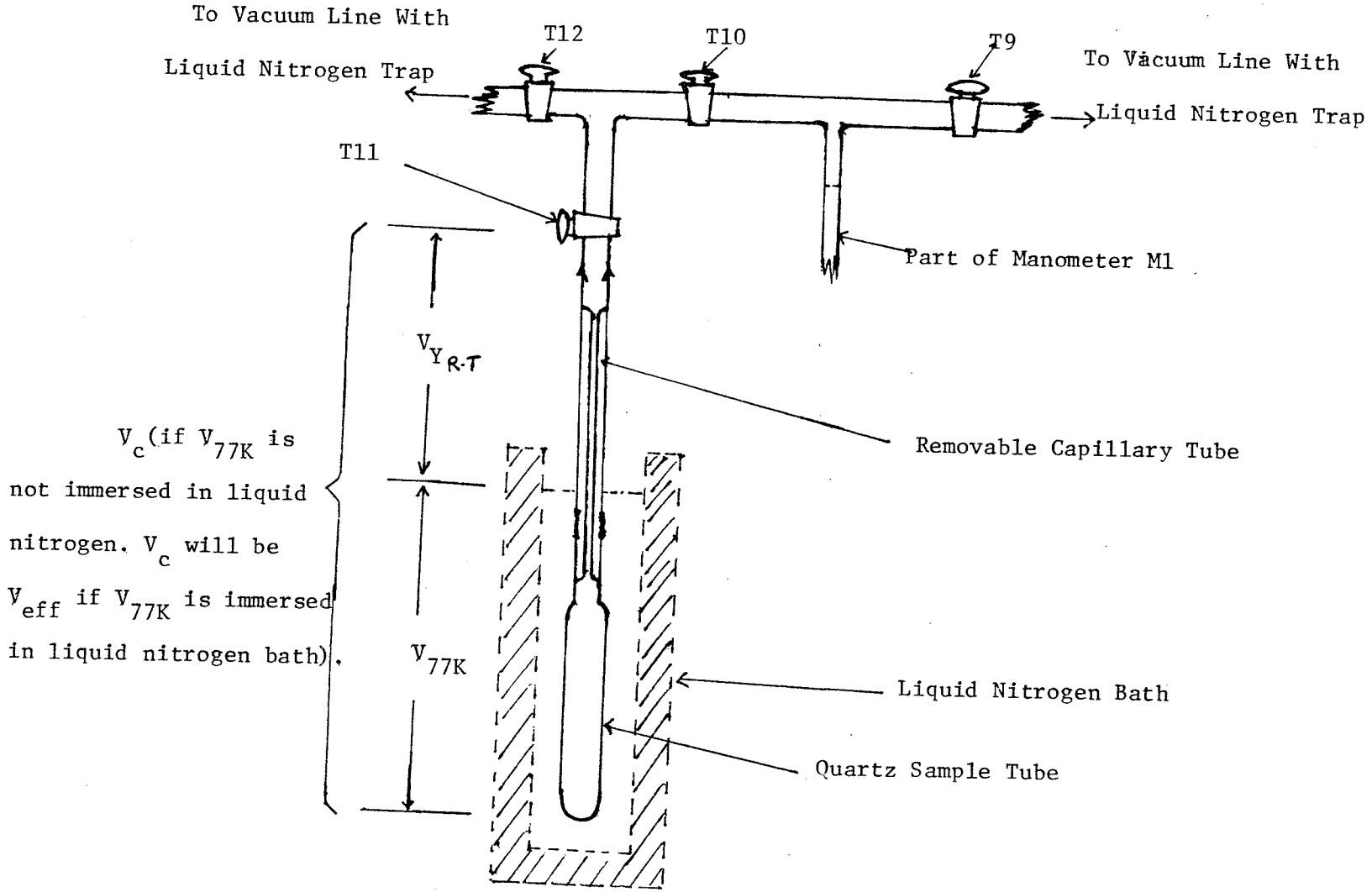

Fig 10: Detail of the BET cell.

Fig 11: A schematic diagram of the BET vacuum system.

A = To atmosphere.

CT = Removable capillary tube.

DP = Mercury diffusion pump

LNTPG = Liquid nitrogen trap with "thirsty glass".

LNT = Liquid nitrogen trap.

M = Manometer.

PG = Pressure gauge.

QST = Quartz sample tube.

R = Reservoir.

R_H = Helium reservoir.

R_{H_2} = Hydrogen reservoir.

R_O = Oxygen reservoir.

R_N = Nitrogen reservoir.

RP = Rotary pump

T = Stopcock.

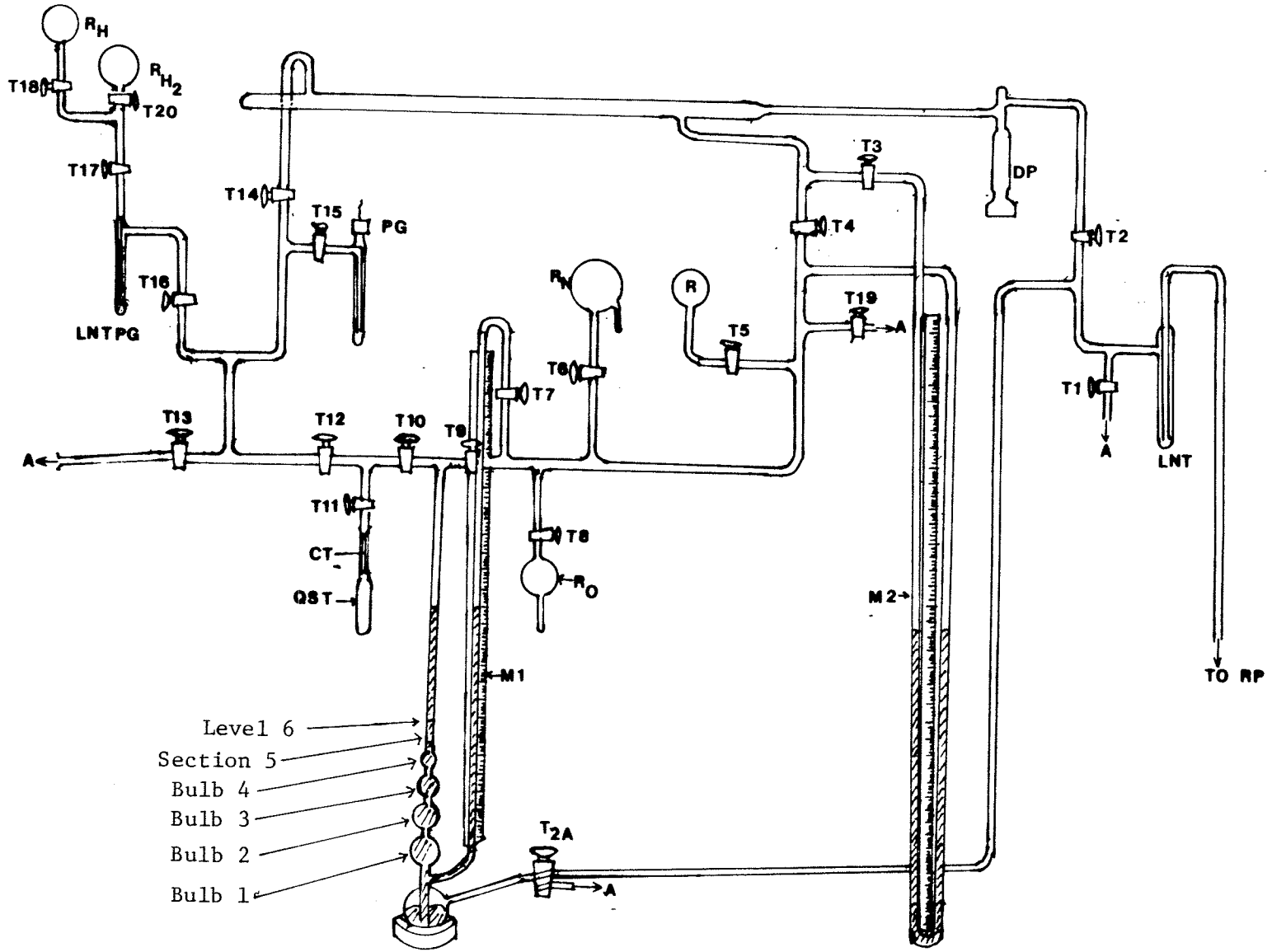
R_H
R_{H_2}
T18
T20
T17
T14
T15
PG
T16
LNTPG
T3
DP
T4
T2
R_N
R
T19
A
T5
T6
T7
T1
A
LNT
T13
T12
T10
T9
A
T11
CT
QST
T8
R_O
M2
M1
TO RP
Level 6
Section 5
Bulb 4
Bulb 3
Bulb 2
Bulb 1
T_{2A}
A

[Bulb 1(57.196 mL), bulb 2(33.312 mL), bulb 3(15.485 mL), bulb 4(5.650 mL), section 5(1.291 mL) radius of capillary = 0.1007 cm and section 6(1.291 mL) was calibrated by Dr. A. Lemire].

It is vital that the system be vacuum tight prior to any experiment or calibration. This was achieved by regreasing all the stopcocks with high vacuum grease (Apiezon N). All the stopcocks were then closed and the system evacuated slowly by opening the stopcocks slowly. The diffusion pump was then switched on. Pinholes or faulty stopcocks were checked by closing all stopcocks. Corrective measures were taken if pinholes or faulty stopcocks were found.

4-4 Calibration

When a sufficient vacuum was achieved, that is $P_{system} < 10^{-4}$ torr, all the stopcocks were closed and the mercury level in manometer M1 was lowered to the last etched line (level six in Fig. 11) by evacuating air through stopcock T2A. The mercury level in manometer M1 was noted. The mercury level was then slowly raised (5 cm) by leaking air through stopcock T2A and the new mercury level in manometer M1 was again noted. The procedure was repeated until a series of heights and their corresponding "pressures" in vacuum was obtained. Next air was admitted into the system by opening stopcock T19 (see Fig. 11) until a desired pressure was obtained and then shut. An appropriate amount of air (200 torr) was allowed to leak into V_A (Fig. 11) via T9 slowly. By raising the mercury level as outlined above, a series of mercury heights and their corresponding "pressures" was obtained. Upon completion, the amount of air was expanded into sections V_B and subsequently V_C, repeating the procedures mentioned above for V_B and V_C each time.

4-4 Calculation

Let P_1 and P_2 be the pressures exerted by air at mercury heights h_1 and h_2 respectively.

Let V_1 and V_2 be the corresponding volume occupied by air at pressures P_1 and P_2 respectively.

At constant temperature,

$$P_1V_1 = P_2V_2 \quad \text{(Boyle's Law)} \tag{4.01}$$

But $$V_1 = \pi r^2 h_1 + V_A^1 \tag{4.02}$$

and $$V_2 = \pi r^2 h_2 + V_A^1 \tag{4.03}$$

where r = radius of capillary

V_A^1 = volume of section V_A

Substitute equations (4.02) and (4.03) into (4.01)

$$P_1(\pi r^2 h_1 + V_A^1) = P_2(\pi r^2 h_2 + V_A^1)$$

Rearranging and simplifying,

$$V_A^1 = \frac{\pi r^2 (P_1h_1 - P_2h_2)}{P_2 - P_1} \tag{4.04}$$

By similar argument and application of Boyle's Law, the volume of $V_B(V_B')$ and $V_C(V_C')$ are given by:

$$V_B^1 = \frac{P_B(\pi r^2 h_B + V_A^1) - P_B^1(\pi r^2 h_B^1 + V_A^1)}{P_B^1 - P_B} \qquad (4.05)$$

and

$$V_C^1 = \frac{P_C(\pi r^2 h_C + V_A^1 + V_B^1) - P_C^1(\pi r^2 h_C^1 + V_A^1 + V_B^1)}{P_C^1 - P_C} \qquad (4.06)$$

where P_B and P_B' = pressures exerted by air (200 torr) at Hg heights h_B and h_B' respectively and P_C and P_C' = pressures exerted by air (200 torr) at heights h_C and h_C' respectively.

4-5 Determination of effective volume V_{eff}

Since part of the sample tube V_C (see Fig. 10) was immersed in a liquid nitrogen bath during the experimental work on surface area determination, the effective volume at 77K must be known with a PTG sample in the sample tube. Helium (Linde, purity = 99.995%) was selected because it does not adsorb appreciably at 77K. It was purified and dried by selective adsorption on "thirsty glass" at 77K whereby the main impurity, air, was removed. An appropriate amount of purified helium was introduced into V_A and V_B via stopcocks T18, T17, T16, T12 and T10, with stopcocks T14, T13 and T11 remaining shut. The pressure exerted by helium and its corresponding mercury height in manometer M1 was noted. By opening stopcock T11, helium was expanded into the sample tube which was partially immersed in liquid nitrogen bath. The pressure and height of mercury level was noted when equilibrium was attained (5 minutes). Stopcock T11 was then closed and more helium was introduced into V_A and V_B. The procedure was repeated until a series of pressures and their corresponding mercury heights was obtained.

4-5.1 Calculation

$$\text{Let } V_{eff} = V_{Y(R.T)} + V_{Z(77K)} \tag{4.07}$$

where

$V_{Y(R.T)}$ and $V_{Z(77K)}$ are the volume occupied by helium at section V_Y and V_Z at room temperature and at 77K respectively.

$$\text{Let } V_1 = V_A' + V_B' + V_X \tag{4.08}$$

where $V_X = \pi r^2 h$

Similarly,

$$V_2 = V_A' + V_B' + V_X' + V_{eff} \tag{4.09}$$

where $V_X' = \pi r^2 h'$

Let P_1 and P_2 be the pressures exerted by helium before and after expanding into the sample tube, h and h' being the heights of the mercury level in manometer M1 respectively.

Applying the relationship $P_1V_1 = P_2V_2$

$$P_1V_1 = P_2(V_A' + V_B' + V_X' + V_X') \tag{4.10}$$

But

$$\frac{V_{eff}}{T_{R.T}} = \frac{V_Y}{T_{R.T}} + \frac{V_Z}{77K}$$

that is

$$V_{eff} = V_Y + \frac{V_Z \times T_{R.T}}{77K} \tag{4.11}$$

In other words, V_{eff} will remain constant and valid if the height of liquid nitrogen level in nitrogen bath is kept constant. The results are illustrated in Table 1.

4-6. Measurement of Isotherm

An appropriate amount (0.03g - 0.18g) of PTG sample was weighed and transferred to the quartz sample tube which was then connected to the vacuum system (Fig. 11). Evacuation and degassing (18 hours) then commenced. When the appropriate pressure was achieved (usually 1.8×10^{-5} torr), all the stopcocks were shut except T10. Nitrogen (Linde, purity = 99.95%) which was dried and purified by selective adsorption on "thirsty glass" was allowed to leak into the system via stopcock T9 which was then closed. The mercury level in manometer M1 was adjusted and it's height h_1 and corresponding "pressure" P_1 were noted. With the sample tube immersed in liquid nitrogen bath, nitrogen was expanded into the evacuated sample tube by opening stopcock T11. The entire system was allowed to equilibrate. When equilibrium was achieved, that is with no further decrease of pressure being observed, the mercury level in manometer M1 (h_2) and its corresponding "pressure" P_2 were noted. Stopcock T11 was then closed and dried nitrogen was again allowed to leak into the system via stopcock T9. The above procedure was repeated with constant replenishing the liquid nitrogen bath to ensure that the liquid nitrogen level in the dewar was kept constant throughout the entire adsorption experiment. Upon completing the adsorption experiment, the entire system was evacuated except the content in the sample tube. Stopcocks T12 and T9 were then shut and the content in the

Table 1: The effective volume (V_{eff}) of the sample cell at 77K.*

H	P	P_o	ΔP	H_1	P_1	P_o	ΔP_1	V_{eff}
cm Hg	torr	torr	torr	cm Hg	torr	torr	torr	cm^3
5.00	554.5	310.3	244.2	24.11	552.8	499.6	53.2	10.307
0.60	580.1	267.8	312.3	20.48	577.9	463.1	114.8	10.290
5.00	613.5	310.3	303.2	19.30	610.2	450.0	160.2	10.498
0.60	540.8	267.8	273.0	21.77	538.3	473.8	61.5	10.439
0.60	663.8	267.8	396.0	25.96	660.1	518.2	141.9	10.410
0.60	692.7	267.8	424.9	21.60	689.5	472.7	216.8	10.201

* = H and H_1 are heights of the mercury level in manometer M1 before and after expanding DRY helium into the sample cell (containing PTG) respectively. P and P_1 are the corresponding pressures of helium before and after expansion into the sample cell respectively. P_o is the corresponding pressure in vacuum.

$\Delta P = P - P_o$

$\Delta P_1 = P_1 - P_o$

V_{eff} is calculated according to equation (4.10), page 64.

$V_A' = 0.759\ cm^3$. $V_B' = 0.798\ cm^3$.

sample tube was expanded into the vacuum system ($V_A + V_B + V_6 + (V_5 + V_4)$) by opening stopcock T11 which was shut when equilibrium was achieved. The pressure and volume occupied by the "desorbed" nitrogen were noted and the system again evacuated. The above procedure was repeated until no appreciable "desorption" was observed.

4-6.1 Calculation

i) Adsorption

$$\text{Let } V_1 = V_A + V_B + V_X$$

where

$$V_X = V_6 + V_5 + (V_4 + V_3)$$

$$\text{Let } V_2 = V_A = V_B + V_{eff} + V_h'$$

where $V_h' = \pi r^2 h_2 + (V_6)$

Let P_1 and P_2 = pressures exerted by nitrogen before and after expanding into sample tube respectively.

Let n = moles of nitrogen adsorbed.

Hence

$$P_1V_1 = P_2V_2 + nRT$$

Solving and simplifying,

$$n = \frac{P_1V_1 - P_2V_2}{RT} \qquad (4.12)$$

By similar argument as above, the successive adsorption will be given by

$$n = \frac{P_i'V_i' + P_{(i-1)}'V_{(i-1)}' - P_{(i+1)}'V_{(i+1)}'}{RT} \qquad (4.13)$$

where P_i' and $P_{(i+1)}$ are pressures exerted by nitrogen before and after

expansion in sample tube respectively, and V_i', $V_{(i+1)}$ are the corresponding volume occupied by nitrogen before and after expansion into sample tube. The additional term $P'_{(i-1)}V'_{(i-1)}$ accounts for the amount of free nitrogen that remains in the sample tube after each adsorption. A computer programme written in BASIC language was used to perform all the calculations (see appendix 1).

ii) Desorption

Let P be the pressure before expanding nitrogen into the vacuum system and V_{eff}, the volume occupied by the free nitrogen gas.

Let P_1 be the pressure after expanding nitrogen into the vacuum line and V_1 the volume occupied by free nitrogen gas. Let n' be the moles of nitrogen "evaporated" from PTG sample.

Hence

$$PV_{eff} = P_1V_1 + n'RT \tag{4.14}$$

where

$$V_1 = (V_A + V_B + V_6 + (V_5 + V_4))$$

Solving and simplifying equation (4.14)

$$n' = \frac{PV_{eff} - P_1V_1}{RT} \tag{4.15}$$

By similar argument, a general equation is thus given by

$$n(I) = \frac{P(I)V_{eff} - P(I+1)V}{RT} \tag{4.16}$$

where I = integer

V = volume occupied by free nitrogen molecule

A computer programme written in BASIC language was once again made to calculate n(I) (see Appendix 2).

4-7 Determination of pore size and pore size distribution

As mentioned earlier, the evaluation of pore size and pore size distribution of PTG samples is based on the Kelvin equation (2.52). For simplicity, the contact angle Φ is assumed to be negligible, that is $\Phi \approx 0°$, hence reducing equation (2.52) to

$$\ln (P/P_o) = \frac{-2\gamma \bar{V}}{r_K RT} \tag{2.66}$$

The values adopted for γ, V and T are identical to Lippens et al. [35], that is

γ = surface tension of liquid nitrogen being 8.27×10^{-3} Nm^{-2}

$\bar{V} = 34.68 \times 10^{-6}$ m^3 $mole^{-1}$

and T = 77K, the boiling point of liquid nitrogen

Substituting the above values into equation (2.51) yields

$$\ln (P/P_o) = \frac{-4.05}{r_K} \tag{4.17}$$

where r_K = Kelvin radius

The volume of nitrogen desorbed (V_{des}) is given by

$$V_{des} = n \times 34.68 \times 10^{-6} \ m^3 \tag{4.18}$$

where n is obtained from equations (4.15) and (4.16). From the plots of volume of nitrogen desorbed (V_{des}) against Kelvin radius (r_K), the pore size distribution curve can then be obtained by plotting the slope of the curve (V_{des} against r_K) [dV_{des}/dr_K] against Kelvin radius at suitable intervals of Kelvin radius (r_K). This procedure was adopted by Foster [34] in his pioneering work in this field.

4-8 Determination of surface area

Surface area of PTG samples were determined using the BET "two-parameter" equation

$$\frac{P}{V_{tot}(P_o - P)} = \frac{1}{V_m C} + \frac{(C-1)P}{V_m C P_o} \qquad (2.44)$$

where

P, P_o = pressure exerted by nitrogen and saturated vapour pressure respectively

V_{tot} = volume adsorbed

V_m = volume of nitrogen required to form a complete monolayer

and C = BET constant

From the plot of $P/(P_0-P)V_{tot}$ against P/P_0, V_m and C are evaluated since the intercept of the straight line graph corresponds to $1/V_m C$ and slope $= (C-1)/V_m C$. Assuming the surface area of one nitrogen molecule to be 16.27×10^{-20} m^2 [35], the total surface area of PTG (S) is calculated according to the relationship:

$$S = \frac{V_m N_A \times 16.27 \times 10^{-20}}{V_{S.T.P.} \times \text{Weight of sample}} \qquad (4.18)$$

where

N_A = Avogadro constant, 6.022×10^{23} $mole^{-1}$

$V_{S.T.P.}$ = volume occupied by one mole of gas, 22.41×10^3 cm^3

Substituting the values into equation (4.18) and simplifying yields

$$S = \frac{4.36 \times V_m}{\text{Weight of sample}} \qquad (4.19)$$

4-9 X-ray diffraction

PTG sample was annealed as described in page 51. It was crushed and smeared onto a slide. X-ray diffraction pattern (XRD) was taken on an automated and computerized Philips PM1710 X-ray diffractor using CuK radiation (λ = 154 pm) with a nickel filter. Each pattern took fifteen minutes to complete (fast scan).

4-10 Results

Degassing the samples in vacuum (pressure = 1.8×10^{-5} torr) caused a brown discoloration which slowly faded when exposed to atmospheric condition. This discoloration may be attributed to impurity adsorbing on the surface of PTG. However, this will be discussed in detail in chapter 6. Fig. 12.1-12.6 shows the adsorption and desorption isotherms of nitrogen on PTG samples annealed at various temperatures. Prominent "knee-bends" were observed together with the prominent hysteresis loops. This suggested that the adsorption isotherms were of Type IV. As shown in Table 2, increasing the annealing temperature caused a simultaneous decrease in surface area. The sample, PTG300R (Fig. 13.1) was predominantly amorphous but resembled anatase as indicated by the broad and poorly resolved peak at 2θ = 25.469°. Since the sample was loaded with platinum (see chapter 5), the weak signal at 2θ = 40.826° (Fig. 13.1) indicated that the concentration of platinum must be very low or the sample was not properly crushed. (Note that the sample PTG 300R used in the surface area studies was not photodeposited with platinum but was from the same piece of PTG which was also used for the photodeposition experiment). Amorphous PTG (annealing temperature =

Fig 12.1: Adsorption and desorption isotherm of PTG 300R.

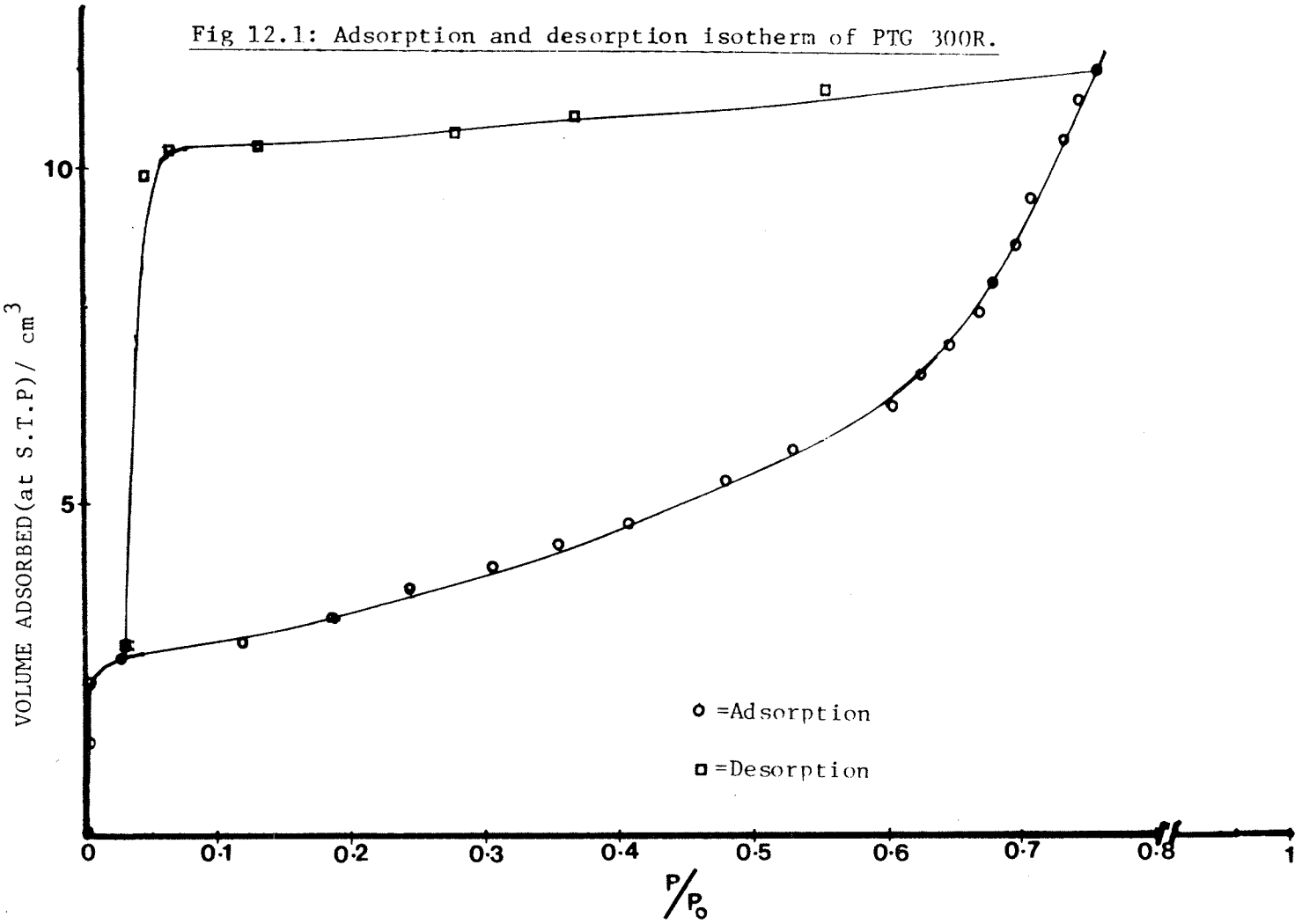

Fig 12.2: Adsorption and desorption isotherm of PTG 320R

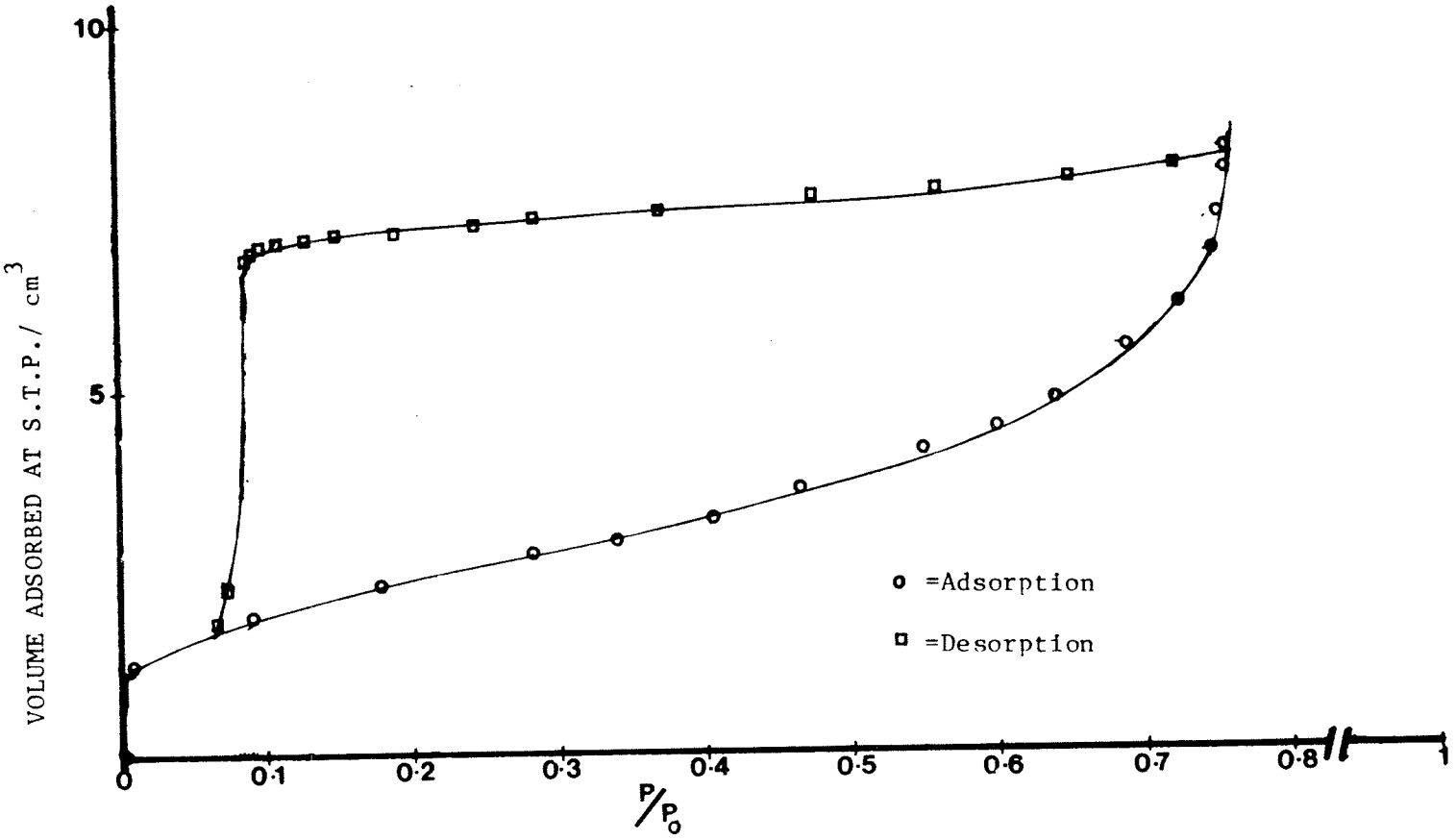

Fig 12.3: Adsorption and desorption isotherm of PTC 360R

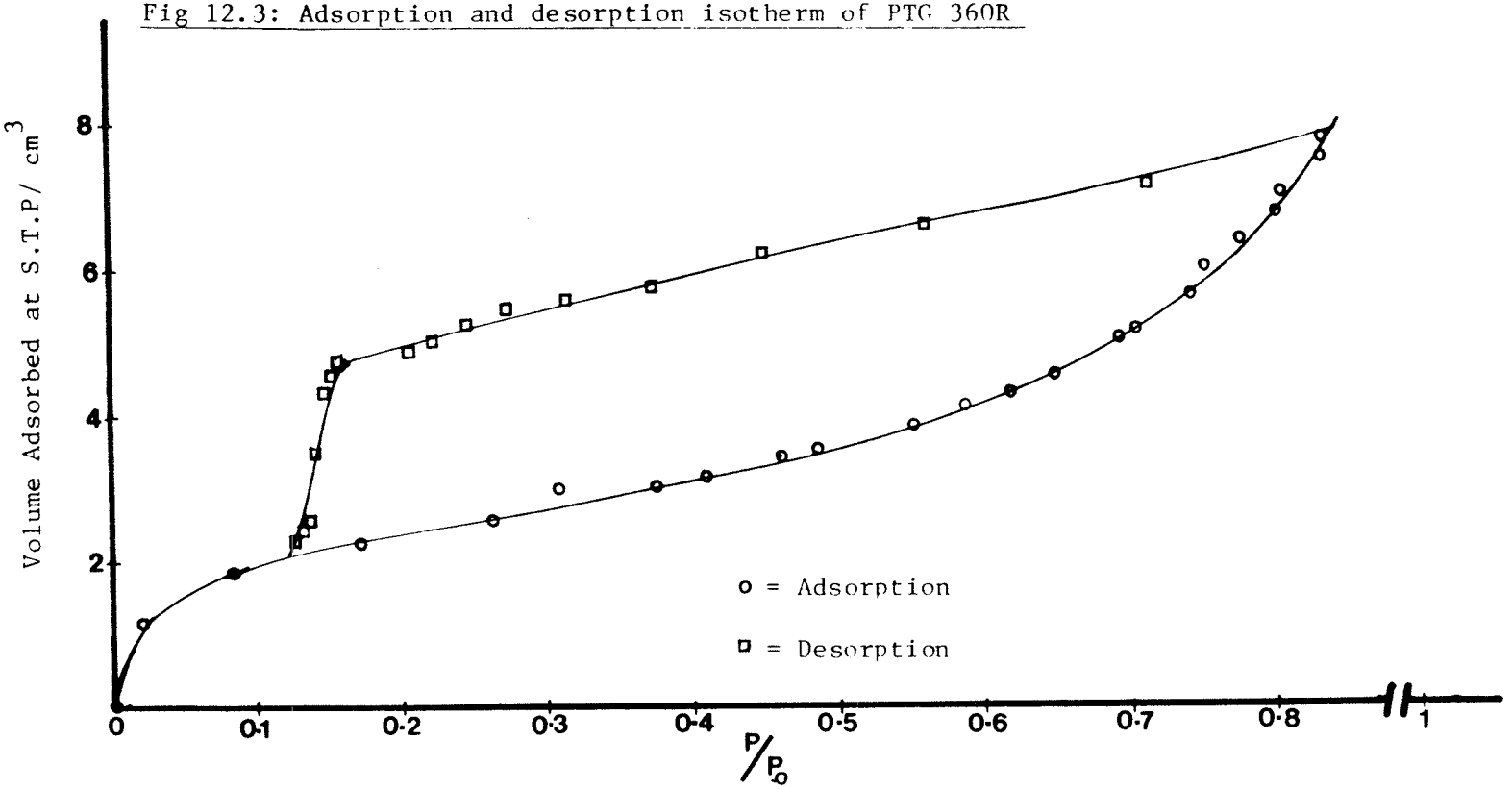

Fig 12.4: Adsorption and desorption isotherm of PTG 410R

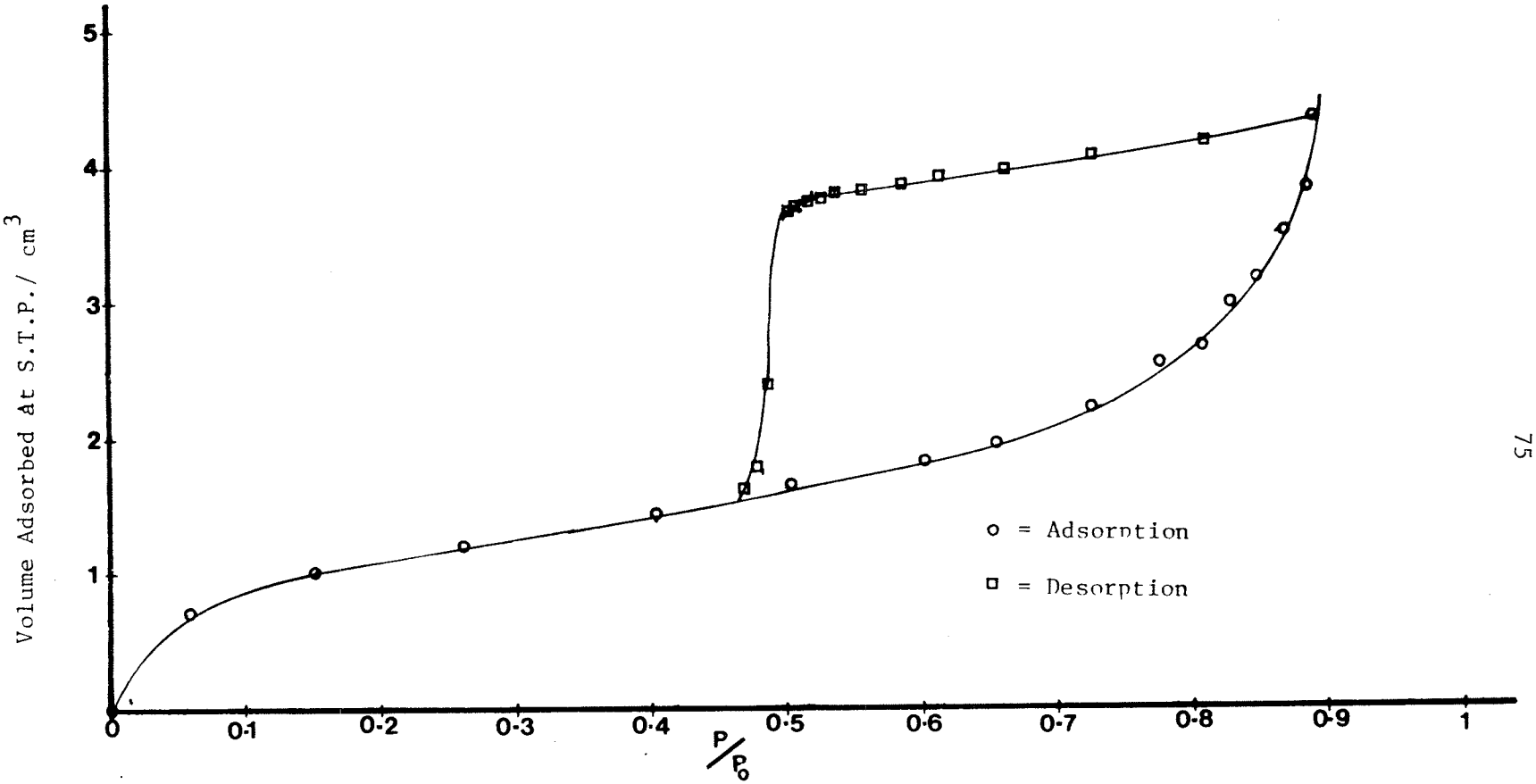

Fig 12.5: Adsorption and desorption isotherm of PTG 440R.

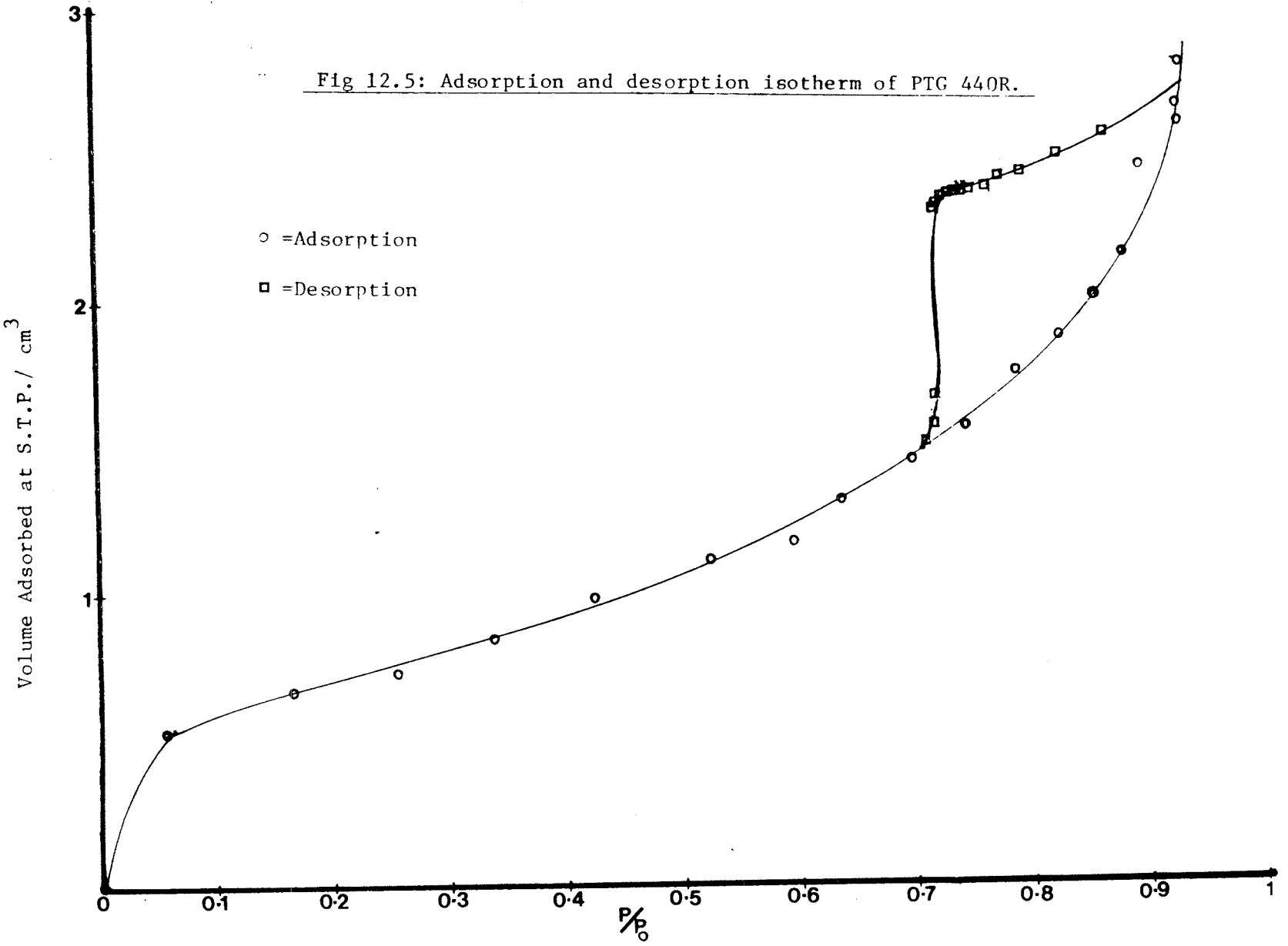

Fig 12.6: Adsorption and desorption isotherm of PTG 460R

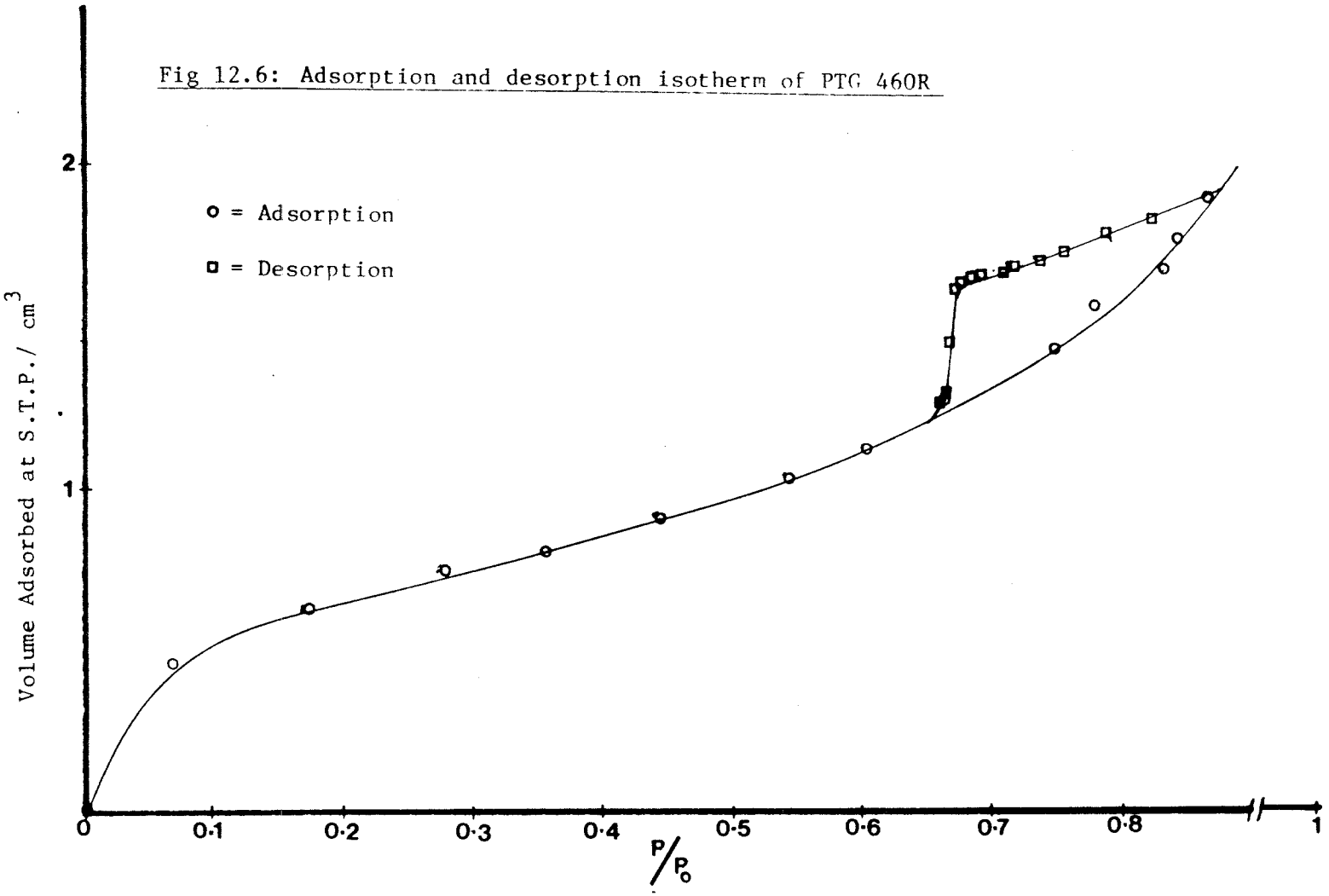

Table 2: Surface area of PTG sample annealed at various temperature*

Sample	Annealing temperature	BET surface area	C-BET constant	E_1
	°C	$m^2\ g^{-1}$		KJ $mole^{-1}$
Porous	300	304	46	-7.07
	320	103	107	-7.18
Titania	360	52	107	-7.18
	410	23	205	-7.37
Glass	440	16	185	-7.33
	460	14	102	-7.17

*Degassing temperature = 200°C

Degassing voltage = 28 volts

Degassing time = 18 hours

Pressure of system = 1.8×10^{-5} torr

Total annealing time for each sample = 14 hours

All the above samples were soaked in doubly distilled water (12 hours) and then soxhleted (24 hours) prior to surface area determination. All the samples were from the same piece of PTG.

E_1 values were calculated using equation (2.47), page 29.

Fig 13.1: X-ray diffraction pattern of PTG300R (Pt loaded) where the following "d" values are calculated from $d = \frac{\lambda}{2 \sin\theta}$, λ being the wavelength (λ = 154 pm) of $CuK\alpha$.

2θ/°	d/Å	Int
15.142	5.8463	290
15.597	5.6765	310
16.931	5.2321	408
17.588	5.0381	400
18.206	4.8686	345
18.415	4.8137	373
21.264	4.1748	245
22.338	3.9765	253
22.877	3.8839	285
23.113	3.8448	245
24.782	3.5895	290
25.469	3.4943	478**
26.200	3.3984	240
27.180	3.2781	210
28.445	3.1351	233
29.168	3.0590	213
40.826	2.2084	175 Pt
41.149	2.1918	205
53.072	1.7241	193
54.131	1.6828	248**
55.222	1.6619	193
64.787	1.4378	143

** = anatase peak. Pt = Platinum peak.

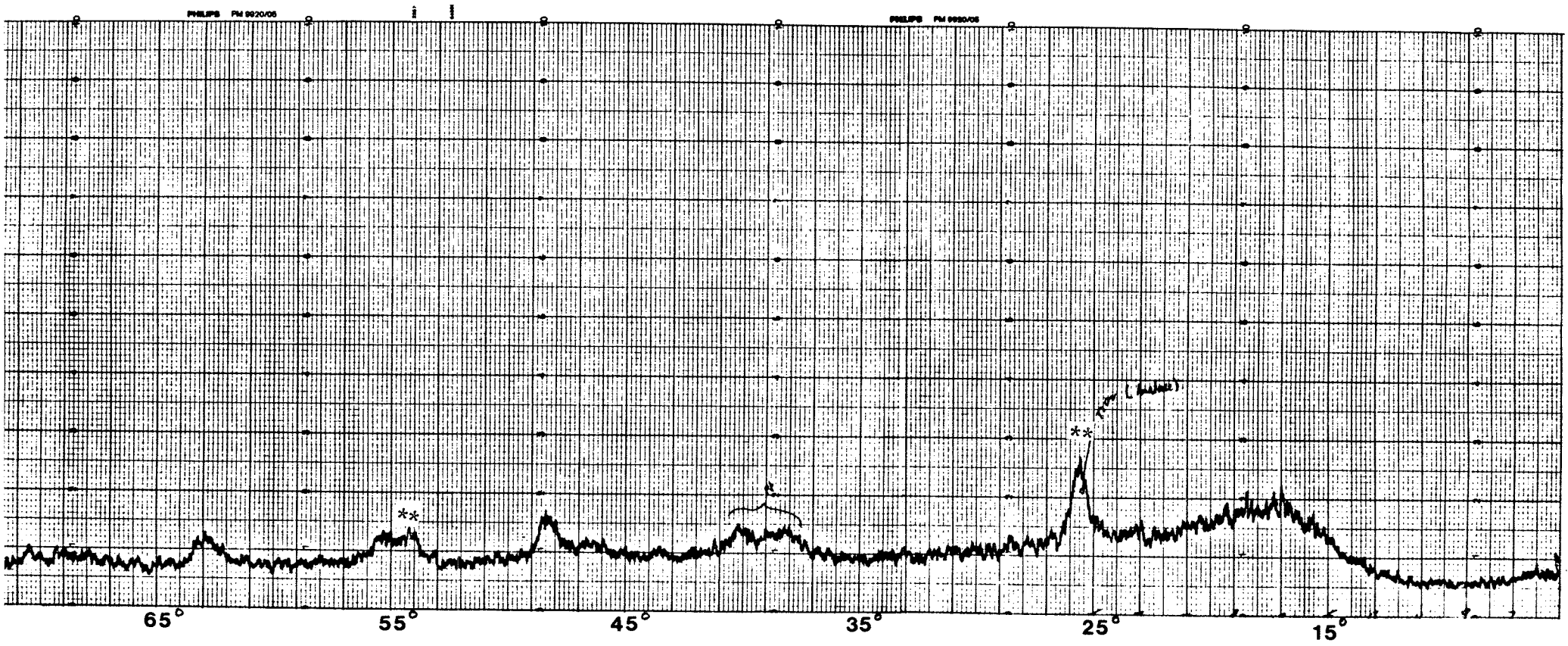
65°
55°
45°
35°
25°
15°
2θ

300°C) was transparent and slightly yellowish in colour. Annealing PTG300R to 360°C caused a 2% loss in weight. The sample (PTG360R) became slightly translucent though the colour was identical to PTG300R. The prominent anatase peak at $2\theta = 25.270°$ is clearly seen in Fig. 13.3 suggesting that PTG360R was now mostly anatase with a slight rutile (<5%) component. Annealing PTG360R to 410°C caused the reduction of anatase character as shown in Fig. 13.4. Rutile component ($2\theta = 27.521°$) was now a major component in the sample (PTG410R) which was completely opaque and white in colour. It was less brittle than the anatase or amorphous analogues. No noticeable loss in weight was observed. Annealing PTG410R at higher temperature (440°C and 460°C) resulted a greater domination of the sample by rutile (Fig. 13.5 - 13.6). It was estimated that increasing the annealing temperature to 480°C will cause a complete domination of the sample by rutile though this has not yet been observed. The samples (PTG440R and PTG460R) were opaque, white and hard.

While the transformation of anatase to rutile was occurring, a change in the hysteresis loop was also observed. The loops diminished in size with increasing annealing temperature while still retaining the Type A characteristics. This diminishing effect was due to the gradual domination of mesopores/macropores over micropores as annealing temperatures were increased. Fig. 14 shows the gradual transformation of micropores to mesopores/macropores as a function of pore size distribution. As shown by the adsorption isotherm, microporous network in the pore structure of PTG samples had a profound effect on the condensation of nitrogen molecules. In a relative pressure region

From $d = \frac{\lambda}{2 \sin\theta}$, λ being the wavelength (λ = 154 pm) of CuK_{α}.

2θ/°	d/Å	Int
25.333	3.5127	853**
27.509	3.2396	303*
32.675	2.7382	40
36.207	2.4788	183*
37.005	2.4272	90
37.549	2.3933	220**
37.988	2.3666	295
38.618	2.3294	158
38.926	2.3117	123
39.252	2.2932	93*
40.379	2.2318	78
41.346	2.1818	103*
42.776	2.1121	48
43.846	2.0630	33
47.966	1.8950	383*
48.403	1.8789	300
53.780	1.7030	205
54.075	1.6945	308
54.385	1.6855	438*
54.967	1.6691	303**
55.210	1.6623	300**
55.432	1.6561	243
55.603	1.6514	175
56.582	1.6252	150*
62.078	1.4938	118**
62.783	1.4787	203
63.624	1.4612	113
63.980	1.4539	70*

* = rutile peak. ** = anatase peak.

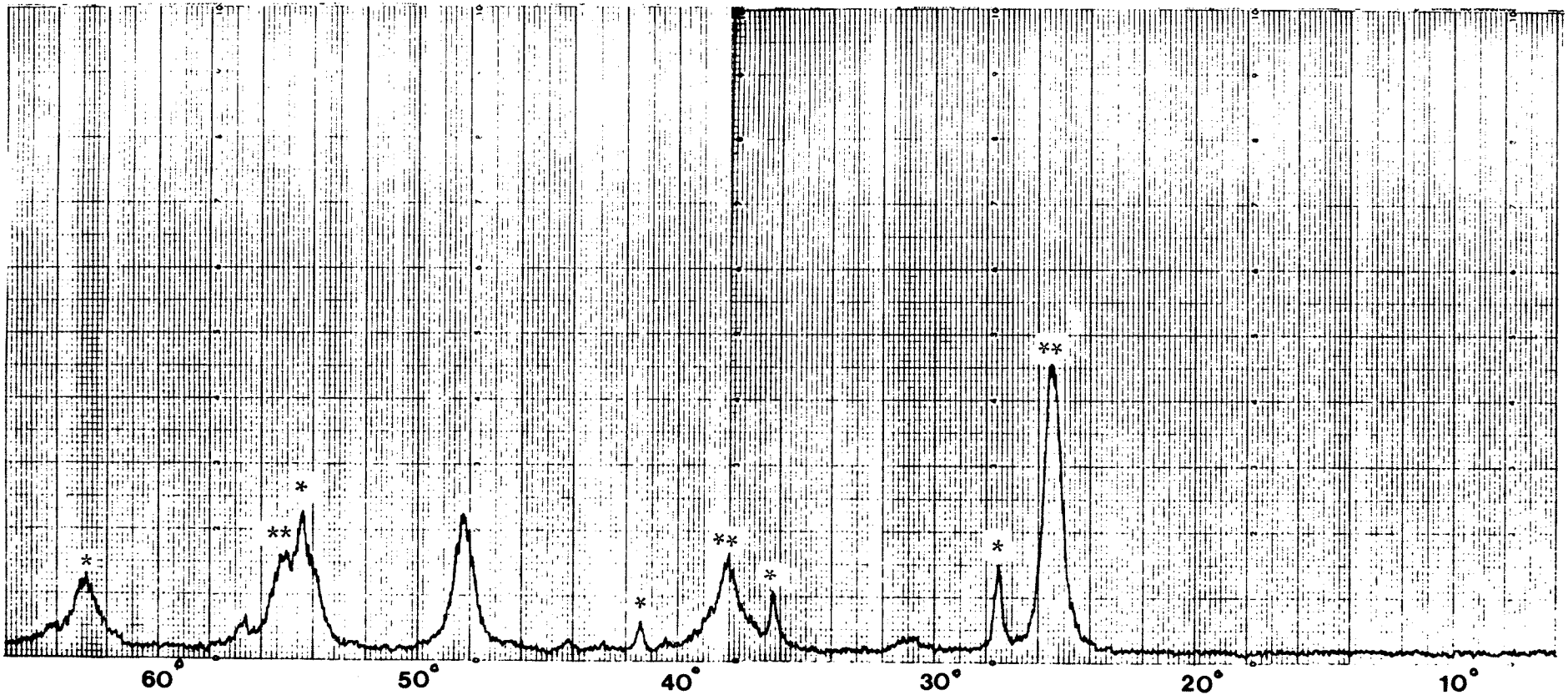
*
**
*
*
**
*
*
**
60°
50°
40°
30°
20°
10°
2θ

Fig 13.3: X-ray diffraction pattern of PTG360R where the following "d" values are calculated from $d = \frac{\lambda}{2 \sin\theta}$, λ being the wavelength (λ = 154 pm) of CuK_α.

2θ/°	d/Å	Int
25.270	3.5214	1208**
27.457	3.2456	160*
36.102	2.4858	123*
36.985	2.4284	158
37.743	2.3814	385**
38.503	2.3361	200**
46.427	1.9542	45
47.246	1.9222	73
48.011	1.8934	610**
53.920	1.6990	375**
54.259	1.6891	363*
56.587	1.6251	113*
62.701	1.4805	355**
62.939	1.4755	243
63.394	1.4660	95
64.818	1.4372	50

* = rutile peak. ** = anatase peak.

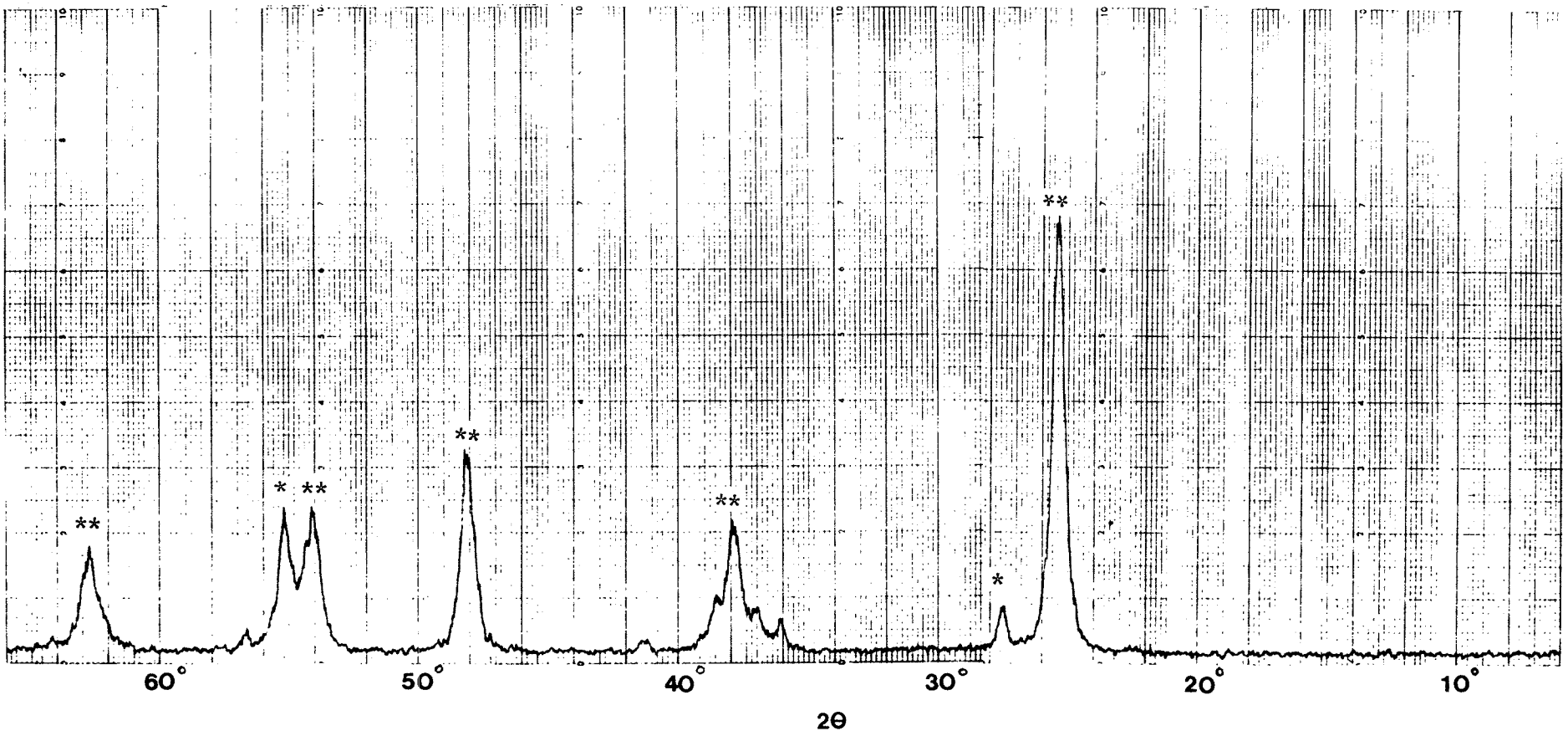
**
* **
**
**
*
**
60°
50°
40°
30°
20°
10°
2θ

Fig 13.4: X-ray diffraction pattern of PTG410R where the following "d" values are calculated from $d = \frac{\lambda}{2 \sin\theta}$, λ being the wavelength (λ = 154 pm) of CuK_α .

2θ/°	d/Å	Int
25.384	3.5057	933**
27.521	3.2382	1220*
36.180	2.4806	715*
37.101	2.4211	108**
37.867	2.3739	318**
38.707	2.3243	128**
39.280	2.2917	130*
41.346	2.1818	435*
44.117	2.0510	148*
48.145	1.8884	445*
54.077	1.6944	370**
54.409	1.6848	1090*
55.129	1.6645	328**
56.702	1.6220	443*
62.184	1.4915	98**
62.341	1.4882	95**
62.808	1.4782	323*
64.175	1.4500	158*

* = rutile peak. ** = anatase peak.

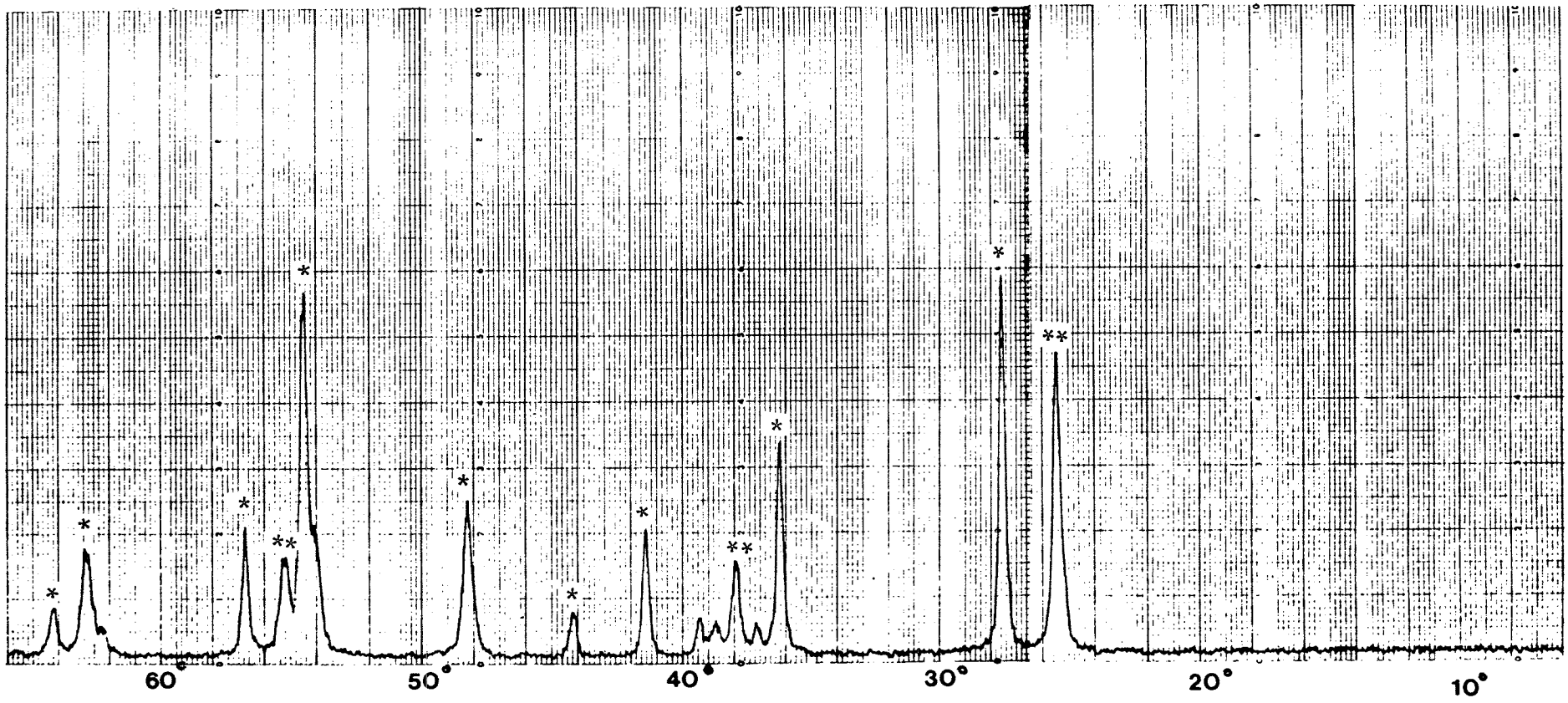
60°
50°
40°
30°
20°
10°
2θ

Fig 13.5: X-ray diffraction of PTG440R where the following "d" values are calculated from $d = \frac{\lambda}{2 \sin\theta}$, λ being the wavelength (λ = 154 pm) of CuK_{α}.

2θ/°	d/Å	Int
7.227	12.2220	38
11.932	7.4109	20
12.561	7.0410	23
25.350	3.5104	668*
26.511	3.3593	43
27.477	3.2433	1713*
36.132	2.4838	1040*
37.108	2.4207	68*
37.779	2.3792	178**
38.704	2.3244	88**
39.238	2.2940	185*
41.302	2.1840	533*
43.590	2.0746	53*
44.061	2.0535	178*
48.122	1.8892	290**
54.388	1.6854	1415*
55.078	1.6659	268**
56.644	1.6236	495*
62.770	1.4790	310*
64.135	1.4508	235*

* = rutile peak. ** = anatase peak.

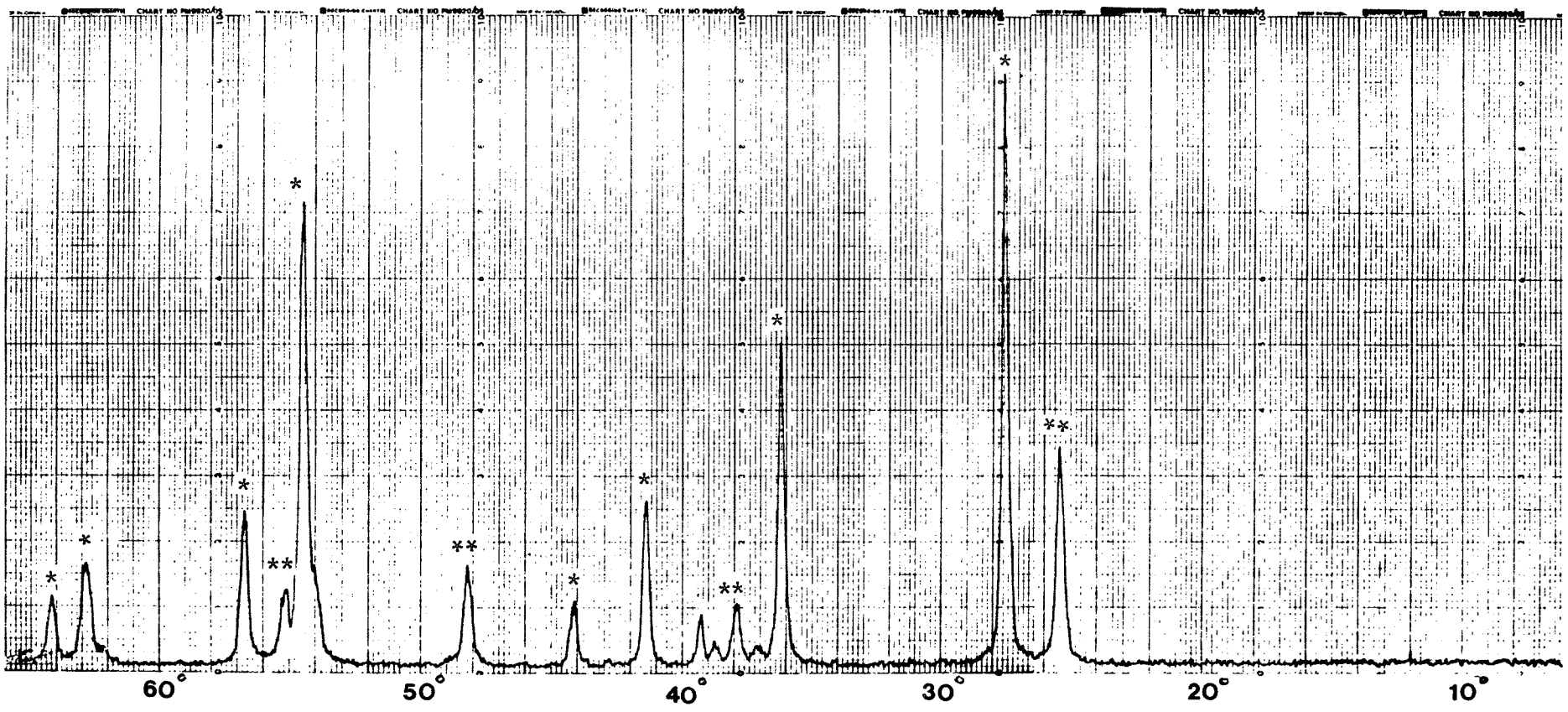
60°
50°
40°
30°
20°
10°
2θ

Fig 13.6: X-ray diffraction pattern of PTG460R where the following "d" values are calculated from $d = \frac{\lambda}{2 \sin\theta}$, λ being the wavelength (λ = 154 pm) of CuK_α.

2θ/°	d/Å	Int
10.786	8.1951	38
25.408	3.5025	335**
27.528	3.2374	1880*
36.180	2.4806	1145*
37.157	2.4176	63
37.882	2.3730	73**
39.285	2.2914	148*
40.635	2.2183	28
41.346	2.1818	640*
43.029	2.1003	35
44.153	2.0494	255*
48.137	1.8887	185**
54.407	1.6849	1738*
55.246	1.6613	140**
56.700	1.6221	503*
61.025	1.5171	40
62.858	1.4772	315*
64.140	1.4507	260*
65.584	1.4222	50*

* = rutile peak. ** = anatase peak.

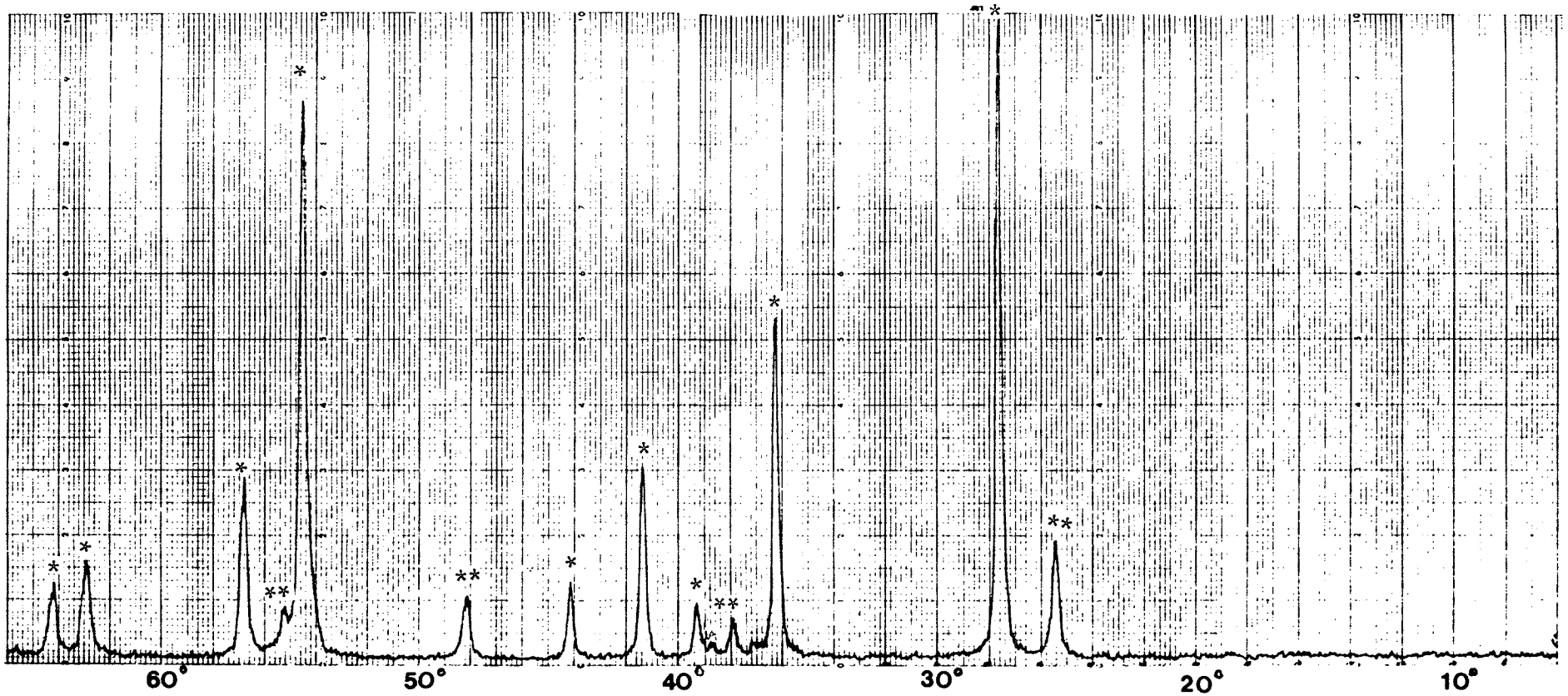
60°
50°
40°
30°
20°
10°
2θ

Fig 14: Pore distribution function of PTG annealed at various temperatures.

PTG300R = PTG sample was annealed at 300°C for 14 hours and cooled to room temperature in an oven (12 hours). The sample was soaked in doubly distilled water overnight and soxhleted (24 hours) prior to surface area determination. The degassing temperature was 200°C and the length of degassing was 18 hours.

PTG360R = PTG sample was annealed at 360°C for 14 hours and subjected to similar treatment as PTG300R.

PTG410R = PTG sample was annealed at 410°C for 14 hours and subjected to similar treatment as PTG300R.

PTG440R = PTG sample was annealed at 440°C for 14 hours and subjected to similar treatment as PTG300R.

PTG460R = PTG sample was annealed at 460°C for 14 hours and subjected to similar treatment as PTG300R.

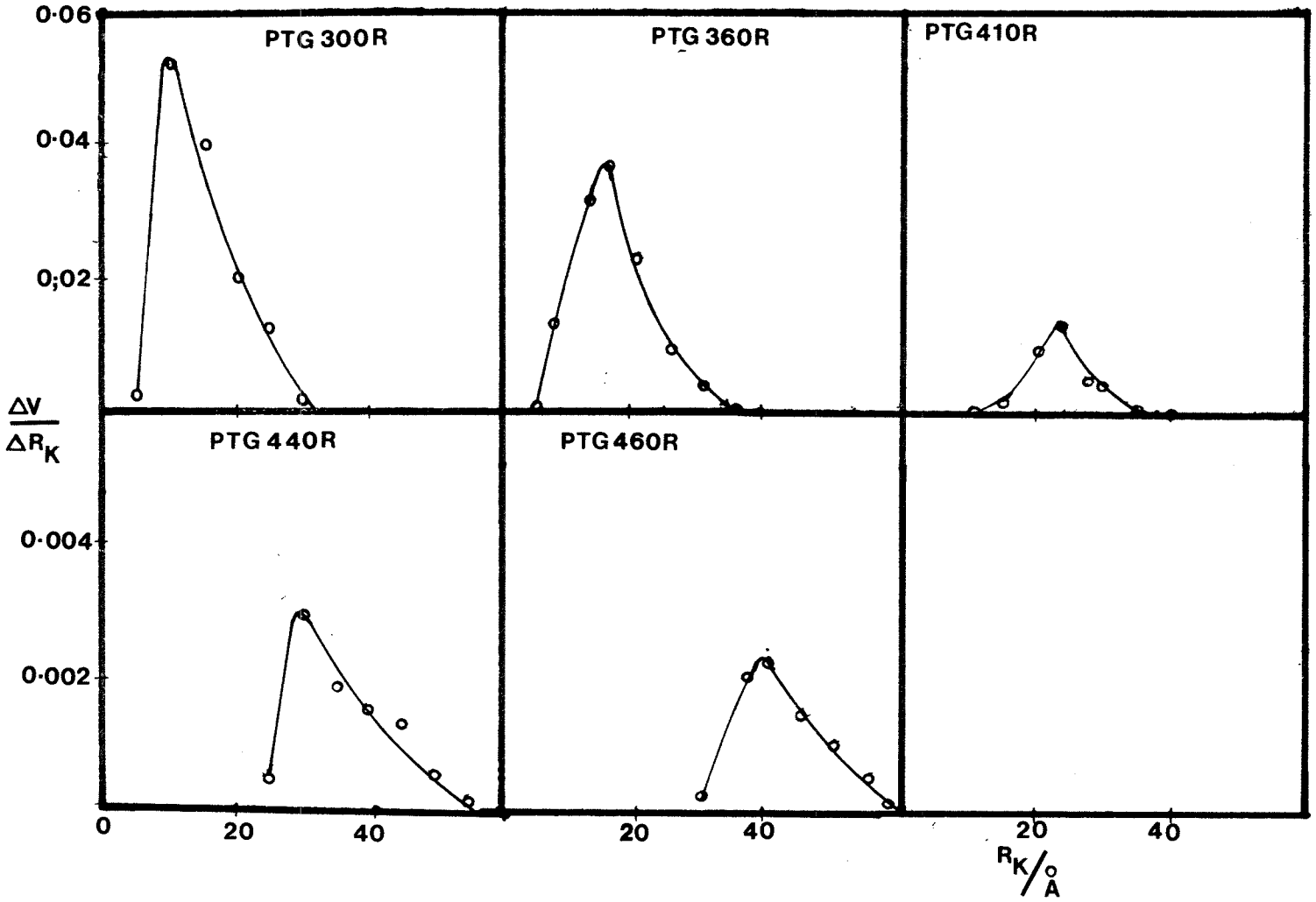
PTG 300R
PTG 360R
PTG 410R
PTG 440R
PTG 460R
0·06
0·04
0;02
0·004
0·002
ΔV/ΔR_K
0
20
40
20
40
20
40
R_K/°A

(P/P_0) between 0.7 - 0.75, condensation occurred when micropores dominated the PTG structures. Conversely, a higher pressure ($P/P_0 \approx$ 0.9) was required to condense the adsorbate molecules. These results were very consistent with the Kelvin equation which predicts that condensation of adsorbate molecules required a lower pressure if the size of the pores is small (micropores) whereas a higher pressure is required for larger pores.

Fig. 15.1-15.3 illustrates the BET plots for samples annealed from 300°C to 460°C. Surface areas were calculated by the application of the BET "two-parameter" equation in the relative pressure region 0.05 - 0.35 [35]. The intercept of the straight line corresponded to $1/V_mC$ and the slope equaled $(C-1)/V_mC$ where C and V_m are BET constant and volume required to complete a monolayer respectively. The variable C-BET constants suggested that the heat of condensation of the first monolayer was not constant, though the variation was not very large (Table 2-4).

The effect of degassing temperature on the surface area was less dramatic as compared to the earlier case. A slight decrease in surface area was observed in both samples, the effect being more apparent on PTG300R. The results are tabulated in Table 3. The samples were still predominantly microporous as illustrated by the pore size distribution in Fig. 16. Table 4 shows the results of surface area against length of annealing time at constant annealing temperature (300°C). No significant surface area change was observed. The pore distribution function (Fig. 17) shows no appreciable change in the pore structure, suggesting that the morphology of the samples used was identical throughout the experiment. The adsorption and desorption isotherms were

Fig 15.1: BET plots of PTG 410R and PTG 440R

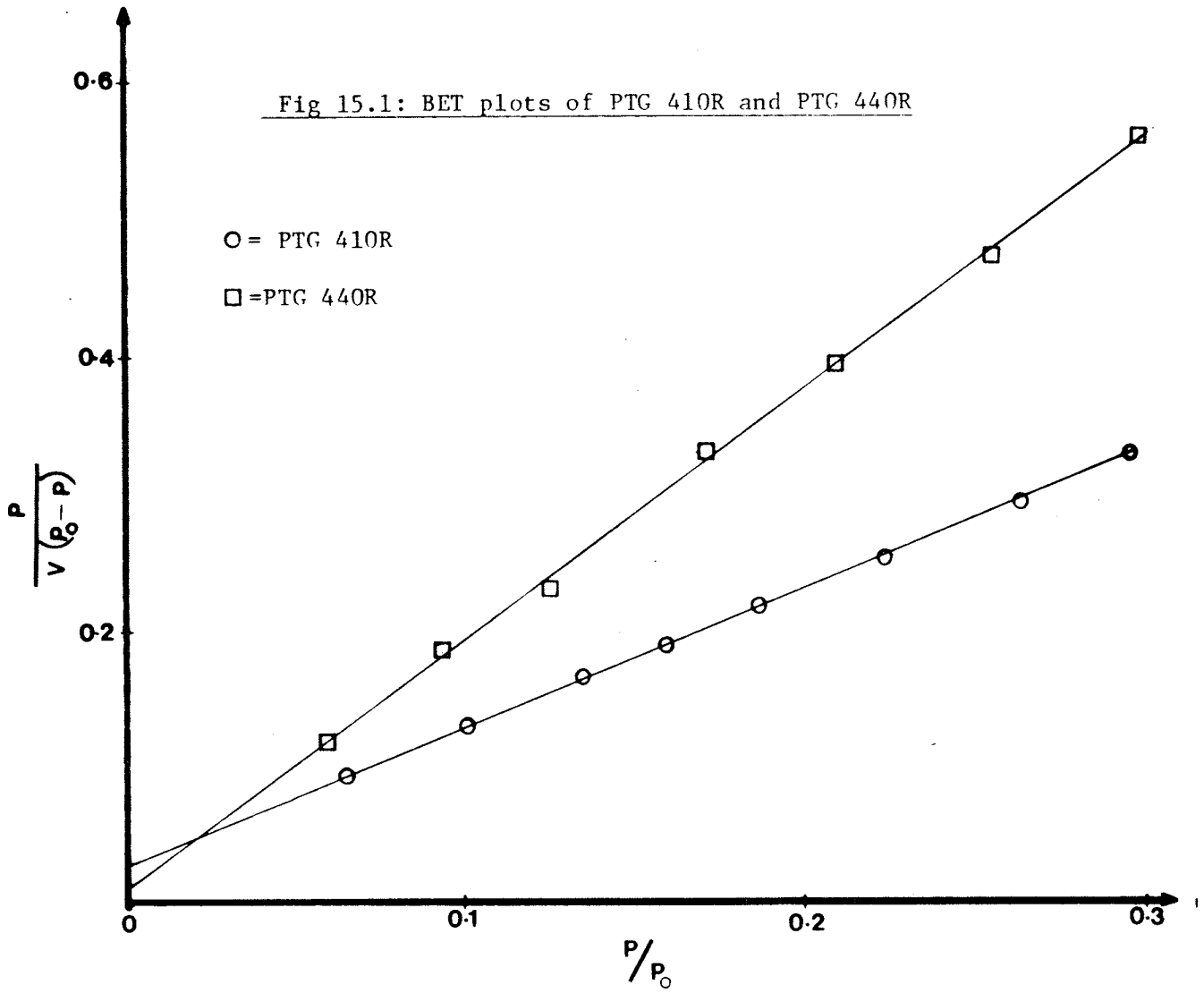

Fig 15.2: BET plots of PTG 300R and PTG 320R

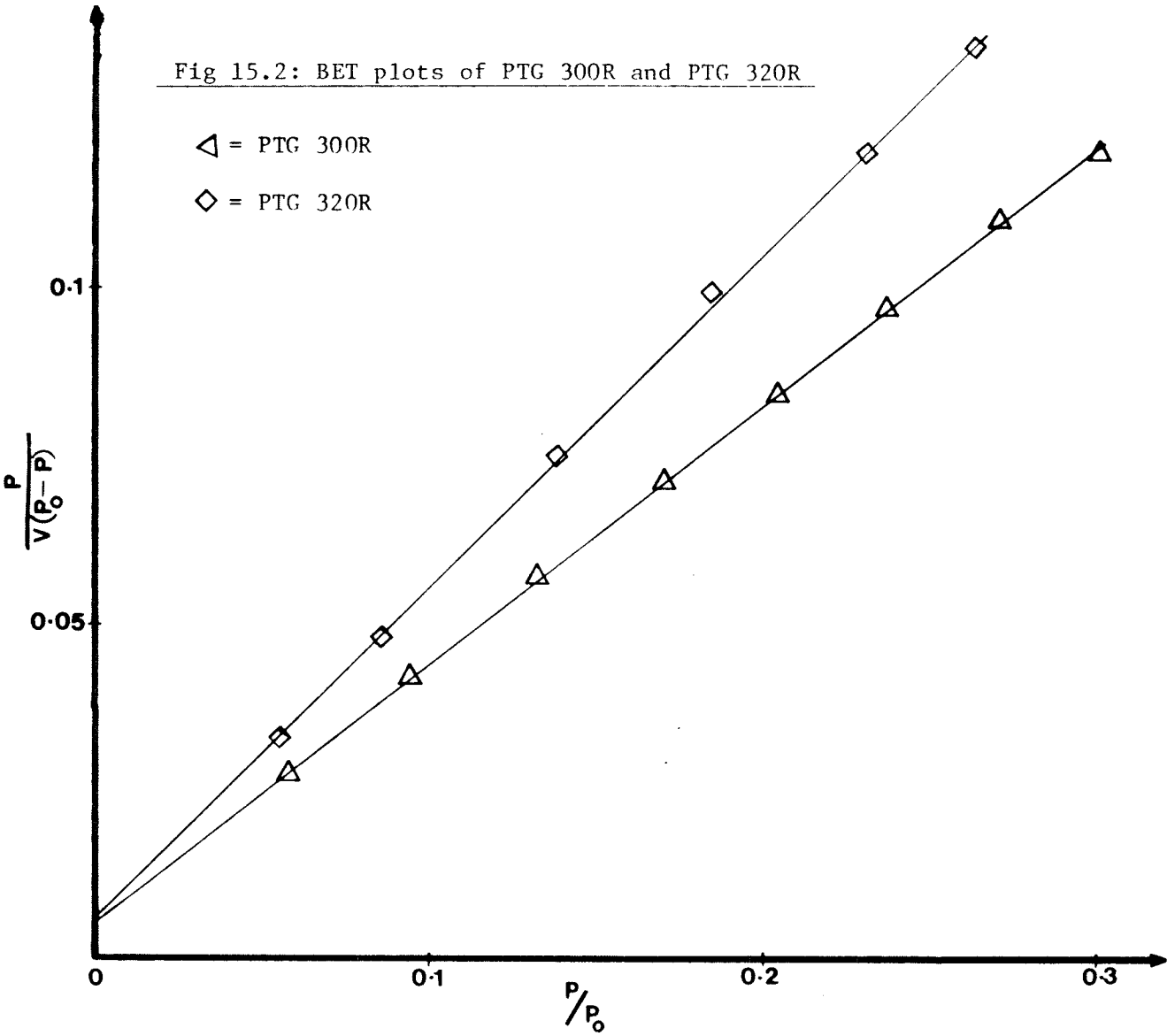

Fig 15.3: BET plots of PTG 300R and PTG 360R

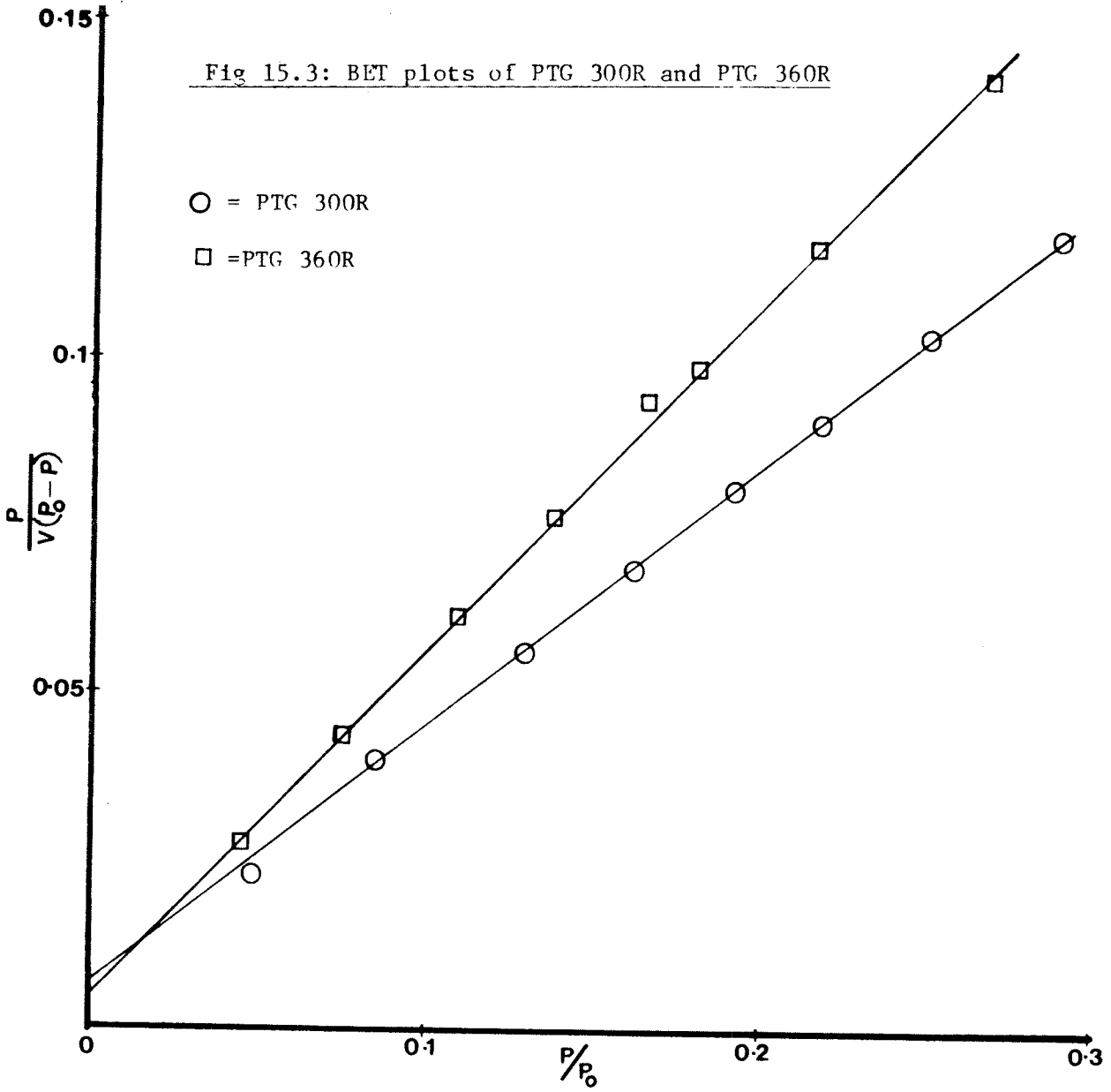

Table 3: Surface area of PTG300R and PTG360R degassed at various temperatures*

Sample	Degassing voltage	Degassing temperature	BET surface area	C-BET constant	E_1
	volt	°C	$m^2\ g^{-1}$		KJ $mole^{-1}$
PTG300R	28	200	304	46	-7.07
	32	249	292	44	-7.07
	35	294	285	74	-7.12
PTG360R	28	200	52	107	-7.18
	32	249	50	99	-7.17
	35	294	50	87	-7.14

*Degassing time = 18 hours

Pressure of system = 1.8×10^{-5} torr

The total annealing time for each sample was 14 hours. All the samples were soaked in doubly distilled water (12 hours) and soxhleted (24 hours) prior to surface area determination. All the samples were from the same piece of PTG.

E_1 values were calculated using equation (2.47), page 29.

Table 4: Variation of surface area of PTG320R with time.*

Sample	Length of annealing time / Hour	Surface area / $m^2 g^{-1}$	C-BET constant	E_1 / KJ $mole^{-1}$
PTG320R	16	103	107	-7.18
	24	105	101	-7;18
	32	105	87	-7.14
	40	105	80	-7.13

*Degassing temperature = 200°C

Degassing voltage = 28 volts

Total degassing time for each sample = 18 hours

Pressure of system = 1.8×10^{-5} torr

All the above samples were annealed at 320°C for 14 hours. The samples were soaked in doubly distilled water after annealing (12 hours) and the soxhleted (24 hours) prior to surface area determination. All the samples were from the same piece of PTG.

E_1 values were calculated using equation (2.47), page 29.

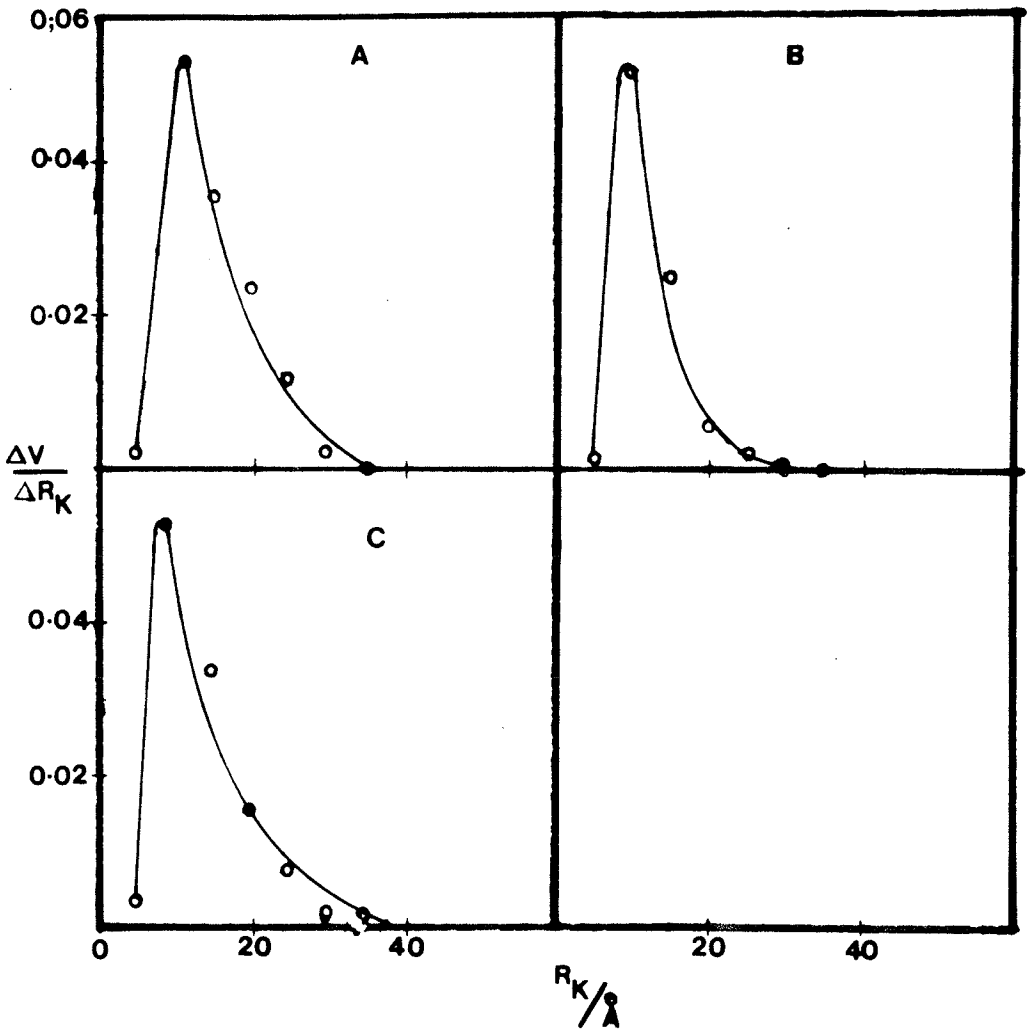

Fig 16: Pore distribution function of PTG 300R. In this diagram, the samples were annealed at 300°C for 14 hours and subsequently cooled to room temperature in the oven. Samples A, B and C were degassed at 200°C, 249°C and 294°C respectively. The total degassing time was 18 hours for each case.

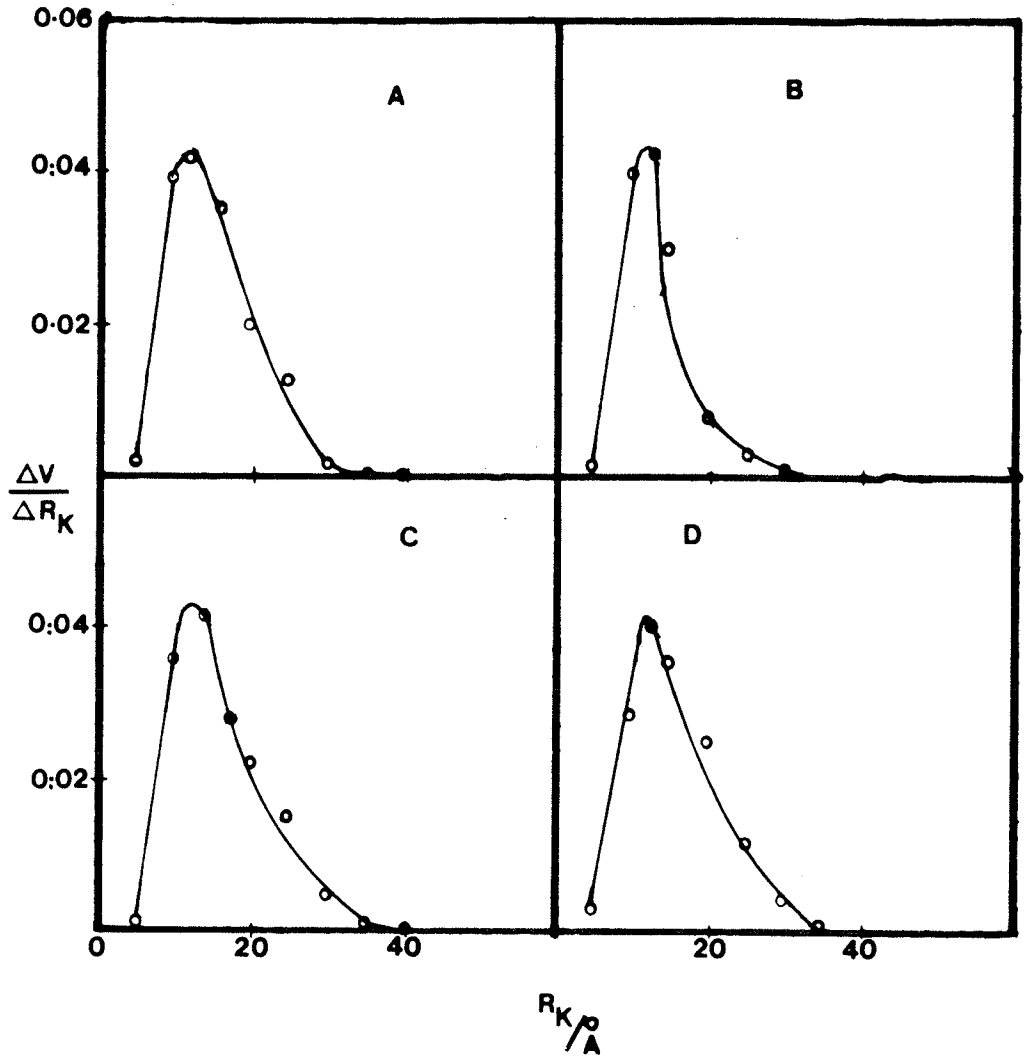

Fig 17: Pore distribution function of PTG 320R (sample was annealed at 320°C).In this diagram,samples A, B, C and D were annealed at 320°C for 16, 24, 32 and 40 hours respectively. The degassing temperature was 200°C.The total degassing time was 18 hours for each case.

identical to those illustrated in Fig. 12.1-12.6, lending further support to the above suggestion. No XRD patterns were taken on the samples used for the above experiments.

4-11 Discussion

Annealing temperature had a profound effect on the surface area and pore size of PTG as illustrated in Table 1. When the sample (PTG300R) was predominantly amorphous, the surface was highly hydroxylated and porous. The number of adsorption sites are plentiful, particularly in the "internal" surface of the porous glass. Thus the surface area derived from nitrogen adsorption at 77K was large. Increasing the annealing temperature caused a permanent and drastic loss of surface area. This trend had also been observed by earlier workers [20,64]. Primet et al. [24] working on anatase TiO_2 postulated that bridging species of type $-Ti\overset{O}{<}Ti-$ were formed upon heating TiO_2 above 300°C. A slight decrease in surface area was reported by the authors who inferred the loss of surface area as caused by the formation of the bridging species. This definitely occurred to PTG samples during the annealing process but certainly the formation of the bridging species cannot account for such a drastic decrease of surface area. Besides, the above only occurred on the surface whereby surface hydroxyl groups (hydrogen species) are available. Therefore another mechanism must be operating during the thermal treatment. However, the 2% loss in weight can easily be accounted by the loss of surface hydroxyl groups and co-ordinated water molecules. This will be discussed in further detail in the later chapter on the dehydroxylation of the surface hydroxyl groups of PTG.

A loss of a large fraction of micropores during the thermal treatment must be the prime cause for the drastic loss of surface area. Wicke [cited from ref[51]] found that micropores were largely responsible for the large surface area observed on charcoal and silica gels. The contribution of mesopores and macropores to the total surface area of the above stated samples was negligible relative to that of micropores. El-Akkad [20], working on anatase titania gel concluded that the loss of micropores was mainly responsible for the drastic decrease of surface area. It is likely that during the heat treatment, a large portion of the micropores were either partially or completely blocked, thus permanently destroying a large portion of adsorption sites. This blocking could arise from the transformation of micropores to mesopores and macropores by cross-linking of —Ti—O—Ti— chain [60,65].

In an earlier study on graphitized carbon black, Joyner and Emmett [46] demonstrated that a uniform surface could result via "graphitizing" the sample at very high temperature (3200°C). Surface area was lost. Considering the thermal treatment of PTG samples and that of carbon black, it is very unlikely that this factor could be the major cause. Beside, the highest annealing temperature was only 460°C. Sintering, smoothing of the pore wall or even weakening of the pore wall has been known as a result of heat treatment. Lippens and De Boer [66] reported that by sintering BOG450 and BOG580 (both well crystallined boehmite) at 750°C caused a substantial decrease of surface area. The authors attributed the disappearance of the narrow pores as the cause of the loss of surface area. In short, it can be concluded that the drastic

loss of surface area is attributed to the loss of the micropores. Cadenhead and Everett [67], working on porous glass noticed that surface area decreased when porous glass was sintered. The above authors also attributed the decrease of surface area as a result of the formation of larger pores. Their results on the adsorption and desorption of benzene on porous glass (Vycor) at 25°C was similar to our results, though their annealing temperatures were about 600-900°C.

Harris and Whitaker [60] claimed that mesopores and macropores were formed when they subjected anatase titania gel to thermal treatment. Cadenhead et al. [43] pointed out that stresses induced during the adsorption process may sometimes be sufficient to distort the morphology of the solid. If the stress is very severe, fracturing of sample occurs. Under such condition, there is no doubt that mesopores and macropores could also result, the extent of formation depending on the population of the weak pore wall. With the combination of the above factors, surface area is expected to decrease substantially if the adsorption sites are being destroyed. This postulate is very consistent with the results obtained, particularly for PTG samples annealed at temperature higher than 410°C where mesopores dominated the structure of the samples.

Degassing temperature caused a slight decrease of surface area and this has been attributed to the formation of $-Ti-\overset{O}{}-Ti-$ species. Again, sintering of sample cannot be ignored. Extending the length of annealing time at constant annealing temperature (320°C) did not cause any structural damage to the samples. In fact, Linsen and van den Heuvel [51] reported that pores can be created by the expulsion of

residual water molecules embedded inside the sample. Earlier, Lippens and De Boer [66] reported that narrow pores were also created by heating well crystallized boehmite (BOG450 and BOG580) at 250°C. By doing so, additional sites are created. This report is in good agreement with my results as shown in Table 3 though the increment in surface area was not very substantial. In short, not many pores were created during the annealing process though the duration had been extended. Presumably the structure was able to resist the heat treatment at that particular temperature.

It has been clarified that the shape and size of the pores determine the nature of the hysteresis loops. If all the samples have pores of similar size and shape, then the size and shape of the loop would be expected to be similar in all cases. This is only partially true with the PTG samples used in the experiments. The prominent hysteresis loops, quite reminiscent to those obtained by Weiser et al. [59] suggested that the shape of the pores was identical in many respects. Based on the classification proposed [51,56], the above hysteresis was Type A when the sample was amorphous or anatase but gradually transforming to Type E at higher annealing temperature ($\geq$ 410°C) when mesopores dominated the structural network of the samples. This transformation had been observed in BOG450 and BOG580 by Lippens and De Boer too [66].

As mentioned earlier, many theories had been proposed to explain the hysteresis phenomenon. McBain [53] believed that hysteresis loop was caused by the presence of pores with constricted necks, that is the radius of the body r_b is substantially larger than the radius of the

constricted neck r_n. Pores will be completely filled at a relative pressure corresponding to r_b but emptying commenced at a pressure corresponding to r_n. In other words, the emptying process was unable to retrace the adsorption path. Linsen and van Heuvel [51] pointed out that if the necks are short and narrow and that $r_b > 2r_n$, then the hysteresis loops will be wide. This was seen as illustrated in Fig. 6.1 and is said to exhibit "ink-bottle" effect because the pores are assumed to resemble the shape of ink-bottle. Cohan [52] suggestd that there may exist pores with constricted neck and wide spheroidal base ($r_b \gg r_n$). In such circumstances, hysteresis is caused by the delay in the formation of a meniscus during adsorption.

When the sample was predominantly amorphous, the hysteresis loops spread to the low relative pressure region. Cadenhead et al. [43] pointed out that if the sample is "loosely structured", that is possessing the ability to expand and contract over wide range of pressure during adsorption, low pressure hysteresis will not be observed. Conversely, if the structure is very strong and rigid, then low pressure hysteresis will not be observed either. Only samples of intermediate rigidity will exhibit low pressure hysteresis. Upon thermal treatment, low pressure hysteresis will be eliminated. This low pressure hysteresis theory developed by the above authors is fairly consistent with the results obtained at this study. If the samples of PTG300R, for example was rigid, the hysteresis loop would not have spread to the low pressure region. As reported earlier, the sample became hard and less brittle compared to the amorphous or anatase analogues. Perhaps, the structure was very rigid and hence a high

pressure hysteresis loop was observed.

Another criterion which determines the exhibition of low pressure hysteresis loop is the pore size. The pore size must be approximately the same size as the adsorbate molecules. If the pores are too large, no low pressure hysteresis loop will be observed. On the other hand, if the adsorbate molecules are large, no hysteresis will be observed either. Charcoal was shown to exhibit low pressure hysteresis loop by Cadenhead *et al.* [43]. Upon activation by steam, the hysteresis loop was completely eliminated, the reason being the enlargement of the pore size. Similarly, during annealing at elevated temperature ($\geq$410°C), mesopores and macropores were formed. These pores were much larger than nitrogen molecule, hence no low pressure hysteresis loop was observed.

In the development of BET theory, Brunauer *et al.* [33] assumed that C-BET constant equals unity. From the experimental evidence (see Table 1-3), C-BET was never constant. Recalling from Chapter 2, C-BET is related to the heat of condensation of the first monolayer (ΔE_1) by

$$C \approx \exp\left[(\Delta E_1 - \Delta E_L)/RT\right] \qquad (2.47)$$

where ΔE_1, ΔE_L, R and T are similarly defined as in page 29. When ΔE_1 varies, C-BET varies. As shown in Table (1-3), ΔE_1 values which are determined using equation (2.47), did not deviate significantly, considering the effect of heat treatment which as mentioned earlier could cause sintering and transformation of micropores to mesopores or macropores. This implies that the slight deviation of ΔE_1 values could be attributed to the lack of uniformity of the van der Waals forces on the surface. However, there is some reservation about the above

statement since no heat of adsorption experiments were conducted. However, Culver and Heath [68] noticed that there existed high energy sites on saran charcoal even though the pore size had been enlarged by 15%, suggesting that the surface was not uniform in many respects. Thus the heat of adsorption varied.

The heat of liquefaction of nitrogen molecule is 6 KJ $mole^{-1}$. As indicated in Tables (1-3), ΔE_1 values are more than 6 KJ $mole^{-1}$. Beebe et al. [69] proposed that if the pores are narrow, then the adsorbate molecule will experience numerous attractive forces arising from other pore walls close to the vicinity of the site it resides at. In short, the adsorbate molecules experience more "induced" effects, hence the heat of condensaton of the first monolayer is substantially greater than the heat of liquefaction of the adsorbate molecules. But Culver and Heath [70] contradicted the above claim. They attributed the higher heat of adsorption as an indication of porous samples, the fact which was confirmed by XRD by Biscoe and Warren [71] while studying spheron particles.

In spite of the variable C-BET, ΔE_1 values are within the heat of physical adsorption range (20 kJ $mole^{-1}$), suggesting that Van der Waals forces were in operation during the adsorption process. Beside, it also implies that there was no dissociation of nitrogen molecules. Had this occurred, that is chemisorption was involved, ΔE_1 values would be entirely different, by at least 2-3 fold of that of ΔE_1 shown in Tables (2-4).

CHAPTER 5

ELECTRICAL CONDUCTIVITY STUDIES ON PLAIN AND PHOTODEPOSITED POROUS TITANIA GLASS

5-1 Introduction

Titanium dioxide (TiO_2) exists in three allotropic forms viz:brookite, anatase and rutile, the latter two being more commonly encountered. Amongst them, rutile is considered the more stable allotrope due to its common occurrence even though thermochemical data indicates that anatase is 8-12 KJ $mole^{-1}$ more stable than rutile at 25°C. Anatase TiO_2 unit cell is tetragonal in shape but elongated along the c-axis. An anatase unit cell (see Fig. 18) is comprised of TiO_6 octahedra with four edges being shared with other octahedra, the top and the bottom octahedra are at right angles to each other. Rutile is also tetragonal in shape but the TiO_6 octahedra is distorted. Only the two opposite edges are shared with other octahedra [10]. Brookite is orthorhombic whereby the TiO_6 octahedra has three of its edges shared with other octahedra [72]. They inter-convert as follows [73]:

$$\text{Brookite} \xrightarrow[\Delta]{460^\circ C} \text{Anatase} \xrightarrow[\Delta]{470^\circ C} \text{Rutile}$$

TiO_2 is commonly used commercially as pigment in white paint. Recently, much attention has been diverted to its electrical properties. In the presence of hydrogen or in its non-stoichiometric form, it behaves as n-type semiconductor with resistivity between 10^3 to $10^8 \Omega$cm which decreases with increasing temperature. However, it is an insulator in its stoichiometric form. Earle [9] and later Cronemeyer [74] concluded that conduction proceeds via free electrons in the TiO_2 pellet (formed from TiO_2 powder under pressure) and synthetic rutile crystal, rather than holes as in other types of defect semiconductors. Breckenridge and

Fig 18: Structure of anatase and rutile TiO_2.

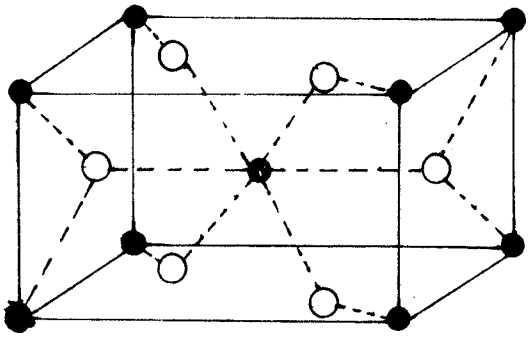

RUTILE

● = Titanium

○ = Oxygen

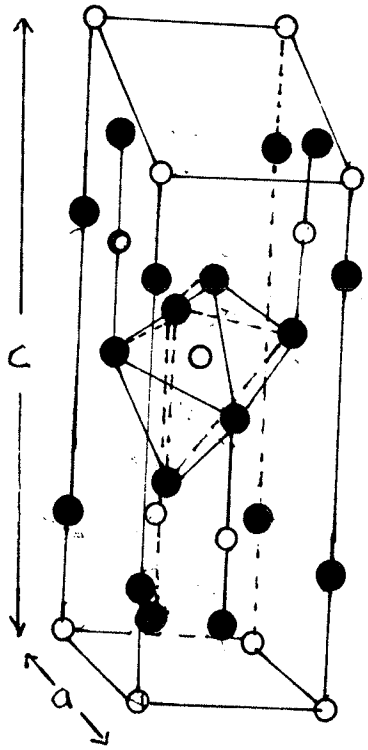

ANATASE

○ = Titanium

● = Oxygen

Hosler [10] suggested that conduction in single crystal TiO_2 (rutile) reduced by hydrogen at high temperature is attributed to impurity or defect bands. Similarly, Castro and Hollander [77] working on rutile TiO_2 concluded that the impurity band is the principal means of conduction. Hasiguti et al. [12], in 1961, proposed that conduction proceeds via Ti^{3+} species formed by the reduction of Ti^{4+} species by hydrogen. At very low temperature ($\approx$20K), conduction is via the impurity band. Apparently, most of the literature available today is focused on rutile TiO_2- single crystal or pellet for obvious reason. Nevertheless, there were a few studies conducted on anatase TiO_2. Iwaki and Miura [78] studied the properties of anatase TiO_2 by measurement of heat of immersion in water but it was not until recently that some conductivity studies were conducted. Harris [22] constructed a hydrogen detector using polycrystalline anatase TiO_2 loaded with platinum. He found that the conduction is purely electronic, the conduction electron arising from the ionisation of hydrogen atoms chemisorbed on the surface. The response to hydrogen was found to be relatively slow at room temperature but increases slightly with increasing temperature. Gesser et al. [21] constructed a hydrogen detector utilizing monolithic amorphous (anatase like) Porous Titania Glass (PTG) loaded with palladium. Conduction is attributed to the formation of Ti^{3+} species by the conversion of O_2^- species to OH^- and subsequently to water in the presence of hydrogen. The electron released is used to reduce Ti^{4+} to Ti^{3+}. In this chapter, temperature coefficient studies on reduced plain and photodeposited PTG will be presented. The effect of Soxhleting, evacuation, exposure to oxygen, water vapour, hydrochloric acid vapour, etc. on platinum loaded PTG will be discussed.

5-2. Experimental

5-2.1 Preparation of sample-PTG410R

A piece of PTG300R was annealed to 410°C at 50°C/hour. When the annealing temperature reached 410°C, it was maintained (total annealing time was fourteen hours. Annealing was done at Chemistry Department, University of Manitoba, Winnipeg) and subsequently cooled to room temperature in the oven (twelve hours). The titania glass was carefully sliced into rectangular strips (approximately 1 mm x 10 mm, 1 mm thick) using a sharp razor. These strips were Soxhleted drastically (seventy-two hours), changing the water every twelve hours. The strips were air-dried under fluorescent lamp and this glass was referred as PTG410R. Note that PTG300R which was annealed before was subjected to similar treatments except for the annealing temperature limit.

5-2.2 Construction of hydrogen detector-M/PTG (M = Pd, Pt, Rh) by photodeposition

Strips of PTG410R were soaked in chloroplatinic acid ([H_2PtCl_6] = 1g/100 mL, Alfa Inorganics, Ventron), palladous chloride ([K_2PdCl_6] = 1g/100 mL, Fisher certified reagent) or rhodium chloride ([$RhCl_3$] = 1g/100 mL, Fisher certified reagent) solutions according to the format below:

Solution	Soaking Time/second	Detector
H_2PtCl_6	300,450,600	Pt/PTG
K_2PdCl_6	300,450,600	Pd/PTG
$RhCl_3$	300,450,600	Rh/PTG

The soaked strips were immersed in methanol (Fisher certified reagent) and subjected to high power ultra-violet irradiation (5-10 minutes). The photodeposited glass was removed from the methanol solution and left to air-dry (10-15 minutes). The detectors were washed with doubly distilled water a few times and air-dried under a fluorescent lamp (1 hour).

5-2.3 The response of M/PTG (M = Pt, Pd, Rh) to hydrogen/air mixtures

A circuit was set up as illustrated in Fig. 19.

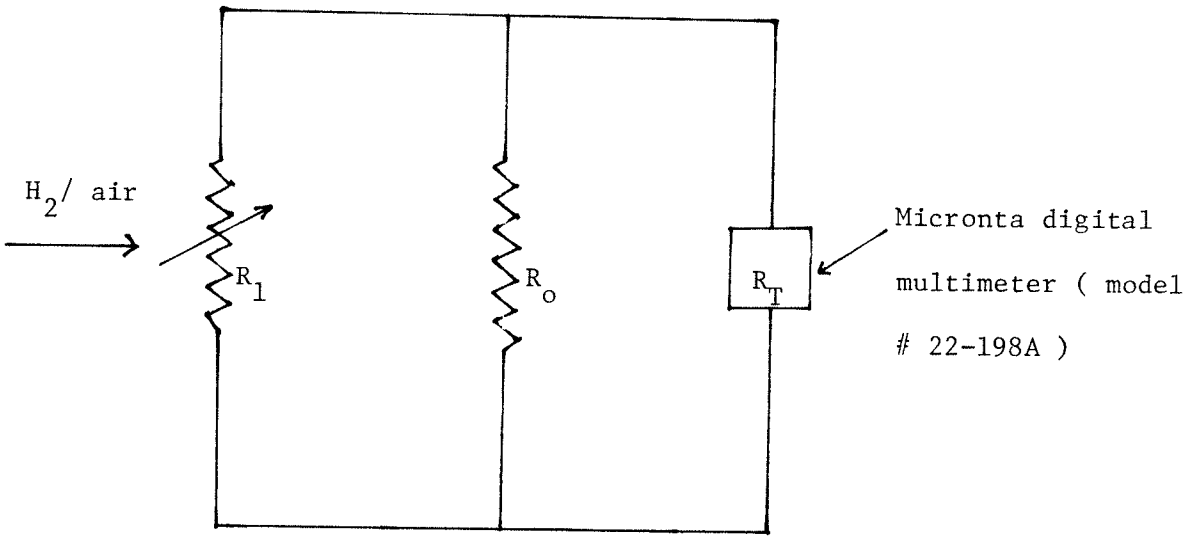

R_T = resistance of complete circuit

R_1 = resistance of M/PTG

R_0 = base resistance (between 19.35 - 19.43 M).

Fig. 19. A schematic circuit diagram used to monitor the response of M/PTG to H_2/air (CO).

In the above circuit, the resistors were arranged in parallel. This was used to bring the measured resistance onto the 20 MΩscale of the multimeter.

The base resistance was first noted prior to any experiments. A detector was then attached to the gold clips (soldered to tungsten electrodes) and the "holder" (see Fig. 20) subsequently mounted to the high vacuum system. Leads were then connected to the tungsten electrodes. The resistance was noted when it ceased to fluctuate. The system (containing 103 cm^3 air) was stirred electromagnetically and an appropriate amount (0.19%, 0.67%, 0.88%, 1.43%, 1.89%, 2.81%, 3.71%) of hydrogen (Linde, purity = 99.95%) was injected into the system via the septum using a syringe (B-D plastipak). The resistance was monitored every minute until the resistance stabilized. The detector was then exposed to air and the resistance noted (every minute) until it stabilized.

5-2.4 The response of Rh/PTG to carbon monoxide

The procedure for this experiment was identical to section (5-2.3) except that carbon monoxide (Matheson, purity = 99.50%) was used instead of hydrogen/air mixture. [The"recovery" experiment, that is exposing the detector to air,was not done as carbon monoxide is a health hazard]).

5-2.5 The response of Pt/PTG to hydrogen after:

a) Soxhleting

Fig 20: A schematic diagram of the flow system used for conductivity studies.

T = Stopcock. M = Manometer.

MLNT = To main manifold with liquid nitrogen trap.

MS = Magnetic stirrer.

RS = Rubber septum.

WE = Tungsten electrode.

H = "holder".

D = Detector.

GS = Gold clips.

S = Stopper.

"Reaction chamber" = Section used to monitor the response of detector to gases.

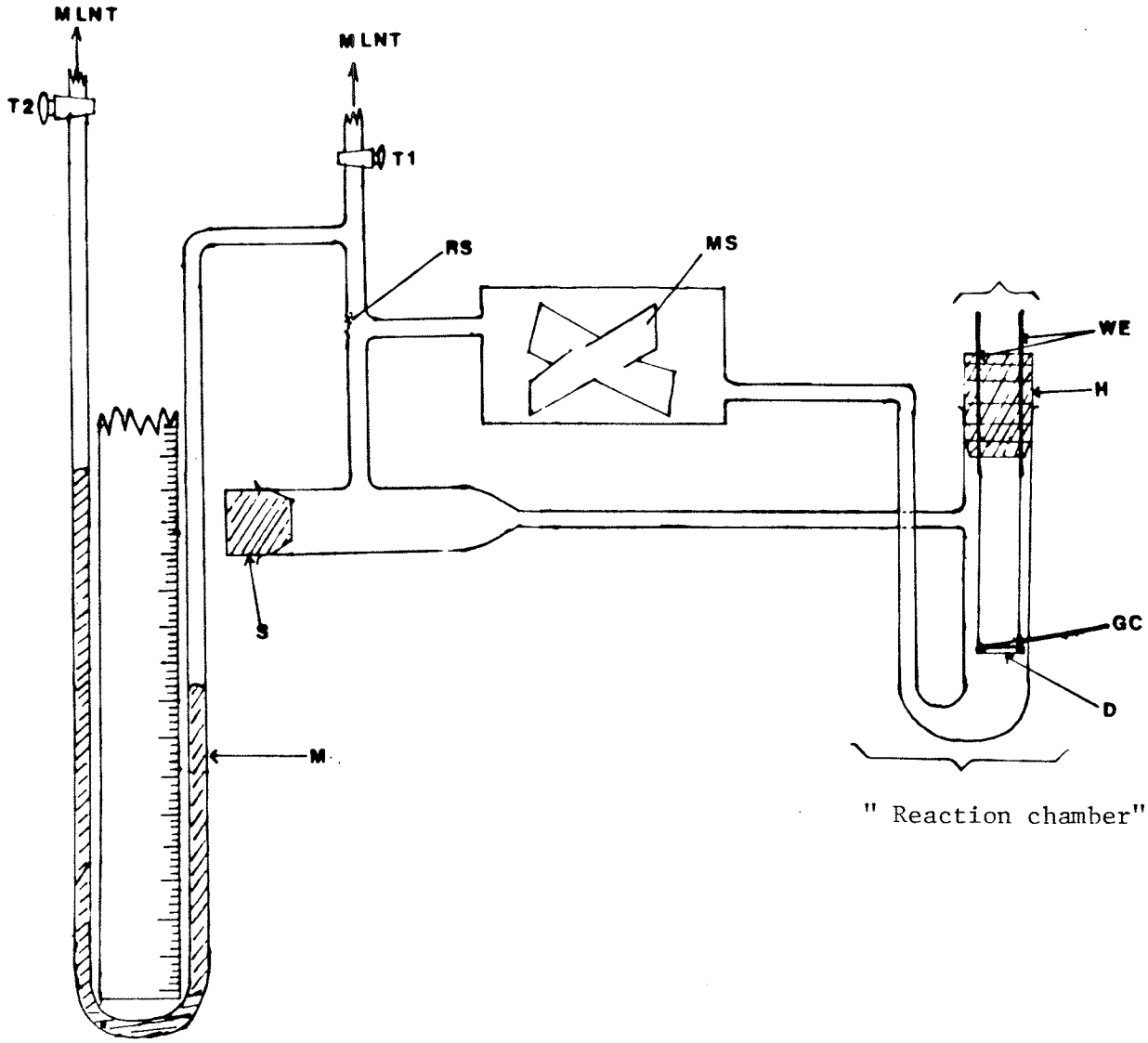

" Reaction chamber"

Pt/PTG was soxhleted (12 hours) and then air-dried under a fluorescent lamp (1 hour). It was then attached to the electrodes and mounted to the vacuum system. Leads were then connected to the electrodes and the system evacuated (3 minutes). Stopcock T (see Fig. 20) was then closed and an appropriate amount of hydrogen (as mentioned in section(5-2.3)) was introduced into the system. The resistance was noted (every minute).

b) Exposure of Pt/PTG to hydrochloric acid vapour

The detector was exposed to hydrochloric acid vapour ([HCl] = 6 mol dm^{-3}, Fisher certified reagent) by suspending it above the solution. The response to hydrogen was monitored as outlined in section(5-2.3).

c) Prolonged evacuation

The system was evacuated with the detector attached to the electrodes (12 hours). Stopcock T (see Fig. 20) was closed and the response of the detector to hydrogen was monitored as outlined in section (5-2.3).

d) Exposure of Pt/PTG (from prolonged evacuation) to oxygen and water vapour

The entire system was evacuated (12 hours). Stopcock T was then shut and 2 cm^3 of oxygen (Linde, purity = 99.60%) was admitted and left to stand (2 minutes). The entire system was then evacuated (3 minutes) and the response to pure hydrogen was then monitored according to the procedure outlined in section(5-2.3). (The effect of water vapour was monitored according to the procedure outlined above. Instead of oxygen,

a tiny amount of doubly distilled water ($\approx$0.1 mL) was introduced into the system via the septum by injection).

5-3 Temperature coefficient studies

5-3.1 M/PTG (M = Pt,Pd) in the presence of air/hydrogen mixture

A detector was attached to the electrodes and then mounted in the vacuum system (volume = 103 cm^3) which contained air (volume of air = 103 cm^3, pressure of system was one atmosphere). The system was stirred electrically (by "magnetic" fan) and hydrogen (4.0%) was introduced into the system. The "reaction chamber" was then immersed in an insulated hot water-bath (70-80°C) and the resistance noted when equilibrium was attained (5-10 minutes). The procedure was repeated by immersing the "reaction chamber" in an insulated water bath (room temperature), insulated ice-bath (0°C) and ethanol (Fisher certified reagent) - dry ice bath (-78°C), noting the resistance each time when equilibrium was achieved.

5-3.2 Electroreduced plain PTG300R

A strip of PTG300R (0.1 cm x 1 cm, 0.1 cm thick) was attached to a gold clip (cathode, Pt electrode was the anode) and immersed in hydrochloric acid solution ([HCl] = 1 x 10^{-3} mol dm^{-3}, Fisher certified reagent). It was reduced electrolytically (current $\simeq$ 5mA) for a specified period (10s - 140s). The reduced PTG was quickly rinsed in doubly distilled water and attached to the electrodes immediately. The entire system was then evacuated and the pressure of the system monitored using the mercury McLeod gauge. When appropriate pressure was achieved (usually 0.001 mm Hg), stopcock T was shut and the "reaction

chamber" immersed in hot water bath, water bath, ice bath and ethanol-dry ice mixture, noting the resistance each time when equilibrium was attained.

5-4 Treatment of data

In this text, PTG either plain or loaded with noble metal is assumed to be a resistor and its behaviour is ohmic (below 9V). Since the resistors were arranged in parallel (Fig. 19), then the resistance (R_1) of titania glass is given by

$$\frac{1}{R_T} = \frac{1}{R_1} + \frac{1}{R_o} \qquad (5.01)$$

where R_0 = base resistance

R_T = resistance of entire circuit

R_1 = resistance of PTG

Rearranging and simplifying equation (5.01)

$$R_1 = \frac{R_o \times R_T}{R_o - R_T} \qquad (5.02)$$

Resistivity $\mathcal{K}$ is given by

$$\mathcal{K} = \frac{R_1 \times A}{L} \qquad (5.03)$$

where A = cross sectional area of resistor

L = length of resistor

But conductivity σ is given by the reciprocal of $\mathcal{K}$

$$\sigma = \frac{1}{\mathcal{K}}$$

$$= \frac{L}{R_1 \times A} \qquad (5.04)$$

Also

$$\sigma = ne\mu \tag{5.05}$$

where n = number of conducting electrons per unit volume or holes in the normally filled valence band

μ = mobility of electron

and e = charge of electron [cited from ref.[79]]

For an intrinsic semiconductor, the number of electrons n is given by [79]

$$n = [2(2\pi mkT/h^2)]^{3/2} \exp(-E_g/2kT)$$

$$= A \exp(-E_g/2kT) \tag{5.06}$$

where Eg = energy gap between conduction and valence band

m = mass of electron

k,h = Boltzmann and Planck constants respectively,

T = temperature

and $A = [2(2\pi mkT/h^2)]^{3/2}$

If the semiconductor contains defect, then

$$n' = A\exp(-E/kT) \tag{5.07}$$

where E being the activation energy for the excitation of electrons from the Fermi level E_f (which is "pinned" for sufficiently large defect density at the impurity level) to the conduction band E_c.

Hence

$$n \approx A \exp(-E/kT) \qquad (5.08)$$

Substitute equation (5.08) into (5.05) and simplifying,

$$\sigma = A \exp(-E/kT).e\mu$$
$$= B\exp(-E/kT) \qquad (5.09)$$

where $B = Ae\mu$

An Arrhenius type plot is obtained if $\ln \sigma$ is plotted against the reciprocal of temperature, the slope corresponding to (-E/k) and intercept equals B. The calculations were done by Apple II computer using the programme written in BASIC language (see appendix 3).

5-5 Results

The soaked samples darkened upon irradiation by ultra-violet light. This darkening was attributed to the photodeposition of a uniform layer of noble metal (Pd,Pt,Rh) on the surface of titania glass (PTG410R). No significant change in the resistance was observed. The response of Pt and Pd detectors to various concentration of hydrogen at room temperature are illustrated in Fig. 21.1-21.4. In most cases the formation of a plateau commenced after the first minute. On the third minute, more than 90% response was observed with one exception (Pt/PTG, 450s soaking, $[H_2]$ = 1.90%) which was caused by uneven flow of hydrogen in the system in the inital stage. The response to hydrogen was less dramatic at lower hydrogen concentration but a shorter recovery

Fig 21.1: Response of Pt/PTG(600s soaking) to various concentration of hydrogen in air at 25°C.

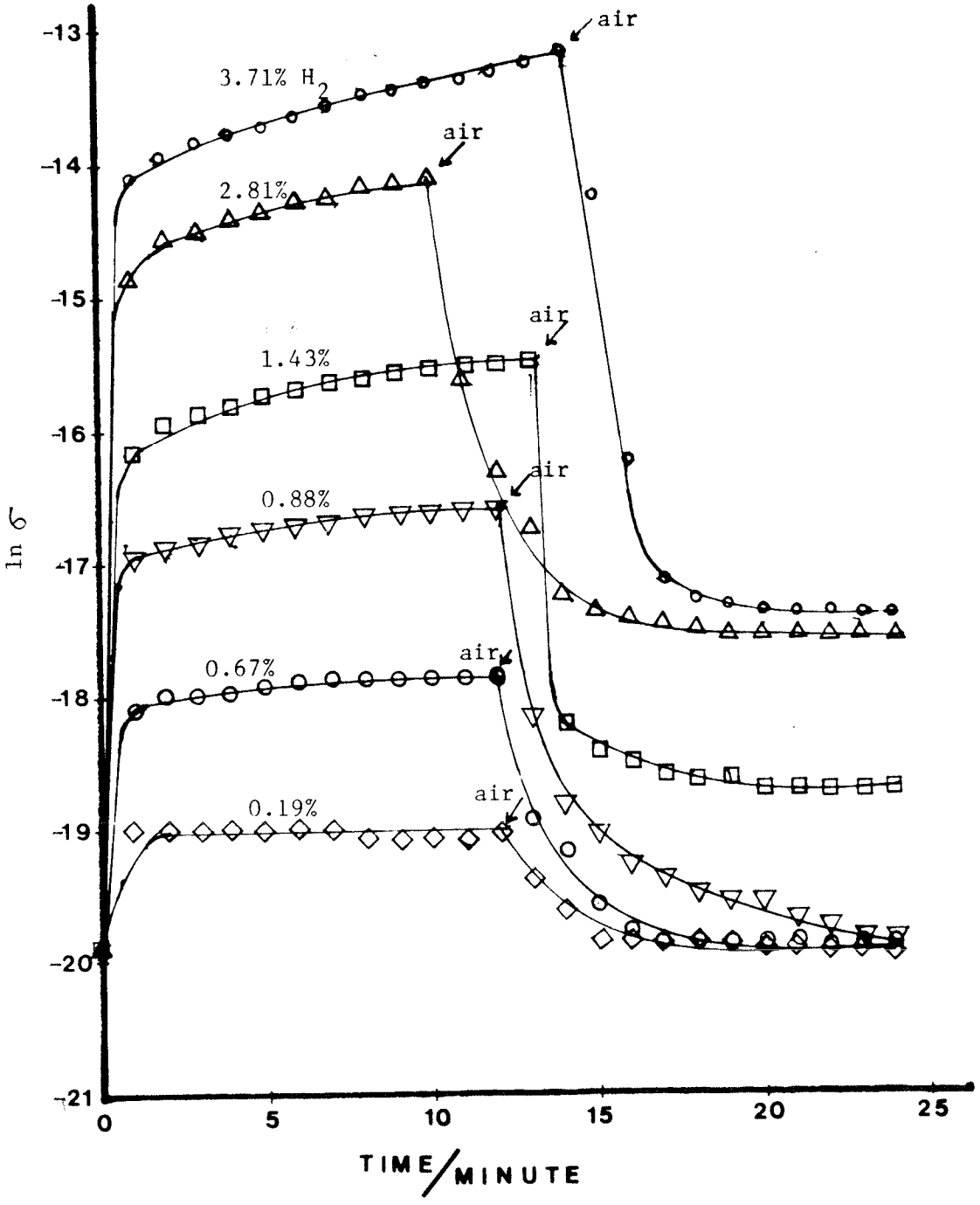

Fig 21.2: Response of Pt/PTG(450s soaking) to various concentration of hydrogen in air at 25°C.

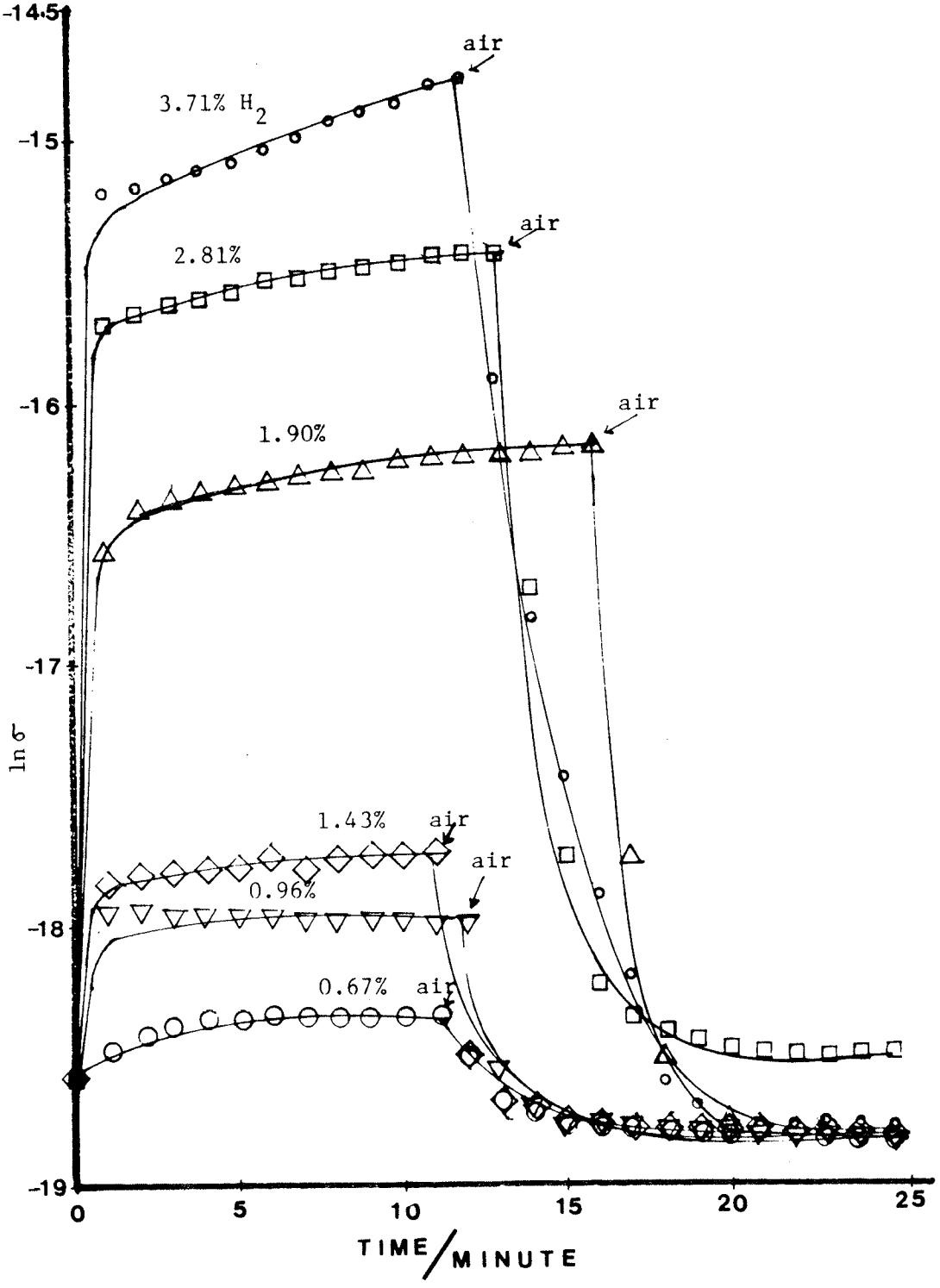

Fig 21.3: Response of Pd/PTG(450s soaking) to various concentration of hydrogen in air at 25°C.

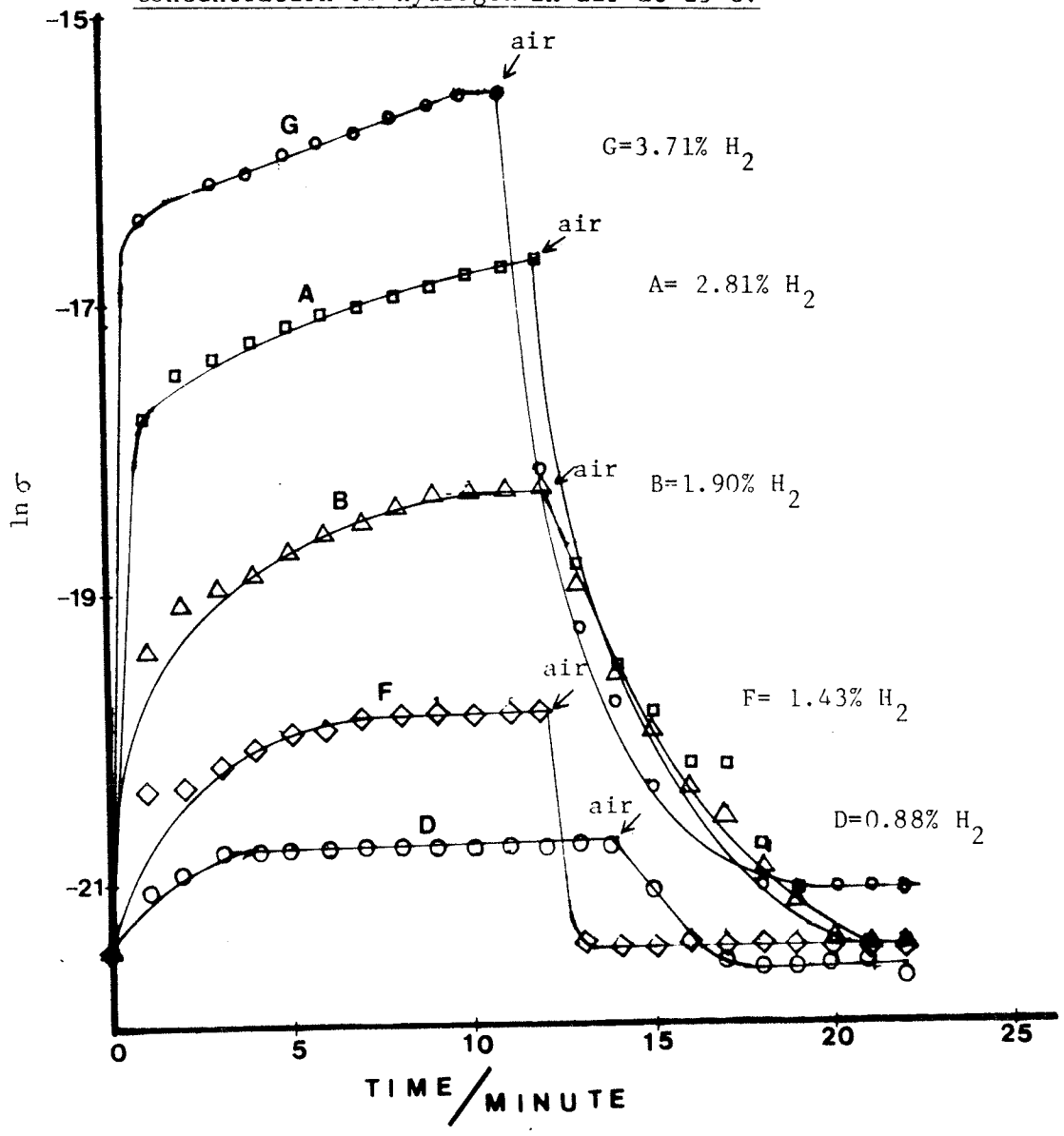

Fig 21.4: Response of Pd/PTG(600s soaking) to various concentration of hydrogen in air at 25°C.

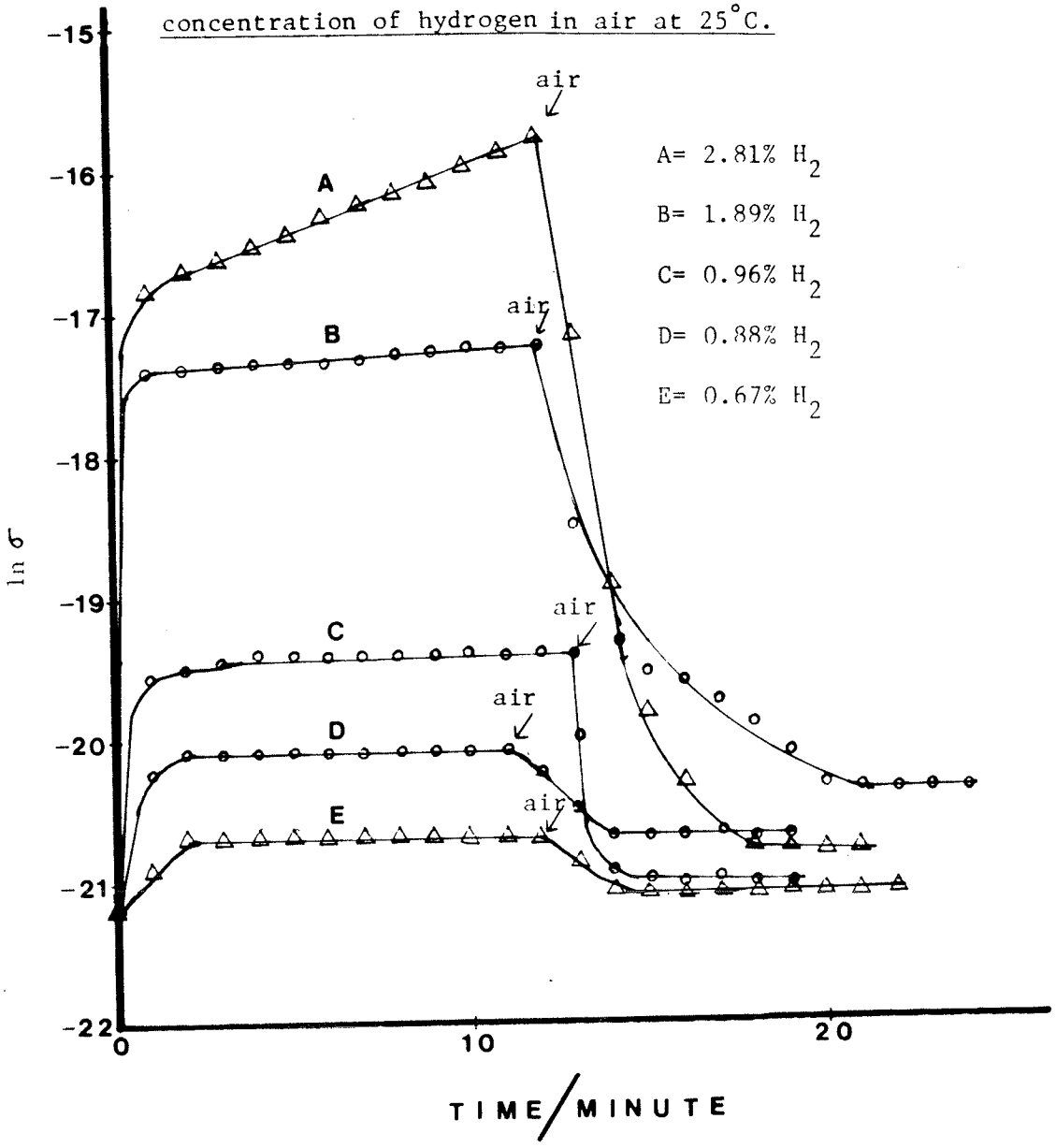

time was required. As hydrogen concentration increased, the response was more dramatic as illustrated by the increasing electrical conductivity values. However, the recovery time increased slightly. This result suggested that electron concentration in the conduction band increases as hydrogen concentration increases.

Clearly it can be seen that the platinum detectors were more sensitive than the palladium counterpart to hydrogen. Sensitivity increased with loading and recycling in hydrogen. Attempts to use lowly loaded (less than 300s soaking) detectors to detect hydrogen at lower concentration was very discouraging. Several attempts to utilise rhodium loaded PTG410R as hydrogen detector proved fruitless due to its poor response to hydrogen relative to platinum or palladium detectors. An attempt to use Rh/PTG to detect carbon monoxide was extremely discouraging due to poor response and inhibition of the sensitivity by the gas. Exposing the inhibited detector to air (five days) failed to revive its sensitivity, not even to pure hydrogen. No further experiment was conducted thereafter.

The detectors "shocked" after being soxhleted drastically. In other words, the resistance of the detector was very large. Prolonged evacuation and exposure to hydrochloric acid vapour inhibited the response of platinum detector to hydrogen too, the latter (HCl) case causing poisoning to the detector. The resistance of the detector decreased after exposure to hydrochloric acid vapour (see Table 5). Soxhleting and exposing the detector to air (five days) failed to recover its response as a detector-even pure hydrogen was not effective. Partial recovery was achieved by soaking the detector in hydrogen peroxide. The effect of oxygen and water vapour on platinum detector

Table 5 : Resistance of M/PTG (M = Pt, Pd, Rh) before and after exposure to HCl vapour.

Sample	Resistance before exposure to HCl / MΩ	Resistance after exposure to HCl. / MΩ
Pd/PTG	2500	77
Pt/PTG	125	110
Rh/PTG	1880	410

Exposure time = 45 minutes

Concentration of HCl = 6 mole dm^{-3}

All the above samples were prepared according to the format listed in 5-2.2, page 105 except that the soaking time was only 300 seconds for each case.

PTG in the above table indicates that PTG 410R was used as the " support " for the noble metals.

(which was evacuated) is illustrated in Fig. 22-23. In the absence of oxygen and/or water vapour, platinum detector was inert to pure hydrogen. The response was initiated upon the introduction of either oxygen or water vapour, indicating that the above mentioned ingredients are vital in the detection of hydrogen by Pt/PTG. Plain PTG410R was inert to hydrogen/air mixture, suggesting that noble metal is a necessity for the construction of M/PTG (M = Pt, Pd, Rh) hydrogen detector.

The electroreduced titania glass (PTG300R) was very susceptible to oxidation. The colour varied from blue to purple, depending on the extent of reduction. This coloration was attributed to the formation of Ti^{3+} species [21,32] or the colour centred species TiO_2^- [80]. Exposing the reduced glass to air restored the original colour (slightly yellowish), indicating that Ti^{4+} was formed. Fig. 24-25 illustrate the changes in electrical conductivity as a function of the reciprocal absolute temperature of electroreduced and photodeposited (PTG410R) titania glass. A reasonable linear relationship is observed according to equation (5.09). The results are listed in Table 6-7. The activation energy of conduction E, decreased as reduction time increased. This may represent an authentic decrease in the energy level of the defect, but there seems little physical basis for this assumption. We assume instead that it results from a decrease in the concentration of defects at an energy E below the conduction band, such that the Fermi level becomes "unpinned" by these centres and is controlled by secondary impurity or defect centres. As a result, conductivity increased as reduction time increased. No attempt was made to utilize PTG360R and PTG410R for the above temperature coefficient studies.

Fig 22: The response of evacuated Pt/PTG410R to hydrogen after various treatments.

P = Evacuate, that is having the mercury diffusion pump and rotary pump evacuating the vacuum system.

O = Addition of pure oxygen (2 cm^3).

AR = Addition of pure argon (2 cm^3).

H_2 = Addition of pure hydrogen (6 cm^3).

E = The response of oxygen treated Pt/PTG410R (evacuated for 12 hours, 80 seconds soaking in chloroplatinic acid) to hydrogen (6 cm^3)

F = The response of argon treated Pt/PTG410R (evacuated for 12 hours, 80 seconds soaking in chloroplatinic acid) to hydrogen (6 cm^3).

K = The response of oxygen treated Pt/PTG410R (evacuated 12 hours, 80 seconds soaking in chloroplatinic acid) to argon (2 cm^3).

Volume of system = 103 cm^3.

Pressure of system = 1 atmosphere.

Temperature of system = 25°C.

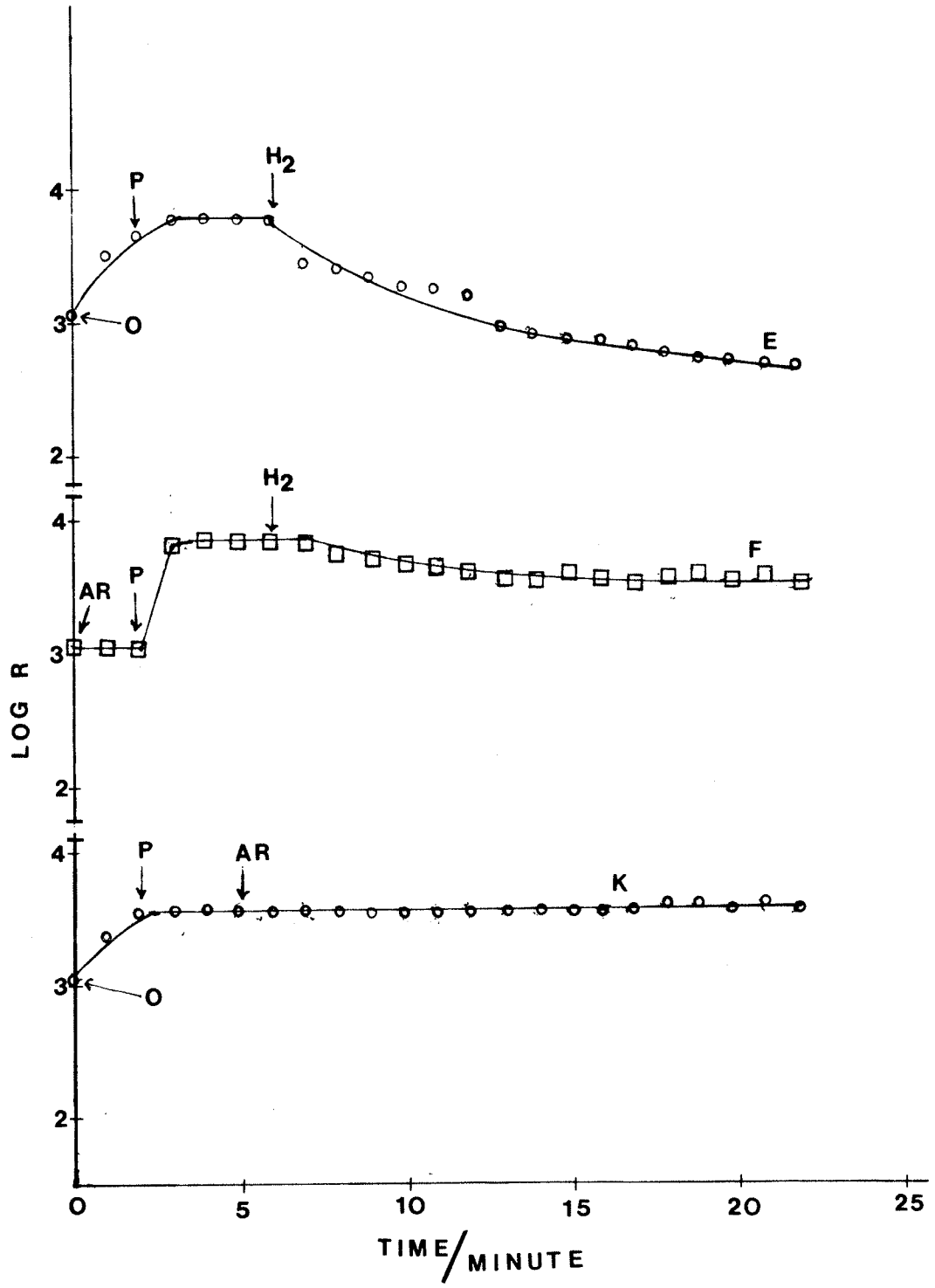
LOG R
4
3
2
P
H_2
O
E
F
AR
K
0
5
10
15
20
25
TIME/MINUTE

Fig 23: The response of Pt/PTG410R to hydrogen after various treatments.

HCl = The response of HCl treated Pt/PTG410R (80 seconds soaking in chloroplatinic acid to pure hydrogen (6 cm^3).

J = Introduction of doubly distilled water (0.1 mL).

P = Evacuate, that is having the mercury diffusion pump and rotary pump evacuating the vacuum system.

H_2 = Addition of pure hydrogen (6 cm^3).

W = The response of moisture treated Pt/PTG410R (evacuated 12 hours, 80 seconds soaking in chloroplatinic acid) to pure hydrogen (6 cm^3).

N = The response of unsoxhleted Pt/PTG410R (80 seconds soaking in chloroplatinic acid) to pure hydrogen (2 cm^3).

G = The response of evacuated Pt/PTG410R (80 seconds soaking in chloroplatinic acid) to pure hydrogen (2 cm^3).

Volume of system = 103 cm^3.

Pressure of system = 1 atmosphere.

Temperature of system = 25°C.

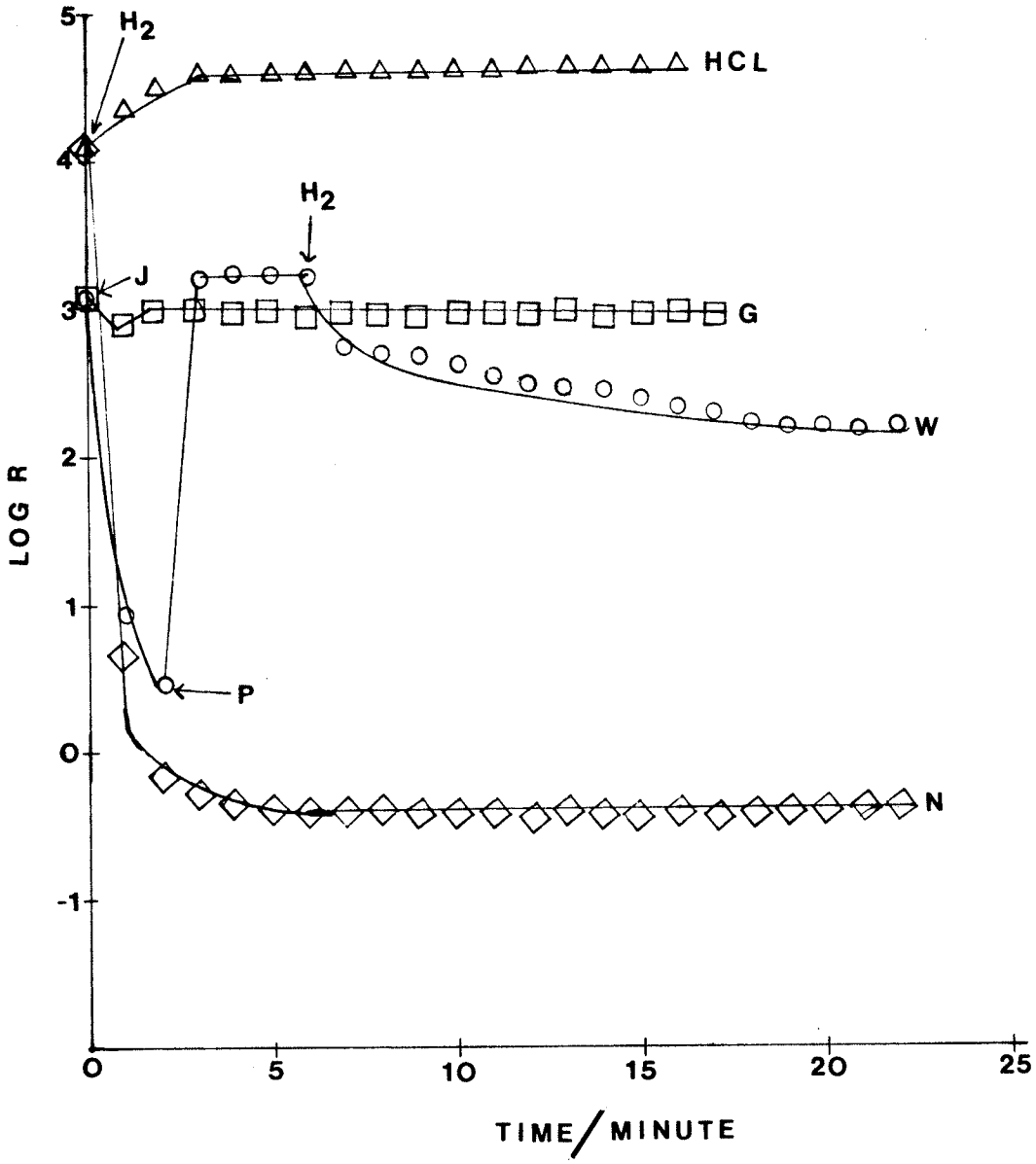
5
4
3
2
1
0
-1
LOG R
H_2
H_2
HCL
G
W
N
J
P
0
5
10
15
20
25
TIME / MINUTE

Fig 24: Plots of the logarithm of electrical conductivity(σ) as a function of the reciprocal absolute temperature of electroreduced PTG 300R.

A = Arrhenius plot of PTG 300R electroreduced for 140 second

B = Arrhenius plot of PTG 300R electroreduced for 100 second

C = Arrhenius plot of PTG 300R electroreduced for 110 second

D = Arrhenius plot of PTG 300R electroreduced for 110 second

E = Arrhenius plot of PTG 300R electroreduced for 130 second

F = Arrhenius plot of PTG 300R electroreduced for 80 second

G = Arrhenius plot of PTG 300R electroreduced for 70 second

H = Arrhenius plot of PTG 300R electroreduced for 50 second

I = Arrhenius plot of PTG 300R electroreduced for 30 second

J = Arrhenius plot of PTG 300R electroreduced for 10 second

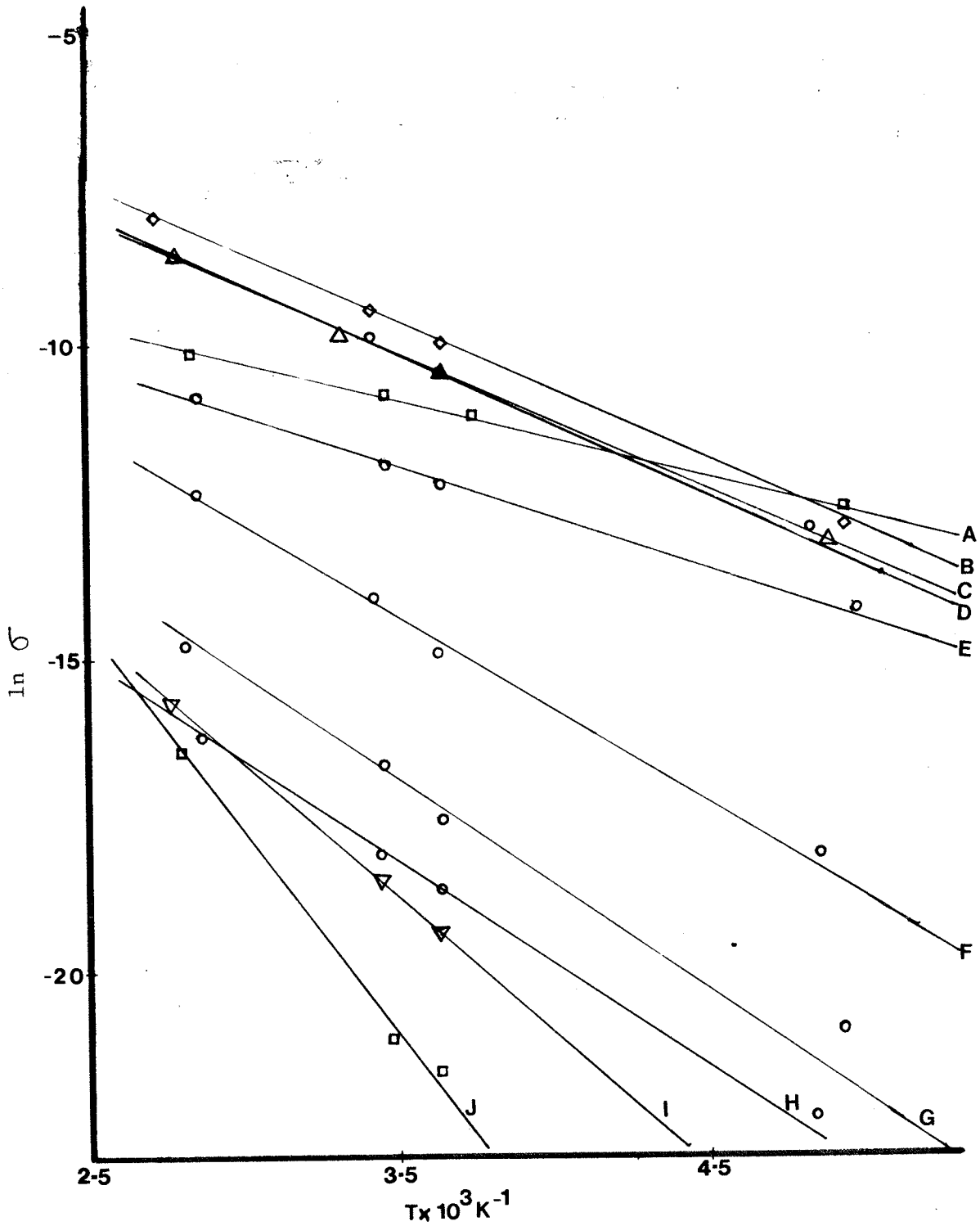
-5
-10
-15
-20
ln σ
2·5
3·5
4·5
T x 10³ K⁻¹
A
B
C
D
E
F
G
H
I
J

Fig 25: Plots of logarithm of electrical conductivity(σ) as a function of the reciprocal absolute temperature of photodeposited PTG 410R.

A = Arrhenius plot of Pt/PTG 410R, soaked in chloroplatinic acid for 450 second.

B = Arrhenius plot of Pt/PTG 410R, soaked in chloroplatinic acid for 600 second.

C = Arrhenius plot of Pd/PTG 410R, soaked in palladous chloride solution for 600 second.

D = Arrhenius plot of Pt/PTG 410R, soaked in chloroplatinic acid for 300 second.

E = Arrhenius plot of Pd/PTG 410R, soaked in palladous chloride solution for 450 second.

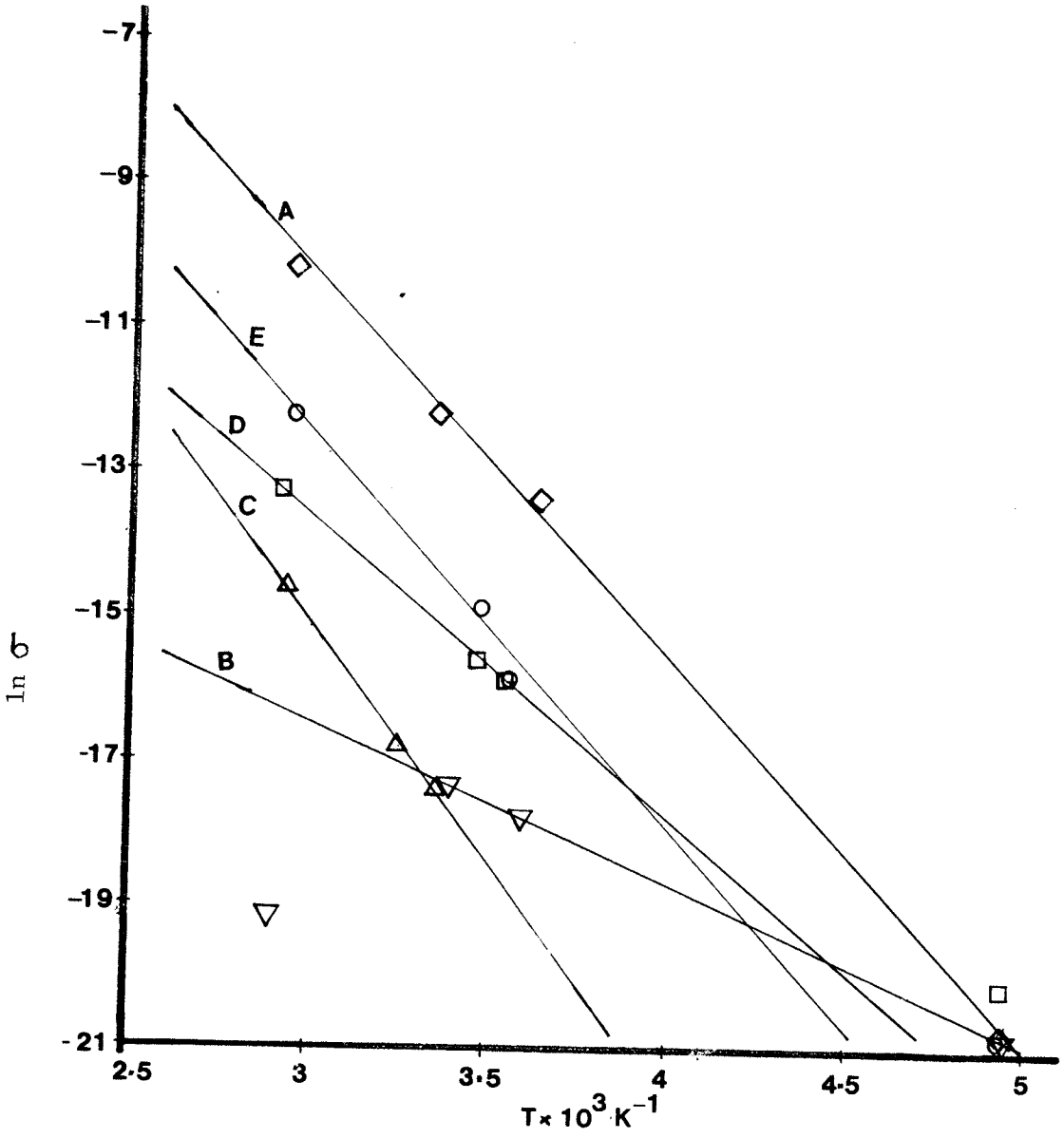
-7
-9
-11
-13
-15
-17
-19
-21
ln σ
A
E
D
C
B
2·5
3
3·5
4
4·5
5
T× 10³ K⁻¹

Table 6 : Compilation of energy seperation (E) between the conduction band (E_c) and the Fermi level (E_f) of electroreduced PTG 300R*

Reduction time / second	E / KJ mole^{-1}	$E_c - E_d$ / KJ mole^{-1}
140	9.70	19.40
130	11.94	23.88
110	15.86	31.72
100	18.99	37.98
80	21.22	42.44
70	22.90	45.80
50	24.76	49.52
30	36.32	72.64
10	56.28	112.56

*The samples were electroreduced in dilute HCl solution (0.001M) according to the procedure outlined in section 5.32, page 110.

Table 7: Compilation of conduction energy (E) of M/PTG (M = Pd, Pt) with various loading in the presence of H_2 (4%)/ air mixture.*

Sample	Soaking time / second	E / KJ mole^{-1}
Pt/PTG	600	23.61
	450	40.33
	300	29.78
Pd/PTG	600	35.89
	450	28.73

* In the above table, PTG410R was used as a "support" for the noble metals. The samples were prepared according to the format listed in section 5-2.2, page 105.

5-6 Discussion

When TiO_2 is immersed in methanol, some of the terminal hydroxyl group will react to form Ti—O—CH_3 species [31] as

$$Ti^{4+}\text{—}OH + CH_3OH \longrightarrow Ti^{4+}\text{—}O\text{—}CH_3 + H_2O \qquad (5a)$$

An analogous reaction will occur to PTG410R when immersed in methanol. Upon irradiation by ultra-violet light, photodeposition of a uniform layer of noble metal occurred which is attributed to the reduction of Ti^{4+} species to Ti^{3+} species which in turn reduces the noble metal cation to it's metallic form [21].

$$\overset{O_2^-}{\vdots}\!Ti^{4+}\text{—}O\text{—}CH_3 \xrightarrow[CH_3OH]{h\nu} Ti^{3+} + CO_2 + \frac{3}{2}H_2 + \frac{1}{2}H_2O$$

$$n\ Ti^{3+} + M^{n+} \xrightarrow[CH_3OH]{} n'\ Ti^{4+} + M^{o} \qquad (5b)$$

where M = noble metal

n,n' = integer

Under these circumstances, methanol serves as an "electron trap", capturing the electron released from reaction (5b) which is used for the reduction of Ti^{4+} to Ti^{3+}. Apart from carbon dioxide, hydrogen and oxygen, methanol, methanal and methanoic acid are also formed during this process [81-82].

The feasibility of reaction (5b) is determined by the Gibbs free

energy (ΔG).

$$\Delta G = -nFE \qquad (5.10)$$

where n = moles of electrons

F = Faraday constant

and E = the standard electrode potential difference between Ti^{3+}(-0.209v) and the cation (Pt^{4+} = 1.44V, Pd^{2+} = 0.68V, Rh^{3+} = 0.44V)

It is well known that hydrogen will chemisorb dissociatively on the platinum surface [22]. Electron Spin Resonance (ESR) studies on PTG indicates that O_2^- species will interact with hydrogen atom via hydrogen spillover, forming a peroxy type species which has been observed in photochemical studies on TiO_2 by Gonzalez-Elipe et al. [83]. Gesser et al. [32] proposed that this interaction causes an electron transfer as

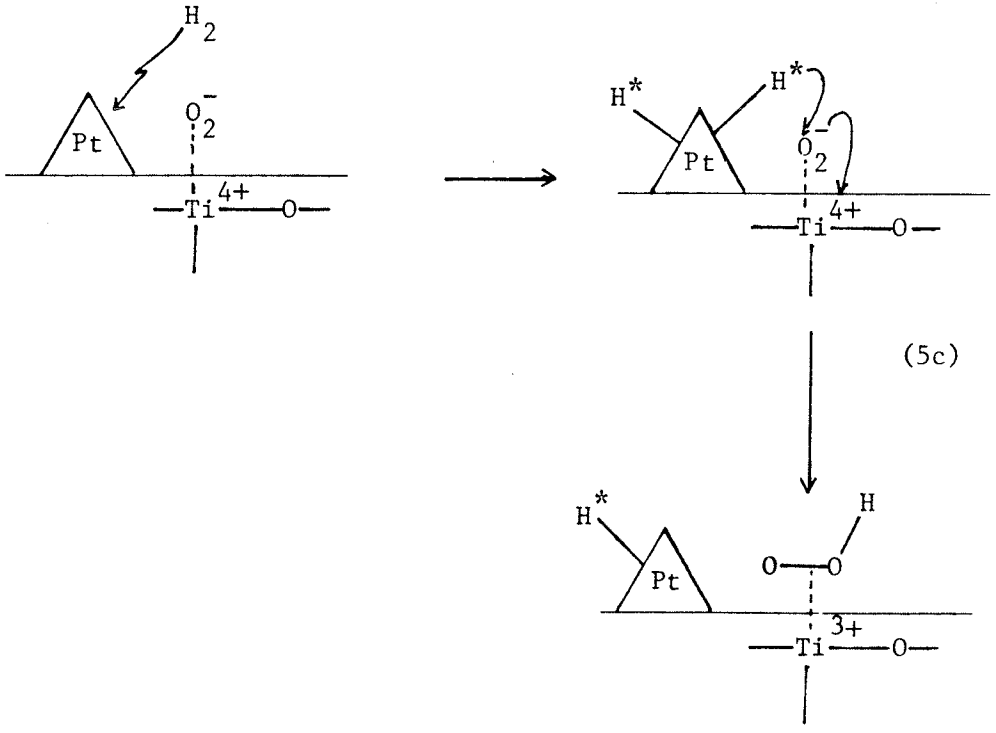

resulting in the formation of Ti^{3+} which diffuses readily in the lattice. Increasing the hydrogen concentration enhances the formation of Pt-H species, thus further facilitating the formation of the donor species Ti^{3+} via hydrogen spillover. As Ti^{3+} concentration increases, conductivity (σ) therefore increases too. Less dramatic change in σ in the later stages is caused by the depletion of O_2^- species, the prerequisite for hydrogen spillover. Exposing the detector to air regenerates the sensitivity. Evidence based on ESR studies in Pd/PTG system indicates that Pd/PTG...O_2^- species is formed [32], which thus serves as the recovery step for the hydrogen detector.

Palladium is known to adsorb tremendous amount of hydrogen relative to it's own volume as compared to platinum. But why Pt/PTG was a better hydrogen detector than Pd/PTG is still unclear, presumably it could be due to the fact that platinum could be a better hydrogen spillover promoter than palladium. The increasing sensitivity of the detectors by recycling is still unclear. Perhaps it could be due to the reduction of traces of cation to it's metallic state. However, this needs to be investigated further.

Carbon monoxide will chemisorb on rhodium surface and the response which was observed can be represented as

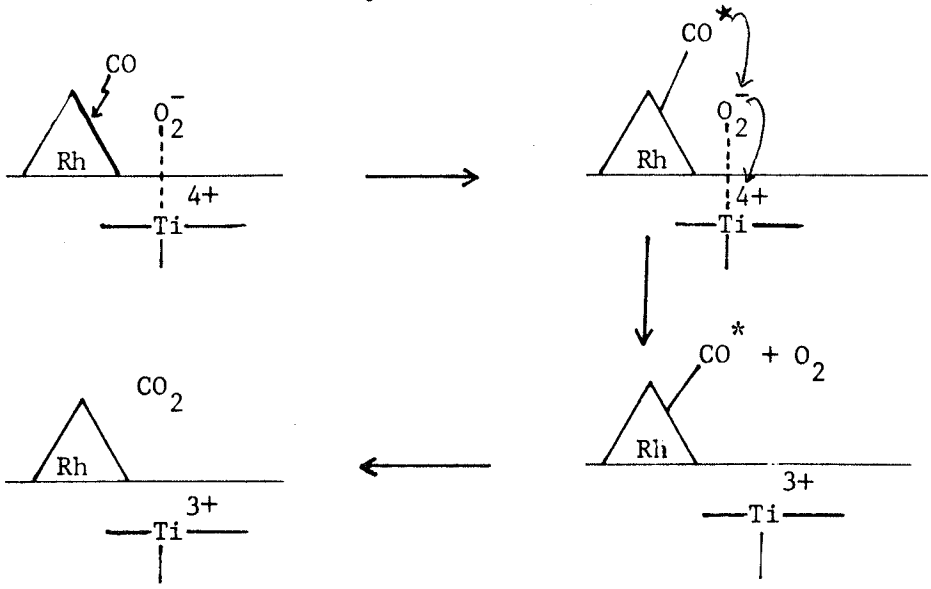

(5d)

Again O_2^- species serves as the prerequisite for Ti^{3+} formation. However, this proposal ought to be investigated further. Yates [23] noticed that carbon dioxide will chemisorb strongly on TiO_2 surface forming CO_2^- type species. Evacuation failed to remove this species but chemisorbed carbon monoxide was completely removed. Recently, Morterra et al. [84] confirmed Yates' identification but other species like bicarbonate type were also formed. Carbon dioxide is formed according to the proposed mechanism. Chemisorption of carbon dioxide on the surface of PTG can therefore occur. Whether the inhibition of Rh/PTG by carbon monoxide was caused by the CO_2^- species or bicarbonate type species has yet to be determined.

Exposure of Pt/PTG to hydrochloric acid vapour completely destroyed the detector. Jones and Hockey [85] found that the surface hydroxyl ions reacted with hydrochloric acid vapour as

$$Ti^{x+}\!\!-\!\!OH^- + HCl \longrightarrow H_2O + Cl^- \qquad (5e)$$

producing species like $Ti^{x+}\!\!-\!\!Cl$, $Ti^{x+}\!\!-\!\!Cl^-$, etc. As mentioned earlier, O_2^- species (which is basic) exists on the surface of PTG. Gesser and Kruczynski [32] have shown that O_2^- and OH^- species can interchange. Presumably the depletion of OH^- species by hydrochloric acid vapour somehow affects O_2^- species, perhaps by decreasing it's concentration on the surface of PTG. However, the direct reaction of O_2^- with hydrochloric acid cannot be ignored since the O_2^- species is basic.

The ease of removing O_2^- species from the surface of PTG was in excellent agreement with earlier work by Gesser and Kruczynski [32]. In the absence of O_2^- species, reduction of Ti^{4+} to Ti^{3+} is not possible. Strong evidence based on ESR studies by the above authors on Pd/PTG

system suggested that oxygen will interact with Pd/PTG to form $Pd/PTG...O_2^-$ species. In the presence of hydrogen, reduction of Ti^{4+} to Ti^{3+} occurs. Oxygen will interact with PTG, forming $PTG...O_2^-$ species. No reduction was observed suggesting that palladium is required to catalyse the reduction of Ti^{4+} to Ti^{3+}. This is in excellent agreement with the present work, suggesting that an identical reaction occurred with the Pt/PTG system upon the introduction of oxygem to the evacuated Pt/PTG.

The introduction of water vapour to the evacuated Pt/PTG system also revitalised the sensitivity of the detector to hydrogen. Earlier, Boudart and Levy [86] showed that the presence of water vapour promotes hydrogen spillover in Pt/WO_3 system. The authors suggested that a solvated proton is formed on the metal which then migrates to the support which serves as the proton acceptor. The proton is subsequently released to the reduction site. Thomson and Harvey [81] noticed that the activation energy of conduction decreases in the presence of moisture in Pt/SiO_2 system. The authors attributed this to increasing protonic conduction. Recently Ambs and Mitchell [88] reported an enhanced hydrogen spillover in a Pt/Al_2O_3 system in the presence of water vapour. They concluded that the OH group is produced via hydrolysis of Al-O bonds by the adsorbed water molecules on the alumina surface. Negative hydrogen spillover was observed in the absence of platinum. In any of the above mechanisms, conductivity is expected to decrease to a certain extent. Herrmann and Pichat [17] reported that the conductivity of platinum loaded TiO_2 increases with increasing platinum loading in the presence of hydrogen. Further investigation is thus required to validate the above proposal regarding the effect of

moisture to Pt/PTG, in particular the "revitalisation" of evacuated Pt/PTG to hydrogen response.

The activation energy of conduction (E) increases with increasing platinum or palladium loading except Pt/PTG with the highest loading (600 second soaking). This abnormality is attributed to the appearance of a quasimetallic nature whereby the uniform layer of platinum on the surface presumably behaves as a conductor which thus causes a decrease in conductivity. This behaviour becomes more apparent at higher temperature as illustrated in Fig. 25. Herrmann and Pichat [17], working on Pt/TiO_2 (anatase) inferred that this increase of E values with increasing loading was due to an "electron pumping" effect, that is an electron is being "pumped" from Ti^{3+} to platinum as

$$e + Pt \rightleftharpoons e_{Pt} \qquad (5f)$$

where e_{Pt} corresponds to an electron trapped by platinum. This is justified by the fact that the work function (ω) of reduced TiO_2 ($\approx$4.60 eV in vacuum) is less than platinum ($\approx$ 5.36 eV). Based on the above results, electron transfer could occur to Pt/PTG system in the presence of hydrogen as well. For the lowly loaded detectors, electrons must have been "pumped" from the shallower donor level (Ti^{3+}), hence E is small. In contrast, electrons have to be extracted from a deeper level, making E larger than the lowly loaded counterparts. In other words, the presence of palladium and platinum will no doubt influence the electronic properties of PTG410R drastically, judging from the results obtained and those of Herrmann and Pichat [17].

The redox reduction of PTG300R is described as:

At cathode

$$Ti^{4+} + e \longrightarrow Ti^{3+}$$

At anode:

$$4\ OH^- \longrightarrow O_2 + 2\ H_2O + 4e \qquad (5g)$$

As can be seen from the Arrhenius type plot of ln σ against the reciprocal absolute temperature (Fig. 24), reasonable straight lines are obtained in accordance to equation $\sigma = \sigma_0 \exp(-E_1/kT)$. This implies that reduced PTG300R behaves as an extrinsic n-type semiconductor in vacuum. Earlier Hasiguti et al. [12] also proposed that the conduction in rutile TiO_2 proceeds via electrons moving in the conduction band, not by the "hopping" mechanism utilising the trapped electrons. The authors indicated too, that the electrons are derived from the $3d^1$ state of titanium, that is Ti^{3+}. Therefore for a slightly reduced PTG, the number of conducting electrons in the conduction band is small since the concentration of Ti^{3+} is small. Hence conductivity σ is small and the Fermi level and the donor level are further apart. As the reduction time increases, more electrons are available to partake in the conduction process due to the increase in Ti^{3+} concentration. Conductivity thus decreases. Judging from the results obtained, it is probably the Fermi level position which is changing with E_c-E_d position remaining fixed. This implies that E_c-E_d position is independent of Ti^{3+} concentration. This result is in good agreement with earlier work

[10,74] and obeys the Meyer's rule which predicts a decrease in E as concentration of electron in the conduction band increases [cited from ref. [79]].

Though PTG300R was reduced electrolytically, the neutrality of the lattice has to be preserved somehow. Breckenridge and Hosler [10], working on rutile TiO_2 postulated the Ti^{3+} probably resides near the oxygen defect O_v which may arise from annealing, for example neutral centres such as $[O_v.2.Ti^{3+}]$, singly ionized centre $[O_v.Ti^{3+}]$ or free vacancies O_v^{2+} have been suggested. Iwaki [13] pointed out that oxygen vacancies which are produced by the removal of oxygen atoms in rutile TiO_2 will generate electrons which may act as donors. However, this explanation can be neglected since this will only occur when the sample is kept in vacuo at high temperature (>700°C) or in hydrogen whereas this work was conducted at room temperature. Pictorially, the location of the conducting species (Ti^{3+}) in reduced PTG300R can be represented as

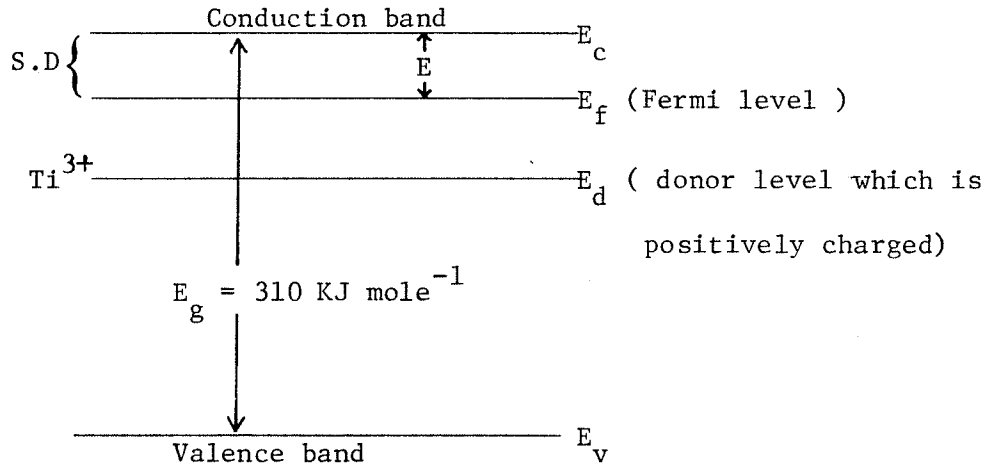

Band structure of PTG (anatase) illustrating the location of conducting species (Ti^{3+}) in electroreduced PTG.

where E_g = energy gap between the conduction band and the valence band

E = energy seperation between the conduction band and the Fermi level, which is approximately equal to $\frac{E_c - E_d}{2}$ for rutile single crystal [13]. This relationship may be applicable to amorphous PTG too.

S.D = other secondary defects (donors).

CHAPTER 6

INFRA-RED STUDIES

6.1 Introduction

The presence of hydroxyl groups (OH) on the surface of both anatase and rutile titania has been widely investigated using infra-red spectroscopic technique. The appearance of the hydroxyl groups, in principle is caused by the interaction of water vapour with the surface of titania in order to satisfy the valency requirement. Proposals have been put forward, hoping to present a quantitative picture of the hydroxylation and dehydroxylation phenomena. Yates [23] first investigated the surface hydroxyl groups of anatase and rutile TiO_2 in 1960. Since then, more details have been revealed. Parfitt and Jackson [26], working on rutile TiO_2 suggested that when water vapour molecule chemisorbs on a bare titanium site, it will decompose, releasing a labile proton which then migrates to the surface oxide ion, leaving the OH group behind on the metal site. In contrast, Primet and co-workers [24] proposed that the hydroxyl groups appear as a result of direct substitution of the surface oxide by OH group. More suggestions have been forwarded and the reader is referred to the review article entitled "The Surface of Titanium Dioxide" by G. D. Parfitt [28].

Little has been done on the surface hydroxyl groups of Porous Titania Glass (PTG), a "polymeric form" of TiO_2 since the publication of the paper by Gesser *et al.* [19]. In this chapter, an infra-red study on the dehydroxylation of the surface hydroxyl groups of PTG will be discussed.

6.2 Experimental

PTG sample (thickness < 0.1 cm) which had been annealed (300°C and 320°C) and drastically Soxhleted (72 hours) was transferred to an infra-red cell as illustrated in Fig. 26. The cell was constructed of Infrasil quartz which was free of OH absorption at 3700 cm^{-1}. The cell was then continuously evacuated and degassed slowly (to prevent the sample from cracking due to rapid loss of moisture) after being mounted to the high vacuum line (pressure $< 10^{-4}$ torr) with liquid nitrogen trap isolating the sample to prevent further contamination (by oil from the rotary pump). Spectra were taken at various intervals using a Perkin-Elmer infra-red spectrometer (model 700). The band width was 0.5 cm^{-1} and the reference used for calibration was polystyrene strip (Perkin-Elmer, 0.05 mm thick, Part Number 186-2082). Degassing temperature was monitored by a chromel-alummel thermocouple placed close to the sample cell. A blank quartz cell was used as the reference throughout the experiment.

6.3 Results

As shown by the X-ray diffraction patterns in the earlier chapter, the sample used (PTG300R and PTG320R) were predominantly amorphous, crystallising to more anatase character at 360°C. At lower degassing temperature ($\lesssim$110°C), a significant amount of residual water was still retained as illustrated by the broad band centred at 3100 cm^{-1} (Fig. 27-28). These obscured bands, which appeared as shoulders in the poorly resolved spectra (Fig. 27-28) are the precursor to the various hydroxyl groups as shall be explained later. At this stage of degassing (temperature = 110°C, pressure $< 10^{-4}$ torr), no apparent change in colour

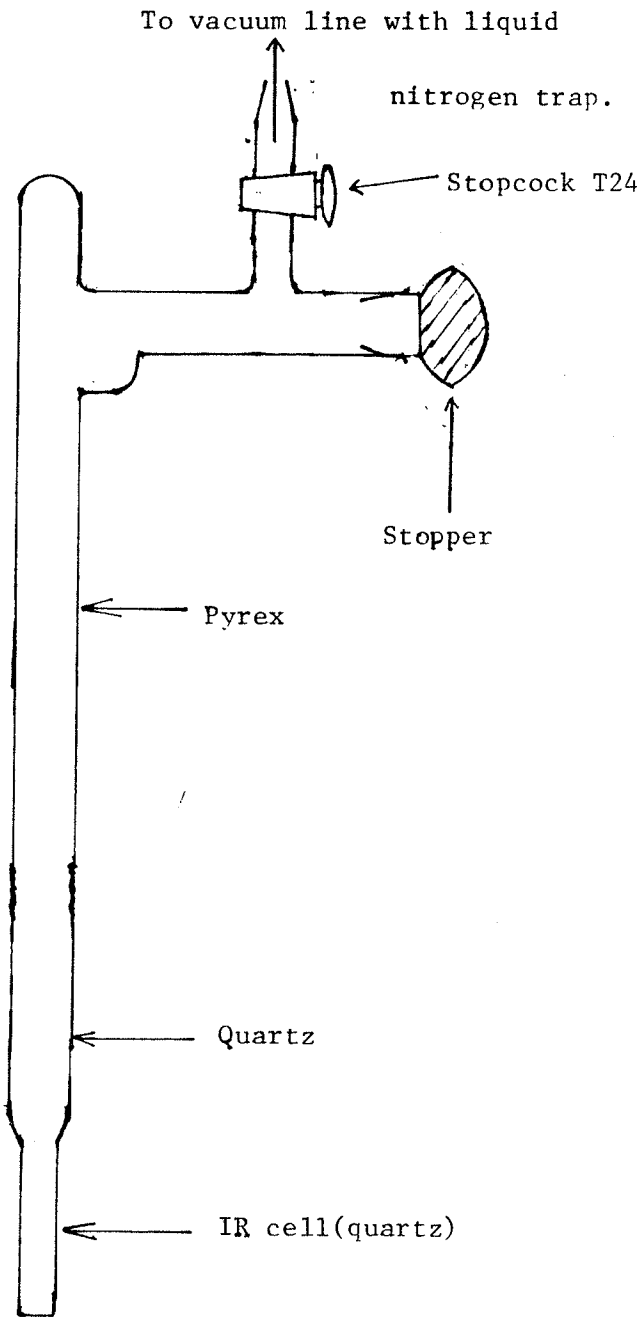

Fig 26: Detail of the IR cell.

Fig 27: IR spectra of PTG320R degassed at various temperatures.

1 = IR spectrum of PTG320R degassed at 110°C for 24 hours.

2 = IR spectrum of PTG320R degassed at 227°C for 5.5 hours.

3 = IR spectrum of PTG320R degassed at 285°C for 30 hours.

4 = IR spectrum of PTG320R degassed at 362°C for 20 hours.

5 = IR spectrum of PTG320R degassed at 382°C for 40 hours.

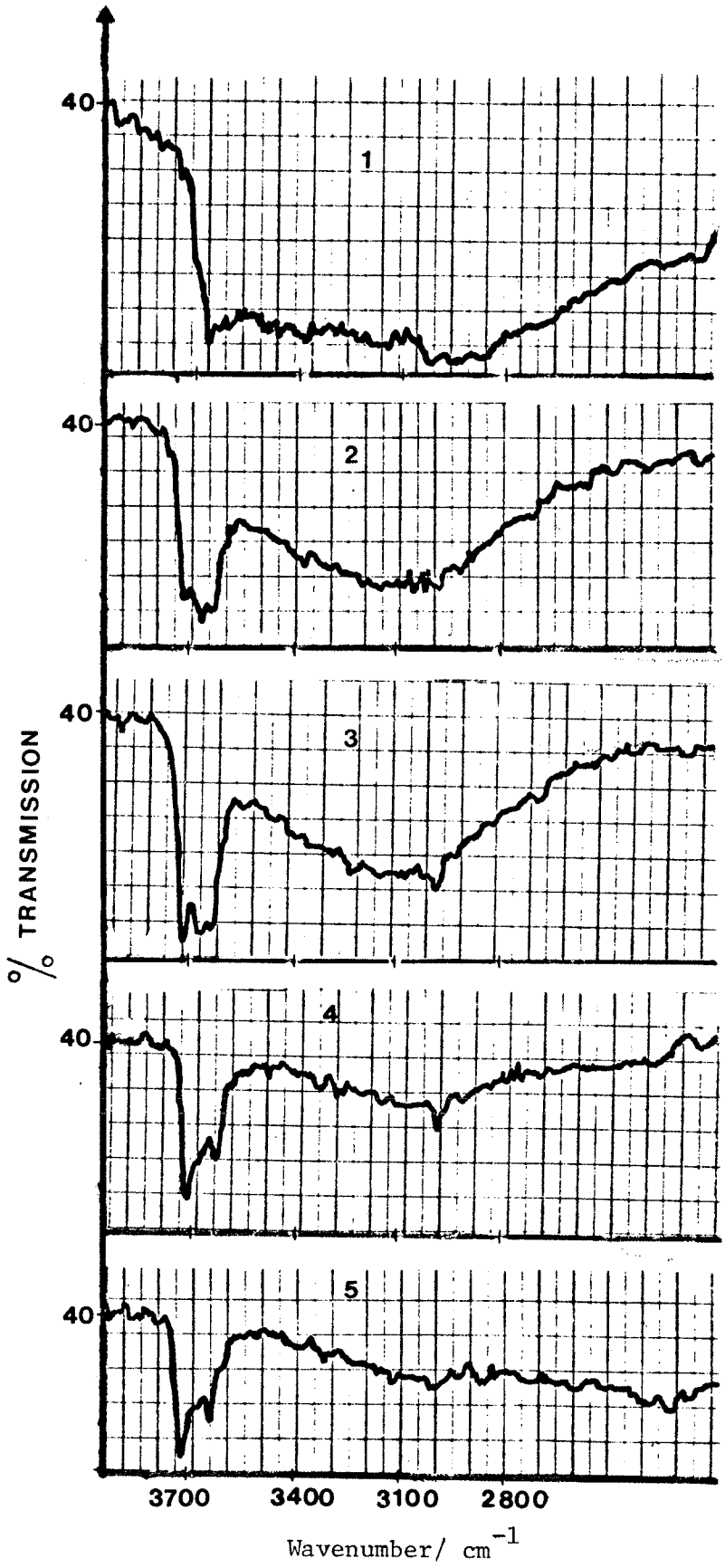
40
1
40
2
40
3
40
4
40
5
% TRANSMISSION
3700
3400
3100
2800
Wavenumber/ cm^{-1}

Fig 28: IR spectra of PTG300R degassed at various temperatures.

6 = IR spectrum of PRG300R degassed at 110°C for 24 hours.

7 = IR spectrum of PTG300R degassed at 227°C for 20 hours.

8 = IR spectrum of PTG300R degassed at 255°C for 20 hours.

9 = IR spectrum of PTG300R degassed at 315°C for 18 hours.

10 = IR spectrum of PTG300R degassed at 362°C for 5 hours.

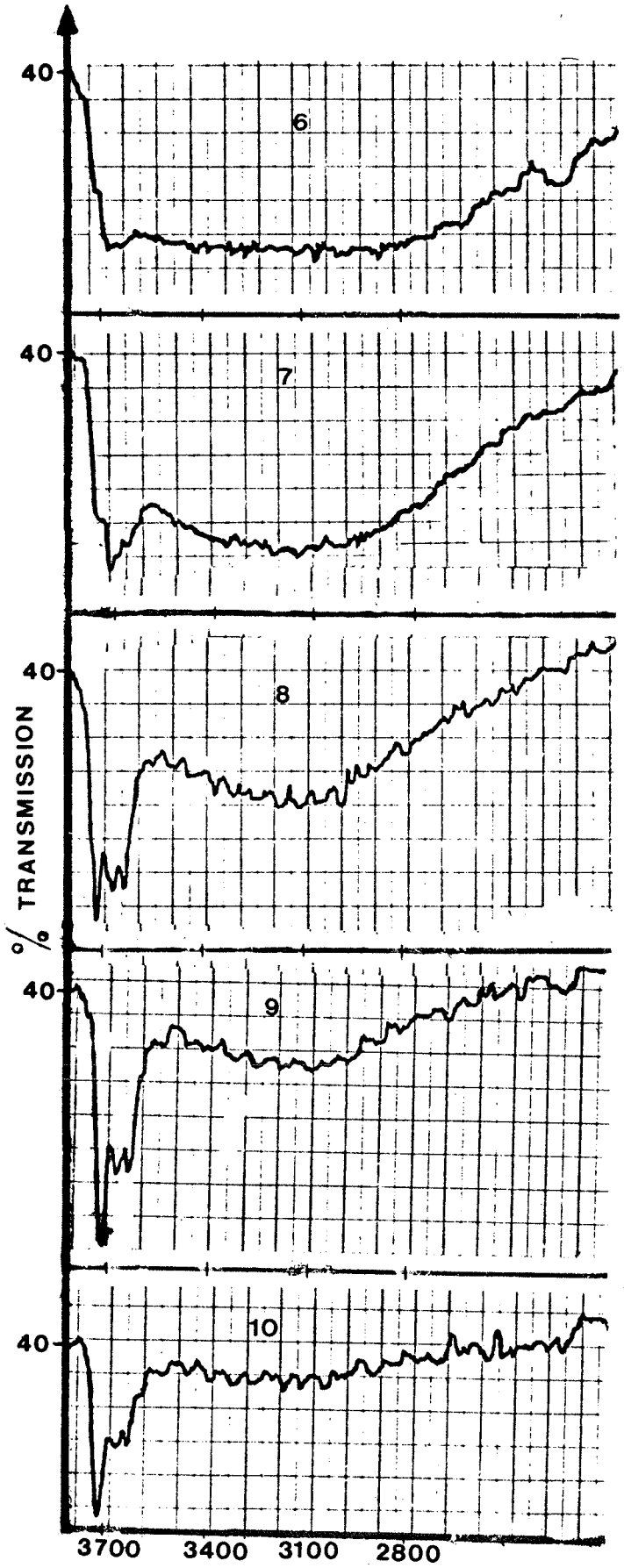
40
6
40
7
40
8
% TRANSMISSION
40
9
40
10
3700
3400
3100
2800
Wavenumber/ cm-1

of the samples was observed. At a slightly higher degassing temperature (>200°C), reduction of residual water occurred as confirmed by the narrowing of the broad water band. Simultaneously, prominent peaks appeared at 3718 cm^{-1}, 3667 cm^{-1} and 3636 cm^{-1} (PTG320R) and 3718 cm^{-1}, 3666 cm^{-1} and 3632 cm^{-1} (PTG300R). However, at this stage of degassing, discoloration of the samples occurred, turning from light brown to dark brown as degassing temperature was increased. This discoloration which was also observed by earlier workers [26,89-91] remained when kept in vacuum but faded slowly to light yellowish (identical to it's original colour prior to experiment) colour when exposed to air. As the band at 3718 cm^{-1} sharpened (degassing temperature >300°C), the bands at the lower frequency region began to diminish and eventually disappeared at very high degassing temperature (>400°C). This stage was not observed but the disappearance of the peaks are illustrated by the diminishing peaks at the lower frequency region.

6.4 Discussion

The discoloration of both anatase and rutile TiO_2 in vacuo is not new. Herrington [92], working on rutile TiO_2 and later Clark and Broadhead [90] working on anatase TiO_2 attributed the discoloration of the sample to contamination of the sample by grease or pump oil. The system used was not grease-free, thus this possibility cannot be ignored. Hollabaugh and Chessick [94] suggested that the hydrated rutile TiO_2 surface consists of two layers -- an inner layer comprising of chemisorbed hydroxyl groups and an outer layer of water molecules hydrogen-bonded across the hydroxyl groups. Upon degassing

and evacuating, the outer layer of water molecules is removed, exposing the inner layer which is susceptible to replacement by impurities. Bearing in mind that the surfaces of rutile and anatase are different, the above model is adopted to explain the discoloration. Following the removal of residual water from the titania glass surface, organic molecules (from grease) are encouraged to displace the inner OH groups. Upon adsorption, the symmetry of the inner hydroxyl groups is disturbed which results in a change in the localised energy levels at the surface of the titania glass. Therefore a brown discoloration resulted. This disturbance is restored following the readsorption of water molecules from the atmosphere. The symmetry of the inner hydroxyl groups is thus regenerated. Contamination by pump oil has been neglected on the basis that the liquid nitrogen trap would have removed the oil vapour, thus prohibiting contamination of the samples.

Jones and Hockey [85] working on rutile TiO_2 demonstrated that the chlorine content on the surface increases upon heating which is inferred as the extrusion of chloride ions from the interior to the surface layers. The chloride ions interact with the surface hydroxyl groups as:

$$Cl^-(\text{ interior }) + 2Ti^{x+}(OH^-)\ (\text{surface}) \longrightarrow Ti^{(x-1)+}\ Cl^-\ (\text{surface}) + Ti^{x+}O^{2-}(\text{surface}) + H_2O\ (\text{desorbed}) \qquad (6a)$$

x = oxidation state of titanium atom

In other words, hydroxyl groups are removed which thus disturbed the symmetry of the inner layer. Hence discoloration occurred. The disappearance of the brown colour may be caused by the readsorption of

water molecule from the atmosphere, hence restoring the symmetry again. Precisely what happened to the adsorbed organic molecules and chloride ions upon readsorption of water molecules remained to be explained. Morterra et al. [30] suggested that the impurity, like chloride is removed as chlorine gas as:

$$2\ Ti^{4+}Cl^{-} \xrightarrow[\Delta]{} 2\ Ti^{3+}\square + \quad Cl_2 \qquad (6b)$$

which results in vacuum reduction of Ti^{4+} ($\square$ = anion vacancy). Upon exposure to atmospheric conditions, discoloration disappeared due to oxidation of Ti^{3+} to Ti^{4+}.

Kaluza and Boehm [91] demonstrated that Hg vapour can cause discoloration to titania too, due to the formation of HgO on the surface. However, the presence of oxygen and ultraviolet light is required. The colour fades in darkness if moisture is present. The authors suggested that fading occurs as a result of the reduction of HgO by the reducing species (possibly Ti^{3+} or TiO_2^{-}) formed during the interaction of TiO_2 with atmospheric water molecules, the process being slow due to the high activation energy involved in the formation of the reducing species.

I believe that this factor probably constitutes a minute role in the discoloration of the PTG samples due to the fact that degassing and evacuating were done at night and the samples partially shielded from direct exposure to fluorescent light by the heater. Cronemeyer and Gilleo [93] and later Heinglein [80] inferred the discoloration to be caused by Ti^{3+} species or the colour centred species TiO_2^{-} respectively. Unlike the latter suggestion, it is unlikely that Ti^{3+} was formed unless the samples were reduced in vacuo or heated at high temperatures (>400°C). But in the presence of ultraviolet light, the appearance of

Ti^{3+} or TiO_2^- species cannot be totally neglected though the probability of it's occurrence is rather small.

The appearance of the sharp band around 3718 cm^{-1} had been observed earlier [19,23,26]. This band is assigned as the free hydroxyl stretching vibration where it is well isolated and not hydrogen-bonded. Generally, bands appearing above 3700 cm^{-1} are typical of metallic oxide of high surface area [cited from ref. [24]], a prediction which agrees very well with the experimental results obtained earlier. Primet et al. [24] claimed that the hydroxylic hydrogen atom of anatase TiO_2 is more acidic than rutile. The electronegative oxygen atoms (designated A in Fig. 29) can polarise the hydroxylic oxygen (designated B in Fig. 29) since they are in close vicinity to each other. Hence an increase in electron density is expected. Therefore the hydroxylic hydrogen becomes more protonic, thus making it the strongest Lewis acid site on the surface of titania. The above authors also demonstrated that the hydroxyl groups are basic. Boehm [25] working on anatase TiO_2 suggested that half of the hydroxyl groups are acidic, the remaining being basic. However, the above has not yet been conducted on the PTG samples. At higher degassing temperature ($\geqslant$382°C), the peak at 3718 cm^{-1} diminished slightly and this is attributed to the removal of OH group via the migration of proton or OH itself. This results in the formation of incompletely co-ordinated Ti atoms and evidence for this had been shown by Primet et al [24]. The reaction is

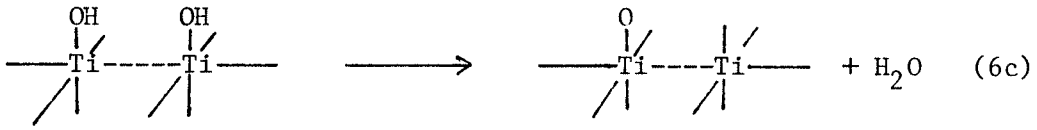

(6c)

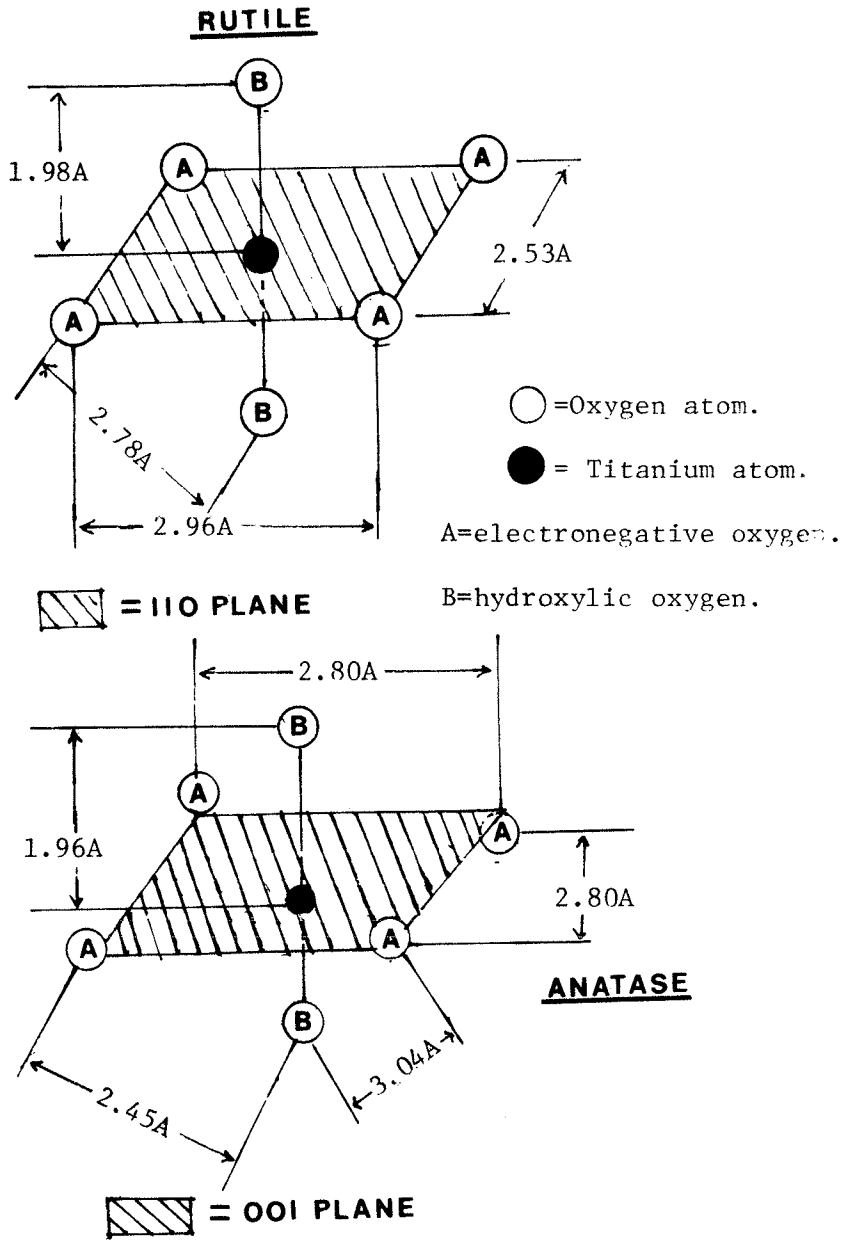

Fig 29. Interatomic distances in anatase and rutile TiO_2.

(Reproduced from reference(24)).

The band at 3667 cm^{-1} (3666 cm^{-1} for PTG300R) is assigned as hydrogen bonded hydroxyl group. Pure anatase will exhibit bands at 3715 cm^{-1} and 3665 cm^{-1} whereas rutile at 3680 cm^{-1}, 3655 cm^{-1} and 3410 cm^{-1} [24]. In short, the above results suggest that the PTG samples used resemble anatase more so than rutile which is in good agreement with the XRD studies earlier. Dehydroxylation of the hydrogen bonded hydroxyl groups (at temperature $\gtrsim$ 300°C) can be accounted as the formation of the bridging species by the removal of the hydroxyl group via the reaction

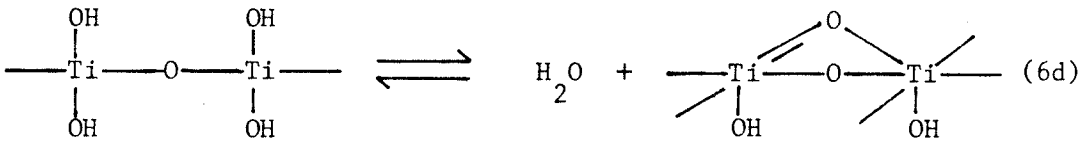

(6d)

The appearance of an entirely different band at 3636 cm^{-1} (3632 cm^{-1} for PTG300R) was in good agreement with earlier studies by Gesser et al. [19]. Terminal hydroxyl groups appear between 3750 cm^{-1} and 3600 cm^{-1} [29,31] while the bridged hydroxyl groups at 3450 cm^{-1} to 3400 cm^{-1} [31]. This tentatively suggests that the band correspond to an unbridged hydroxyl group. It is very unlikely that the above band will correspond to an overlapping anatase and rutile band unless hydrogen bonding occurs whereby the band will be shifted slightly to the lower frequency region. Finklea and Vithanage [31] assigned the peak at 3650 cm^{-1} as the overlapping anatase and rutile peak where the anatase:

rutile ratio is 85:15. Earlier, the XRD patterns illustrated that the samples were predominantly amorphous with increasing anatase characteristic with increasing annealing temperature. Judging from the poor correlation between the two results, it is most unlikely the peak at 3636 (3632) cm^{-1} is of the overlapping nature. Perhaps this band may arise from another crystal face. However, more work is needed to confirm the appearance of this band.

The broad band centred at 3100 cm^{-1} is assigned as the strongly co-ordinated water molecules which were completely removed at elevated temperature (>360°C). By degassing the PTG samples at different temperature, a slight decrease in surface area can thus be accounted for by the formation of bridging species and incompletely co-ordinated species which presumably decreases the number of vacant sites by hindering the adsorption of nitrogen molecules.

CHAPTER 7

CONCLUSION

7-1 This dissertation is primarily devoted to the characterisation and some surface studies on PTG which had been successfully fabricated by the controlled hydrolysis of titanium tetrachloride and careful dehydration. As can be seen, the adsorption isotherms resemble the Type IV isotherm in the BDDT classification whereas the desorption isotherms bear the resemblance of Type A hysteresis loop which subsequently changed to Type E at elevated annealing temperature. This transition was attributed to the enlargement of the pores during the thermal treatment. Beside, the PTG samples were amorphous at lower annealing temperature (300°C), gradually changing to anatase and finally to rutile at higher annealing temperature (460°C). The thermal history did not conclude there. Surface area, determined by adopting the volumetric method using nitrogen as adsorbate at 77K decreased from 304 m^2g^{-1} to 14 m^2g^{-1} over a range of 160°C (300°C - 460°C). The pore size increased from 12Å to 41Å. This severe loss of surface area was caused by the loss of a large fraction of micropores due to sintering and probable formation of Ti-O-Ti chain. Mesopores and macropores resulted at the expense of micropores during the thermal treatment.

Degassing temperature did not significantly reduce the surface area as compared to annealing temperature. A small reduction of surface area was a result of the formation of the bridging species $Ti\overset{O}{\diagdown\diagup}Ti$ and perhaps a slight sintering. Pore size studies indicated no dramatic increase of pore radius, suggesting that "internal" sites which were plentiful "inside" the glass were still accessible to the adsorbate molecules. Prolonging the length of annealing time at constant annealing temperature (320°C) did not cause any morphological change to PTG320R. In fact, a slight increment in surface area was presumably a

result of the creation of new adsorption site by the expulsion of "embedded" residual water molecule or OH groups.

PTG, photodeposited with uniform layer of noble metal (Pt,Pd,Rh) has been used as hydrogen detector. The criterion that determines the feasibility of photodeposition process is the Gibbs free energy ΔG° according to the equation

$$G^\circ = -nFE^\circ$$

The sensitivity of the hydrogen detector (Pt/PTG and Pd/PTG) was greatly improved by recycling in hydrogen and increasing metal loading. Oxygen and/or moisture is vital for hydrogen detection by the detector. In the absence of oxygen and/or moisture, the sensitivity to hydrogen was significantly reduced. This dramatic loss of sensitivity was attributed to the lack of O_2^- species which is the prerequisite for the formation of Ti^{3+} species via the hydrogen spillover mechanism. A noble metal (Pt,Pd) is a necessary ingredient since it promotes the hydrogen spillover mechanism as:

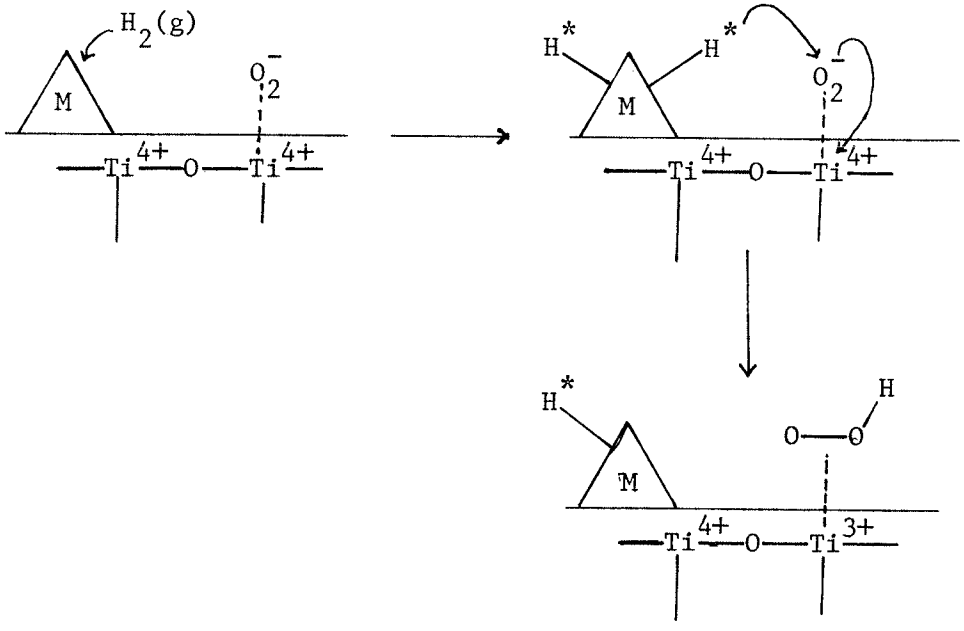

The sensitivity of the platinum detector was completely destroyed by hydrochloric acid vapour, an inhibition probably caused by direct displacement of O_2^- or OH^- species. In contrast, the platinum detector was shown to be more sensitive to hydrogen than the palladium analogue, presumably due to platinum being a better hydrogen spillover promoter than palladium.

Electroreduction of PTG300R caused a dark blue coloration which was attributed to the Ti^{3+} species or the colour-centred TiO_2^- species. By prolonging the reduction, the energy separation between the conduction band and Fermi level E_f narrowed, thus indicating that more electrons are being promoted to the conduction band, causing the resistance to decrease.

Infra-red studies on the dehydroxylation process on PTG indicated three different OH species. The prominent and "heat" resistant peak at 3718 cm^{-1} corresponded to the well isolated and not hydrogen-bonded hydroxyl group. The band at 3667 cm^{-1} was assigned the hydrogen-bonded hydroxyl group which was easily removed at elevated degassing temperature causing the formation of the bridging species $-Ti\overset{O}{<}Ti-$. The band at 3636 cm^{-1} has not yet been assigned and more work has to be done to elucidate the nature of this band. The discoloration caused by degassing may be the result of impurities (Cl^-, organic molecules, etc) residing on the surface of PTG or due to the loss of oxygen from the surface.

7-2. Recommendations for Further Work

With the present day economy, the rising cost of chemicals do impose many disadvantages to both researchers and users. Since the

fabrication of PTG was relatively cheap, more work should be done to evaluate its possible uses.

1. Catalytic work should be very interesting since titania supported catalysts are very resistant to sulphur poisoning, the advantage which it enjoys compared to alumina or silica supported catalysts [95].
2. Transmission Electron Microscopy (TEM) will be useful since it further characterises the catalyst prepared and the nature of the deposited metal.
3. X-ray diffraction (XRD) will be useful too in characterising the catalyst.
4. As to whether the PTG sample used was ohmic or not, has to be investigated further. Varying the length, area, voltage and current may provide the above information.
5. The basic and acidic characteristics of the hydroxyl groups ought to be determined, either by methylation or adsorption of pyridine and hydrochloric acid vapour.
6. The poisoning of rhodium detector by carbon monoxide should be investigated, perhaps by Electron Spin Resonance spectroscopy (ESR) or infra-red spectroscopy.
7. Earlier, Cronemeyer [74] pointed out that brookite and anatase should transform to rutile by heating close to 1000°C. Dachille *et al*. [73] predicted that the transformation of anatase to rutile occurs at 470°C at one atmosphere pressure. Rao [96] contradicted Dachille *et al*.'s work. The author claimed that the transition temperature is 630°C. Since there is controversy over the

transition temperature, future work should be done to clarify the above uncertainty.

Appendix 1

Computer Programmes

Adsorption:

```
10  DIM A(50), B(50), D(50), F(50), G(50), H(50), L(50), M(50), N(50),
    S(50), Q(50), W(50), Y(50), X(50), V(50)

20  GOTO 120

30  PRINT "A(I) = PRESSURE OF GAS BEFORE EXPANDING INTO SAMPLE TUBE"

40  PRINT "D(I) = PRESSURE OF GAS AFTER EXPANDING INTO SAMPLE TUBE"

50  PRINT "B(I) AND E(I) = CORRESPONDING PRESSURE IN VACUUM"

60  PRINT "C AND T = SATURATED VAPOUR PRESSURE AND TEMPERATRUE
    RESPECTIVELY"

70  PRINT "H(I) AND L(I) = HEIGHTS OF MERCURY COLUMN"

80  PRINT "M(I) = EQUILIBRIUM PRESSURE"

90  PRINT "W(I) = VOLUME OF GAS ADSORBED"

100 PRINT "P(I) = C(S.V.P.) - M(I)"
```

```
110  PRINT "Y(I) = M(I)/(Z*N(I)*(C-M(I))) WHERE N(I) IS THE NUMBER OF
     MOLES OF GAS ADSORBED"

120  REM "A-BET"

130  INPUT C,T

140  FOR I = 1 TO 20

150  INPUT A(I), B(I), D(I), E(I), S(I), Q(I), F(I), G(I)

160  V(I) = A(I) - B(I)

170  M(I) = D(I) - E(I)

180  H(I) = 41.5 - S(I)

190  L(I) = 41.5 - Q(I)

200  NEXT I

210  J = 0.101325/(C*T*8.314)

220  K = (22*0.1007*0.1007)/7

230  Z = 280134/12.506
```

```
240  N(1) = J*(V(1)*(K*H(1) + 1.507 + F(1) + G(1) - M(1)*(K*L(1) +
     13.234)))

250  W(1) = N(1)*Z

260  FOR I = 2 TO 20

270  N(I) = J*(V(I)*(K*H(I) + 1.507 + F(I) + G(I) + M(I-1)*11.727 -
     M(I)*(K*L(I) + 13.234)))

280  W(I) = N(I)*Z + W(I-1)

290  NEXT I

300  FOR I = 1 TO 20

310  Y(I) = M(I)/(W(I)*(C=M(I)))

320  X(I) = M(I)/C

330  PRINT W(I), Y(I), X(I)

340  NEXT I

350  END
```

Appendix 1 : The flow-chart for programme " A-BET "

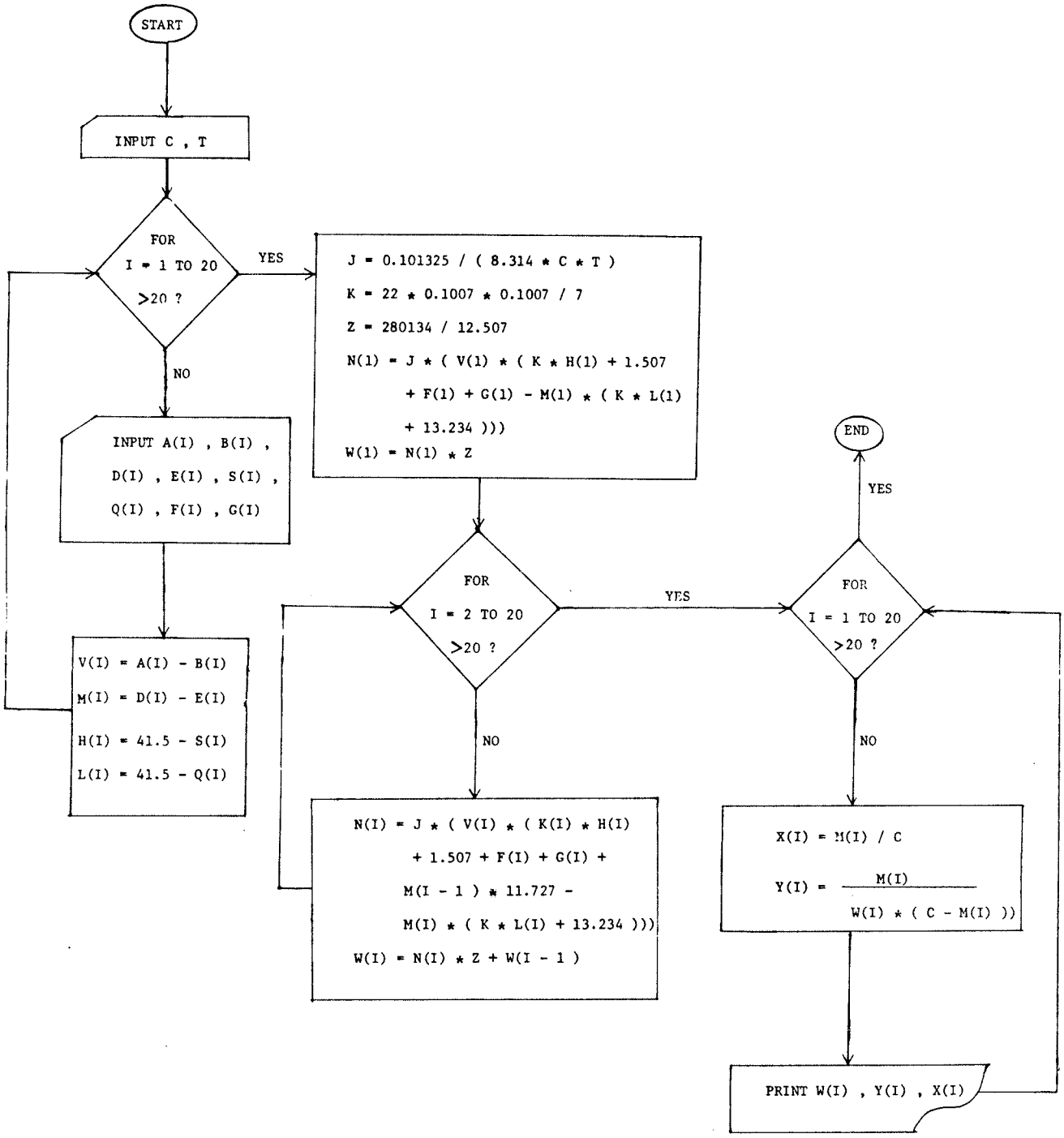

Appendix 2

Desorption

```
10  DIM A(50), B(50), D(50), E(50), F(50), G(50), H(50), L(50), M(50),
    N(50), W(50), X(50), P(50), Q(50)

20  REM "D-BET"

30  INPUT C,T

40  Z = 280134/12.507

50  J = (22*0.1007*0.1007)/7

60  K = 0.101325/(8.314*C*T)

70  FOR I = 1 to 15

80  INPUT A(I), B(I), D(I), E(I), F(I), G(I), H(I), L(I)

90  M(I) = 41.5 - A(I)

100 P(I) = B(I) - D(I)

110 Q(I) = E(I) - F(I)
```

```
120  N(I) = P(I)*(13.234 + G(I) + H(I) + L(I) + J*M(I)) - Q(I)*11.727

130  W(I) = N(I)*Z

140  X(I) = P(I)/C

150  PRINT W(I), X(I)

160  NEXT I

170  END
```

Appendix 2 : The flow-chart of programme " D-BET ".

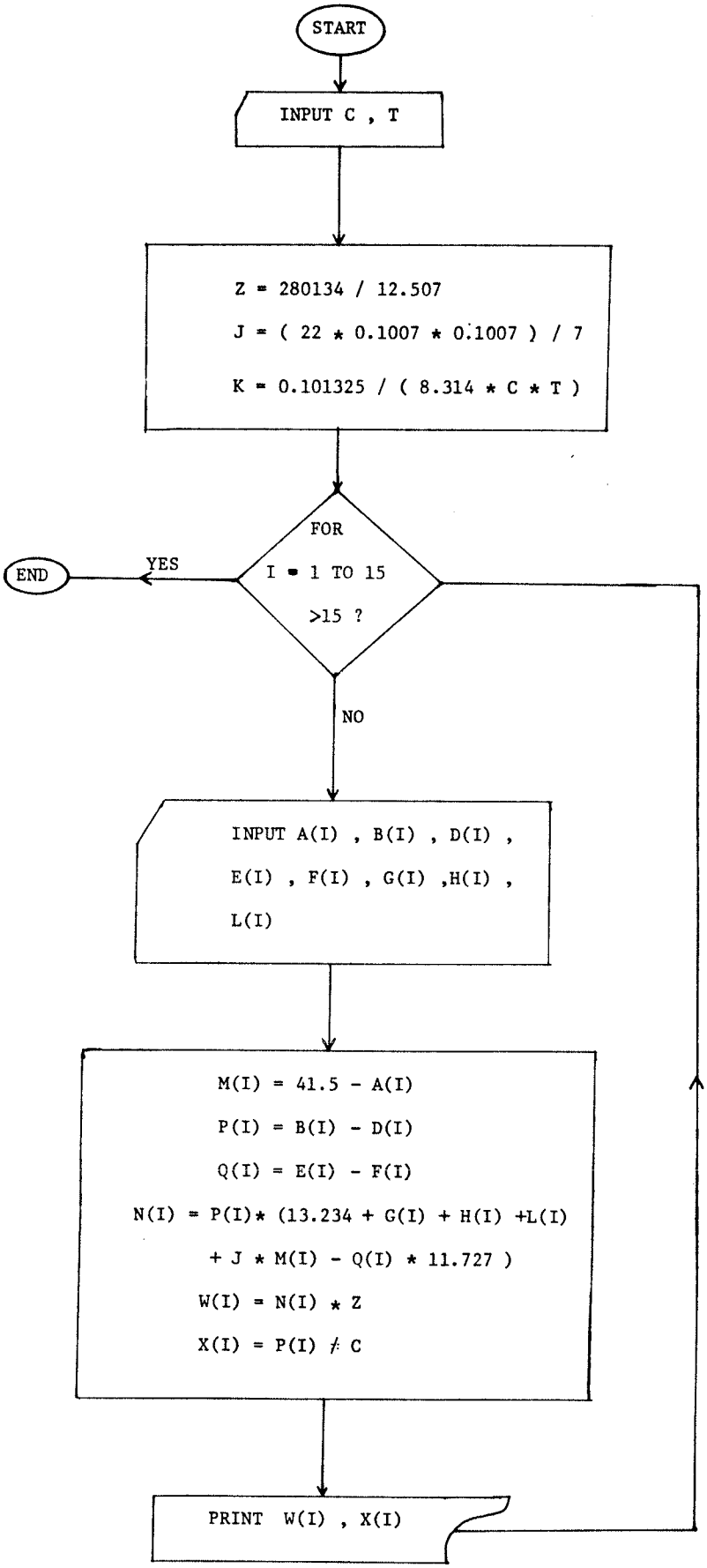

Appendix 3

Conductivity Calculation

```
10   DIM R(50), S(50), J(50)

20   REM "OHM"

30   INPUT R2, L, A

40   K = L/A

50   FOR I = 1 to 50

60   INPUT R(I)

70   J(I) = R2*R(I)/(R2 - R(I))

80   S(I) = J(I)*K

90   PRINT J(I), S(I)

100  NEXT I

110  END
```

Appendix 3 : The flow-chart of programme " OHM ".

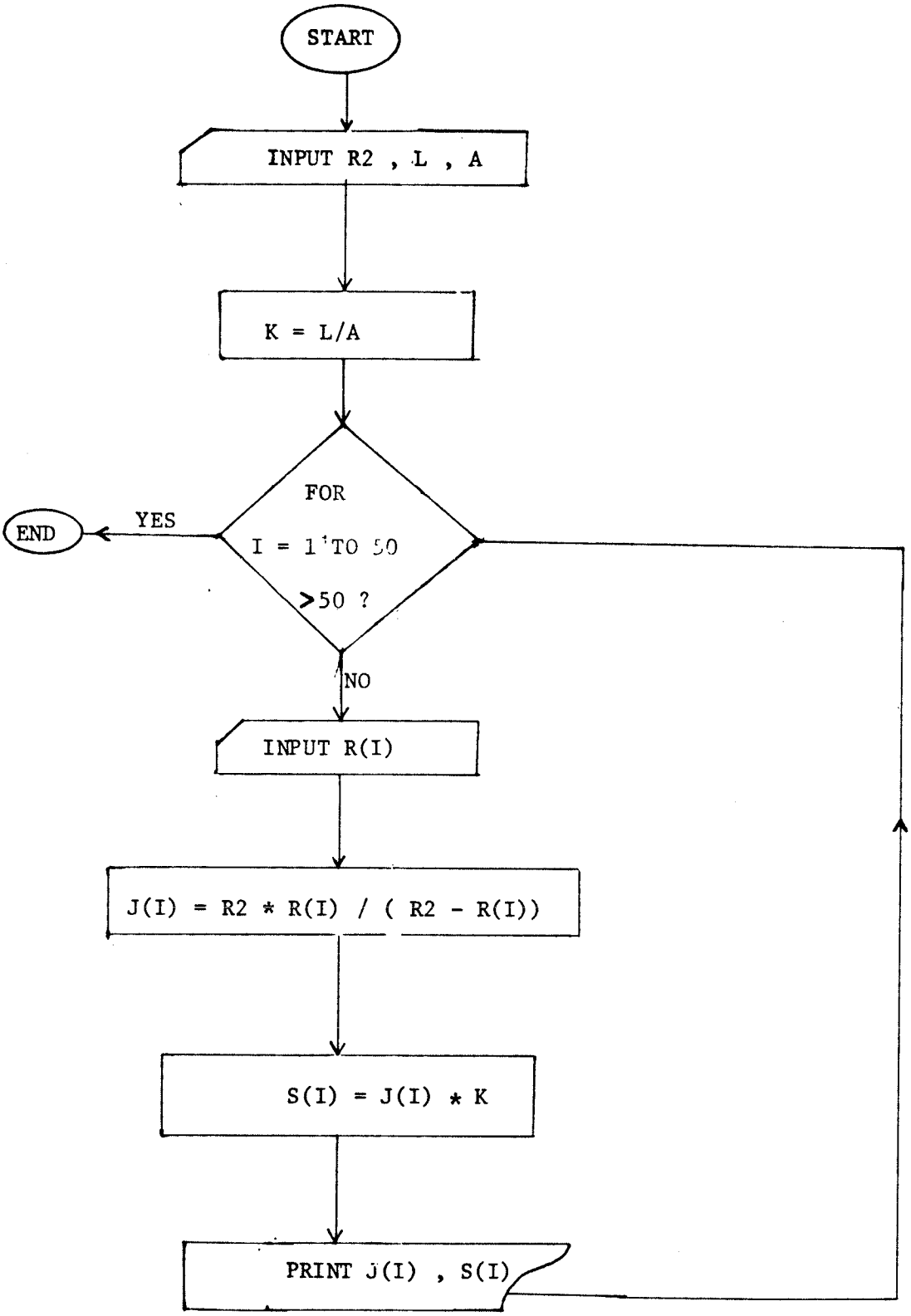

Table 8: Standards on the Joint Committee on Powder Diffraction.

21-1272

d	3.52	1.89	2.38	3.52	TiO_2
I/I_1	100	35	20	100	Titanium Oxide (Anatase)

Rad. $CuK\alpha_1$ λ 1.54056 Filter Mono. Dia.
Cut off I/I_1 Diffractometer $I/I_{cor.}$ =4.3
Ref. National Bureau of Standards, Mono. 25, Sec. 7, 82 (1969)

Sys. Tetragonal S.G. $I4_1/amd$ (141)
a_0 3.7852 b_0 c_0 9.5139 A C 2.5134
α β γ Z 4 Dx 3.893
Ref. Ibid.

εα nωβ εγ Sign
2V D mp Color Colorless
Ref. Ibid.

Pattern at 25°C. Internal standard: W.
Sample obtained from National Lead Co., South Amboy, New Jersey, USA.
Anatase and another polymorph brookite (orthorhombic) are converted to rutile (tetragonal) by heating above 700°C.
Merck Index, 8th Ed., p. 1054.

d A	I/I_1	hkl	d A	I/I_1	hkl
3.52	100	101	1.0436	4	321
2.431	10	103	1.0182	2	109
2.378	20	004	1.0070	2	208
2.332	10	112	0.9967	2	323
1.892	35	200	.9555	4	316
1.6999	20	105	.9464	4	400
1.6665	20	211	.9246	<2	307
1.4930	4	213	.9192	2	325
1.4808	14	204	.9138	2	411
1.3641	6	116	.8966	4	219,1110
1.3378	6	220	.8890	2	228
1.2795	<2	107	.8819	<2	413
1.2649	10	215	.8793	2	404
1.2509	4	301	.8464	2	420
1.1894	<2	008	.8308	<2	327
1.1725	2	303	.8268	4	415
1.1664	6	224	.8162	2	309
1.1608	4	312	.7974	4	424
1.0600	2	217	.7928	2	0012
1.0517	4	305			

d	3.25	1.69	2.49	3.25	TiO_2
I/I_1	100	60	50	100	Titanium Oxide (Rutile)

Rad. $CuK\alpha_1$ λ 1.54056 Filter Mono. Dia.
Cut off I/I_1 Diffractometer $I/I_{cor.}$ =3.4
Ref. National Bureau of Standards, Mono. 25, Sec. 7, 83 (1969)

Sys. Tetragonal S.G. $P4_2/mnm$ (136)
a_0 4.5933 b_0 c_0 2.9592 A C 0.6442
α β γ Z 2 Dx 4.250
Ref. Ibid.

εα nωβ εγ Sign
2V D mp Color
Ref.

No impurity over 0.001%
Sample obtained from National Lead Co., South Amboy, New Jersey, USA.
Pattern at 25°C. Internal standard: W. Rutile group.
Two other polymorphs anatase (tetragonal) and brookite (orthorhombic) converted to rutile on heating above 700°C. Merck Index, 8th Ed., p. 1054.

d A	I/I_1	hkl	d A	I/I_1	hkl
3.247	100	110	1.0425	6	411
2.487	50	101	1.0364	6	312
2.297	8	200	1.0271	4	420
2.188	25	111	0.9703	2	421
2.054	10	210	.9644	2	103
1.6874	60	211	.9458	2	113
1.6237	20	220	.9072	4	402
1.4797	10	002	.9009	4	510
1.4528	10	310	.8892	8	212
1.4243	2	221	.8774	8	431
1.3598	20	301	.8738	8	332
1.3465	12	112	.8437	6	422
1.3041	2	311	.8292	8	303
1.2441	4	202	.8196	12	521
1.2006	2	212	.8120	2	440
1.1702	6	321	.7877	2	530
1.1483	4	400			
1.1143	2	410			
1.0936	8	222			
1.0827	4	330			

29-1360 29-1361

d	3.51	2.90	3.47	3.51	TiO_2
I/I_1	100	90	80	100	Titanium Oxide Brookite

Rad. $CuK\alpha_1$ λ 1.5405 Filter Ni Dia.
Cut off I/I_1 Diffractometer $I/I_{cor.}$
Ref. Nat. Bur. Stand. (U.S.) Monogr. 25, Sec. 3 (1964)

Sys. Orthorhombic S.G. Pcab (61)
a_0 5.4558 b_0 9.1819 c_0 5.1429 A 0.59419(0.56011
α β γ Z 8 Dx 4.120
Ref. Ibid V 257.63Å³

εα 2.5831 nωβ 2.5843 εγ 2.7004(Na) Sign +
2V ∿28°* D 4.14±.06 mp Color Black
Ref. Dana's System of Mineralogy, 7th Ed., 1 588 (1944)

Specimen from Magnet Cove, Arkansas, USA (USNM 97661). *2E becomes 0 at 555.5 (25°C).
Spectrographic analysis: 0.1-1.0% Si; 0.01-0.1% each of Al, Fe, and V; 0.001-0.01% Mg. Niobian brookite from Mozambique [Chem. anal.(%). TiO_2 80.7; Nb_2O_5 14.1; FeO 5.53]; Carvalho et al., Rev. Cien. Geol. Ser. A, 7 61 (1974) gives an identical pattern. Pattern was made at 25°C. To replace 16-617.

d A	I/I_1	hkl	d A	I/I_1	hkl
3.51	100	120	1.649	5	151
3.47	80	111	1.610	13	113
2.900	90	121	1.597	2	232
2.729	4	200	1.541	7	123
2.476	25	012	1.494	10	052
2.409	18	201	1.473	4	160
2.370	6	131	1.466	9	312
2.344	4	220	1.461	12	251
2.332	4	211	1.452	12	203
2.296	5	040	1.442	6	152
2.254	8	112	1.434	10	213
2.244	18	022	1.417	9	161
2.153	16	221	1.364	5	400
1.969	16	032	1.336	8	332
1.893	30	231	1.319	3	401
1.851	18	132	1.312	2	233
1.833	3	212	1.285	2	004
1.757	3	240	1.238	10	024,171
1.691	20	320	1.211	2	431
1.662	30	241	10 reflections to 0.982		

REFERENCES

1. Vannice, M. A.,
"Titania Supported Metals as CO Hydrogenation Catalysts",
J. Catal., 74, 199 (1982).

2. Fang, S. M., Chen, B. H. and White, J. M.,
"Photoassisted Water-Gas Shift Reaction On Platinized Titania. The Influence of Preparation Parameters",
J. Phys. Chem., 86, 3126 (1982).

3. Disdier, J., Herrmann, J. M. and Pichat, P.,
"Platinum/Titanium Dioxide Catalysts",
J. Chem. Soc. Faraday Trans. 1, 79, 651 (1983).

4. Harvey, P. R., Rudham, R. and Ward, S.,
"Photocatalytic Oxidation of Liquid Propan-2-ol by Titanium Dioxide",
J. Chem. Soc. Faraday Trans. 1, 79, 1381 (1983).

5. Tsai, S. C., Kao, C. C. and Chung, Y. W.,
"Photoassisted Water-Gas Shift Reaction Over Pt/TiO_2 (100)",
J. Catal., 79, 451 (1983).

6. Tsai, W., Schwarz, J. A. and Driscoll, C. T.,
"Differential Cation Exchange Capacity of Platinum Supported On Titania",
J. Phys. Chem., 87, 1619 (1983).

7. Chen, B. H., White, J. M., Brostrom, L. R. and Devlney, M. L.,
"Electron Microscopy Investigation of Platinum Supported on TiO_2 and TiO",

J. Phys. Chem., 87, 2423 (1983).

8. Magliozzo, R. S. and Krasna, A. J.,
"Hydrogen and Oxygen Photoproduction by Titanate Powders",
Photochem. and Photobiology, 38, 15 (1983).

9. Earle, M. D.,
"The Electrical Conductivity of Titanium Dioxide",
Phys. Rev., 61, 56 (1942).

10. Breckenridge, R. G. and Hosler, W. R.,
"Electrical Properties of Titanium Dioxide Semiconductors",
Phys. Rev., 91, 793 (1953).

11. Gray, T. J., McCain, C. C. and Masse, N. G.,
"Defect Structure and Catalysis in the TiO_2 System (Semiconducting and Magnetic Properties)",
J. Phys. Chem., 63, 472 (1958).

12. Hasiguti, R. R., Minami, K. and Yonemitsu, H.,
"Electrical Resistivity and Defect Energy Levels in Reduced Titanium Dioxide at Low Temperatures",
J. Phys. Soc. Jpn., 16, 2223 (1961).

13. Iwaki, T.,
"Studies of the Surface of Rutile Single Crystals by Means of Electrical Conductivity",
Bull. Chem. Soc. Jpn., 46, 1631 (1973).

14. Yamamoto, N., Tonomura, S., Matsuoka, T. and Tsubomura, H.,
"A Study on a Palladium-Titanium Oxide Schottky Diode as a Detector for Gaseous Components",
Surf. Sci., 92, 400 (1980).

15. Tauster, S. J., Fung, S. C. and Garten, R. L.,

"Strong Metal-Support Interactions. Group 8 Noble Metals Supported on TiO_2",
J. Amer. Chem. Soc., 100, 170 (1978).

16. Horsley, J. A.,
"A Molecular Orbital Study of Strong Metal Support Interaction Between Platinum and Titanium Dioxide",
J. Amer. Chem. Soc., 101, 2870 (1979).

17. Herrmann, J. M. and Pichat, P.,
"Metal-Support Interactions: An In Situ Electrical Conductivity Study of Pt/TiO_2 Catalysts",
J. Catal., 78, 425 (1982).

18. Resasco, D. E. and Haller, G. L.,
"A Model of Metal-Oxide Support Interaction For Rh on TiO_2",
J. Catal. 82, 279 (1983).

19. Gesser, H. D., Kruczysnki, L., Turner, C. W. and Speers, E. A.,
"Porous Titania Glass as a Photocatalyst for Hydrogen Production from Water",
Nature, 291, 399 (1981).

20. El-Akkad, T. M.,
"Surface Areas, Pore Structures, and Heats of Immersion of Titania Gel in Correlation to Thermal Treatment",
J. Colloid Interface Sci., 76, 67 (1980).

21. Gesser, H. D., Kruczysnki, L. and Speers, E. A.,
"A Simple Detector for Hydrogen in Air",
Alternative Energy Sources V. Part D:
Biomass/Hydrocarbons/Hydrogen, Elsevier Science Publisher, 469 (1983).

22. Harris, L. A.,

"A Titanium Dioxide Hydrogen Detector",

Solid State Science and Technology, 2657 (1980).

23. Yates, D. J. C.,

"Infrared Studies of the Surface Hydroxyl Groups on Titanium Dioxide, and of the Chemisorption of Carbon Monoxide and Carbon Dioxide",

J. Phys. Chem., 65, 746 (1961).

24. Primet, M., Pichat, P. and Mathieu, M. V.,

"Infra-red Study of the Surface of Titanium Dioxides. I. Hydroxyl Groups",

J. Phys. Chem., 75, 1216 (1973).

25. Boehm, H. P.,

"Acidic and Basic Properties of Hydroxylated Metal Oxide Surfaces",

Discussions of the Faraday Society, 52, 264 (1971).

26. Jackson, P. and Parfitt, G. D.,

"Infra-red Study of the Surface Properties of Rutile-Water and Surface Hydroxyl Species",

J. Chem. Soc. Faraday Trans. I, 67, 2469 (1971).

27. Jackson, P. and Parfitt, G. D.,

"Infra-red Study of the Surface Properties of Rutile-Adsorption of Ethanol, n-Butanol and n-Hexanol",

J. Chem. Soc. Faraday Trans. I, 68, 1443 (1972).

28. Parfitt, G. D.,

"The Surface of Titanium Dioxide",

Prog. Surf. Membr. Sci., 11, 181 (1976).

29. Griffiths, D. M. and Rochester, C. H.,

"Infra-red Study of the Adsorption of Water on to the Surface of Rutile",

J. Chem. Soc. Faraday Trans. I, 73, 1510 (1977).

30. Morterra, C., Chiorino, A., Zecchina, A. and Fisicaro, E., "A Spectroscopic Study of Anatase Properties. I. Characterisation of A via-Chloride Preparation",

Gazzetta Chimica Italiana, 109, 683, (1979).

31. Finklea, H. O. and Vithanage, R., "Infrared Adsorption Spectroscopy of Chemically Modified Titanium Dioxide",

J. Phys. Chem., 86, 3621 (1982).

32. Gesser, H. D. and Kruczynski, L., "An ESR Study of the Role of O_2^- in the Reduction of Palladium-Supported Porous Titania Glass",

J. Phys. Chem. (in press).

33. Brunauer, S., Emmett, P. H. and Teller, E., "Adsorption of Gases in Multimolecular Layers",

J. Amer. Chem. Soc., 60, 309 (1938).

34. Foster, A. G., "Sorption Hysteresis. Part II. The Role of the Cylindrical Meniscus Effect",

J. Chem. Soc. Part 2, 1807 (1952).

35. Lippens, B. C., Linsen, B. G. and De Boer, J. H., "Studies on Pore Systems in Catalysts I. The Adsorption of Nitrogen, Apparatus and Calculation",

J. Catal., 3, 32 (1964).

36. Brunauer, S.,

"The Adsorption of Gas and Vapours",

Princeton University Press, (1943).

37. Taylor, H. S.,

"The Activation Energy of Adsorption Processes",

J. Amer. Chem. Soc. 53, 579 (1931).

38. Young, D. M. and Crowell, A. D.,

"Physical Adsorption of Gases",

Butterworths, (1962).

39. Dubinin, M. M., Bering, B. P. and Serpinski, V. V.,

"Physical Adsorption at the Solid-Gas Interface",

Prog. Surf. Membr. Sci., 2, 1 (1964).

40. Langmuir, I.,

"The Adsorption of Gases on Plane Surfaces of Glass, Mica and Platinum",

J. Amer. Chem. Soc., 40, 1361 (1936).

41. Brunauer, S., Deming, L. S., Deming, W. E. and Teller, W.,

"On a Theory of the Van der Waals Adsorption of Gases",

J. Amer. Chem. Soc., 62, 1723 (1940).

42. Sing, K. S. W.,

"The Characterisation of Porous Solids by Gas Adsorption",

Berichte der Bunsen-Gesellschalf, 9, 724 (1975).

43. Cadenhead, D. A., Bailey, A., Davies, D. H.,Everett, D. H. and Miles, A. J.,

"Low Pressure Hysteresis in the Adsorption of Organic Vapours by Porous Carbons",

Faraday Society Transactions, 67, 231 (1971).

44. Brunauer, S., Copeland, L. E. and Kantro, D. L.,

"The Langmuir and BET Theories",

Chapter 3, Vol. 1, Marcel Dekker Inc. (1967).

45. McMillan, W. G. and Teller, E.,

"The Assumptions of the BET Theory",

J. Phys. Chem., 55, 17 (1951).

46. Joyner, L. G. and Emmett, P. H.,

"Differential Heats of Adsorption of Nitrogen on Carbon Blacks",

J. Amer. Chem. Soc., 70, 2353 (1948).

47. Brunauer, S. and Emmett, P. H.,

"The Use of Low Temperature Van der Waals Adsorption Isotherms in Determining the Surface Area of Iron Synthetic Ammonia Catalysts",

J. Amer. Chem. Soc., 59, 1533 (1937).

48. Halsey, G. D.,

"A New Multilayer Isotherm Equation with Reference to Surface Area",

J. Amer. Chem. Soc., 73, 2693 (1951).

49. White, L.,

"A Limitation of the Determination of Surface Area by the 'Point B' Method",

J. Phys. Chem., 51, 644 (1947).

50. Barrer, R. M., McKenzie, N. and Reay, J. S. S.,

"Capillary Condensation in Single Pores",

J. Colloid Sci., 11, 479 (1956).

51. Linsen, B. G. and van den Heuvel, A.,

"Pore Structures",

Solid-Gas Interface, Chapter 35, Vol. 2, Marcell Dekker Inc., (1967).

52. Cohan, L. H.,

"Sorption Hysteresis and the Vapour Pressure of Concave Surfaces",

J. Amer. Chem. Soc., 60, 433 (1938).

53. McBain, J. W.,

"An Explanation of Hysteresis in the Hydration and Dehydration of Gels",

J. Amer. Chem. Soc., 57, 699 (1935).

54. Cohan, L. H.,

"Hysteresis and the Capillary Theory of Adsorption of Vapours",

J. Amer. Chem. Soc., 66, 98 (1944).

55. Mineral Powder Diffraction File-Group Data Book,

Joint Committee on Powder Diffraction Standards, (1983).

56. Everett, D. H.,

"Adsorption Hysteresis",

Solid-Gas Interface, Chapter 36, Vol. 2, Marcel Dekker Inc. (1967).

57. Yoldas, B. E.,

"Monolithic Glass Formation by Chemical Polymerisation",

J. Mater. Sci., 14, 1843 (1979).

58. Klosky, S. and Marzano, C.,

"Titania Jellies",

J. Phys. Chem., 29, 1125 (1925).

59. Weiser, H. B., Milligan, W. O. and Simpson, W. C.,

"The Elimination of Sorption-Desorption Hysteresis In Hydrous Oxide Gels. II. Tantalum Pentoxide, Stannic Oxide, and Titanium Dioxide",

J. Phys. Chem., 46, 1051 (1942).

60. Harris, M. R. and Whitaker, G.,
"Surface Properties of Hydrolysed Titania. I. Titania Prepared from Titanium Tetra-Alkoxides",
J. Appl. Chem., 12, 490 (1962).

61. Handbook of Chemistry and Physics, 50th Edition,
The Chemical Rubber Co., (1969-1970).

62. Kruczynski, L.,
"Preparation of Porous Titania Glass",
(unpublished).

63. Long, D. A., and Davies, J. E. D.,
"The Vibrational Spectra of Titanium Tetrachloride-Hydrochloric Acid and Titanium Tetrachloride-Tri-n-butyl Phosphate Systems and the Hexachloro-anions of Zirconium (IV), Hafnium (IV), Niobium (V) and Tantalum (V)",
J. Chem. Soc. (A), 2560 (1968).

64. Gesser, H. D. and Speers, E. A.,
"A Report on the Development of an Efficient Photo-catalytic System to Produce Hydrogen when Immersed in Water and Exposed to Sunlight",
D. S. S. Contract 04SX. 31155-8-2623, (1980).

65. Boyd, T.,
"Preparation and Properties of Esters of Polyorthotitanic Acid",
J. Polym. Sci., 6, 591 (1951).

66. Lippens, B. C. and De Boer, J. J.,
"Studies on Pore System in Catalysts. II. The Shapes of Pores in Aluminum Oxide Systems",
J. Catal., 3, 38 (1964).

67. Cadenhead, D. A. and Everett, D. H.,
"The Sintering of Porous Glass: Benzene Adsorption by Heat-Treated Porous Glasses",
J. Phys. Chem., 72, 3201 (1968).

68. Culver, R. V. and Heath, N. S.,
"Saran Charcoals. Part 1. Activation and Adsorption Studies",
Faraday Society Transactions, 51, 1569 (1955).

69. Beebe, R. A., Millard, B., and Cynarski, J.,
"Heats of Adsorption of Nitrogen and Argon on Porous and Non-Porous Carbon Adsorbents at -195°C",
J. Amer. Chem. Soc., 75, 839 (1953).

70. Culver, R. V. and Heath, N. S.,
"Saran Charcoals. Part 2. Thermodynamics of Adsorption",
Faraday Society Transactions, 51, 1575 (1955).

71. Biscoe, J. and Warren, B. E.,
"An X-ray Study on Carbon Black",
J. Appl. Phys., 13, 364 (1942).

72. Wyckoff, R. W. G.,
"Crystal Structures",
page 17, Chapter 4, Volume 1, Interscience Publishers Inc., (1951).

73. Dachille, F., Simons, P. Y. and Roy, R.,
"Pressure-Temperature Studies of Anatase, Brookite, Rutile and TiO_2-H",
Amer. Mineralogist, 53, 1929 (1968).

74. Cronemeyer, D. C.,
"Electrical and Optical Properties of Rutile Single Crystals",
Phys. Rev., 87, 876 (1952).

75. Bond, G. C.,
"Heterogenous Catalysis - Principles and Application",
Chapter 2, page 20, Claredon Press, (1974).

76. Thomas, J. M. and Thomas, W.J.,
"Introduction to the Principle of Heterogenous Catalysis",
Chapter 4, page 198, Academic Press (1967).

77. Castro, P. L. and Hollander, L. E.,
"Anisotropic Conduction in Non-Stoichiometric Rule (TiO_2)",
Phys. Rev., 119, 1882 (1960).

78. Iwaki, T. and Miura, M.,
"Studies on the Surface of Titanium Dioxide. I. The Effect of Reduction by Hydrogen on the Heat of Immersion in Water",
Bull. Chem. Soc. Jpn., 44, 1754 (1971).

79. Clark, A.,
"The Theory of Adsorption and Catalysis",
Chapter 8, page 194, Academic Press (1970).

80. Heiglein, A.,
"Colloidal TiO_2 Catalysed Photo- and Radiation Chemical Processes in Aqueous Solution",
Ber. Bunsenges, Phys. Chem., 86, 241 (1982).

81. Oosawa, Y.,
"Photocatalytic Hydrogen Evolution from an Aqueous Methanol Solution Over Ceramics-Electrocatalyst/TiO_2",
Chem. Letts. Chem. Soc. Jpn., 577 (1983).

82. Kawai, T., Kawai, M., Naito, S. and Tamaru, K.,
"The Mechanism of Photocatalytic Hydrogen Production from Gaseous Methanol and Water: IR Spectroscopic Approach",

Chem. Phys. Lett., 98, 377 (1983).

83. Gonzalez-Elipe, A. R., Muneira, G. and Soria, J., "Photo-adsorption and Photo-desorption of Oxygen on Highly Hydroxylated TiO_2 Surfaces. Part 2. Study of Radical Intermediates by Electron Paramagnetic Resonance", J. Chem. Soc. Faraday Trans. 1, 75, 748 (1979).

84. Morterra, C., Chiorino, A., Boccuzzi, F. and Fisicaro, E., "A Spectroscopic Study of Anatase Properties-Adsorption of CO_2", Z. Phys. Chem., 124, 211 (1981).

85. Jones, P. and Hockey, J. A. "Infra-red Studies on Rutile Surfaces", Trans Faraday Soc. 67, 2669 (1971).

86. Boudart, M. and Levy, R. B., "The Kinetics and Mechanism of Spillover", J. Catal. 32, 304 (1974).

87. Thomson, S. J. and Harvey, G. A., "The Electrical Conductivity of Supported Metal Catalysts", J. Catal., 22, 359 (1971).

88. Ambs, W. J. and Mitchell, M. M., "Hydrogen Spillover on Platinum-Alumina-Effect of Water", J. Catal., 82, 226 (1983).

89. Clark, W. C. and Broadhead, P., "Optical Studies of Surface Impurities on Titanium Dioxide", J. Appl. Chem., 20, 354 (1970).

90. Clark, W. C. and Broadhead, P., "Discoloration at Anatase Titanium Dioxide Surfaces by Organic Contamination",

J. Appl. Chem., 21, 101 (1971).

91. Kaluza, U. and Boehm, H. P.,
"Titanium Dioxide Catalysed Photooxidation of Mercury",
J. Catal., 22, 347 (1971).

92. Gebhart, J. and Herrington, K. J.,
"Reduction of Contaminated Rutile Surfaces by Degassing",
J. Phys. Chem., 62, 120 (1958).

93. Cronemeyer, D. C. and Gilleo, M. A.,
"The Optical and Photoconductivity of Rutile",
Phys. Rev., 82, 975 (1951).

94. Hollabaugh, C. M. and Chessick, J. J.,
"Adsorption of Water and Polar Paraffinic Compounds onto Rutile",
J. Phys. Chem., 65, 109 (1961).

95. Matsuda, S. and Kato, A.,
"Titanium Oxide Based Catalysts-A Review",
Appl. Catalysis, 8, 149 (1983).

96. Rao, C. N. R.,
"Kinetics and Thermodynamics of the Crystal Structure
Transformation of Spectroscopically Pure Anatase to Rutile",
Can. J. Chem., 39, 498 (1961).